fjl: POWR

Development of Electricity Generation and Sensor Systems for a Hydropower Propagating Wave Turbine

24 March 2016

Authors

Elizabeth Tomko emtomko@wpi.edu
James Whyte jswhyte@wpi.edu

Advisors

Prof. Fred J. Looft fjlooft@wpi.edu
Prof. Brian J. Savilonis bjs@wpi.edu

This Major Qualifying Project is submitted in partial fulfillment of the degree requirements of Worcester Polytechnic Institute. The views and opinions expressed herein are those of the authors and do not necessarily reflect the positions or opinions Worcester Polytechnic Institute.

Abstract

The Propagating Wave Turbine Project focused on the design, construction, and verification of an energy generation system that converted the mechanical energy of a low speed, high torque shaft into electrical energy. A maximum power point tracking system created the optimal load profile between the voltage and current produced by an electromechanical generator. To test the design, a sensor system was developed to measure power generator and transformation characteristics between the input rotational power, through the mechanical power generator, and through the power point tracking electronics. In addition to the design of the electromechanical power generation system, a nacelle was designed and built to hold the generator, sensors, and electronics. The nacelle was designed to be attached to a Propagating Wave Turbine built by a separate project team. The generator and electronic modules operated successfully, but it was determined that the final system was not optimal for use with the propagating wave turbine since the shaft speed of the propagating wave turbine was not compatible with the necessary shaft speed of the electromechanical generator. Recommendations are provided at the end of the report to improve power generation using a Propagating Wave Turbine system.

Table of Contents

Table of Figures

Table of Tables

1. Introduction

Hydropower has been an important renewable energy source for generations. Early in the 3rd century BCE water wheels were used for grinding wheat into flour (World, n.d.) and, much later, were used as part of the industrial revolution to power factories (Australia, n.d.). Direct water wheel systems are still used and developed in countries that have historically used water wheels to grind grain and perform other daily functions. However, direct, mechanical water wheel power systems have mostly disappeared in favor of extracting energy from flowing water by generating electricity. (Centre for Rural Technology, 2009)

The first hydropower dam to produce electricity was built in 1882 (Story, n.d.). The dam, shown in Figure 1-1, was located on the Fox River in Appleton, Wisconsin and generated enough electricity to power the dam facilities, a nearby building, and the house of H. J. Rogers, the man who pioneered the project. (Story, n.d.) By comparison, as of 2014 there were 2,198 active hydropower installations in the United States alone, with a total generating capacity of 79.64GW (Uria-Martinez, 2014). In 2013, United States hydropower installations generated about 10% of the nation's electricity, while all hydroelectric power installations generated approximately 15% of the world's energy. (Gadonneix, 2013)

Figure 1-1: The First Hydroelectric Power Plant, located in Wisconsin (Story, n.d.)

Most hydropower installations consist of a dam or a reservoir feeding a turbine system powered by water released from higher elevation. An illustration of this type of installation is shown in **Error! Reference source not found.Error! Reference source not found.**. Water from a river collects behind a dam and is directed through a channel in the dam wall. The kinetic energy of the water is converted to mechanical energy by a turbine and then to electricity by an electric generator. Hydropower installations of varying sizes have been in use since 1882 (Story, n.d.) and continue to serve small and large communities all over the world. (Facts About Hydropower, 2013)

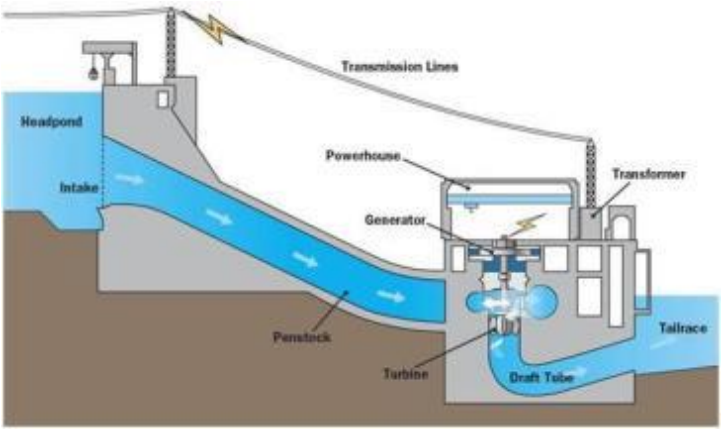

Figure 1-2: How a Hydroelectric Dam Works (William, 2010)

1.1 Propagating Wave Turbine Concept

An alternative method of hydropower for electricity generation based on a 'Propagating Wave Turbine' was recently proposed and developed (Costanzo, 2015). A propagating wave turbine uses a 'ribbon fin,' seen in Figure 1-3. The fin oscillates when water flows parallel to its length and wave motion is translated from one end to the other. This mechanism is usually found on animals such as eels and rays that use the oscillating motion as a means of propulsion. Instead of powering the fin to move through water, moving water can mechanically power the fin. This mechanical energy can then be converted into electrical energy.

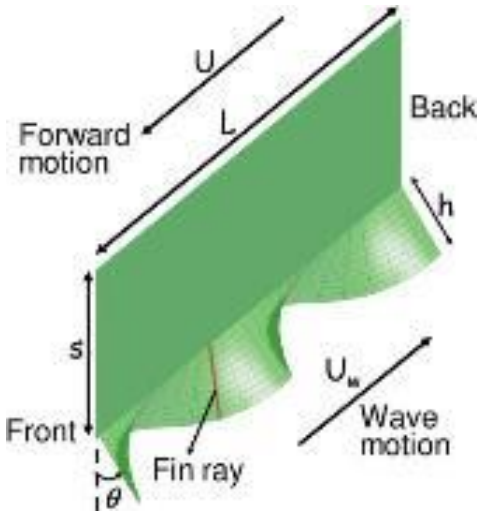

Figure 1-3: Basic Ribbon Fin Design for Propulsion (Bale, 2014)

There are four main benefits of the ribbon fin concept that make the fin an intriguing source of hydropower. First, a ribbon fin system has the ability to create power from a moving current of water without requiring a change in elevation, such as a dam, to create a 'head' of water pressure as needed by a conventional hydroelectric system. Second, a ribbon fin power generation system interacts with a volume of moving water rather than an area. Conventional turbines employ blades rotating about an axis to extract kinetic energy from a current that is moving normal to an area. The ribbon fin system also has a frontal swept area through which water moves, but then extracts energy from a volume of fluid with a fin that extends parallel to the flow. The fin has the potential to remove more kinetic energy from the fluid than a conventional turbine. Third, a fin can generate electricity with minimal disruption of sea life. Conventional turbine systems have to make allowances for marine life in the operating environment and may require screens to prevent fish from entering a spinning turbine generator. The reciprocal motion of a ribbon fin is significantly slower than the rotational motion of a conventional turbine. The fin is not enclosed, and the mechanical motion of the fin does not endanger sea life that enter the fin's operational volume. Finally, similar to turbine based hydro systems, power generation systems based on a ribbon fin are scalable in size to fit an assortment of installation environments and required levels of power generation.

1.2 Project Statement and Objectives

The goal of our project was to develop a method of extracting energy from moving water with a minimal environmental impact by improving on the design of a previously developed ribbon fin energy generation system.

The specific objectives of the project were to:

1. Evaluate previous work on the hydrofin systems to identify specific aspects of the design that could be improved.
2. Collaborate with an ME project team working on a fin and mechanical powertrain to develop a combined mechanical/electrical energy generation system.
3. Develop electronic and control modules and sensor systems needed to generate electricity based on the ME project team mechanical powertrain.
4. Integrate the ME powertrain and electricity generation modules into a complete, deployable prototype.
5. Test the prototype, determine the effectiveness and efficiency of the design, and fully document the results.

Testing by a previous project team demonstrated the ability of a propagating wave turbine device to extract energy from moving water while minimizing environmental impacts. Our project team focused on the design and development of an electricity generation and transmission system, sensors and instrumentation, and a nacelle. Complete details regarding the objectives are in the System Design Chapter.

1.3 Summary

This section has provided an overview of the issues the project has set out to address, with a brief review of the history of hydroelectric power and a brief description of the project objectives. In the following section, basic background information on the ribbon fin system under development by an ME project team will be described along with other topics that are central to understanding the goals and objectives of this project.

2. Background

2.1 Introduction

This chapter provides an overview of existing water energy harvesting technologies from commonplace to experimental. The methods of energy harvesting are explained and economic impacts discussed. This chapter also provides an explanation of the previous design and development of propagating wave turbine prototypes.

2.2 Methods of Water Energy Harvesting

An ocean wave is caused by interfacing bodies and is a combined result of water depth and prevailing winds. Fundamentally, the kinetic energy in a wave comes from the wind. This energy is stored in the moving "mass" of the wave. Waves are enhanced by wind. (Hadhazy, 2013).

Multiple technologies have been developed that capture energy from waves, such as underwater turbines and line attenuators. One example is the Wave Buoy, shown in Figure 2-1. The buoy moves vertically with surface waves and the vertical motion is converted into rotational motion to turn an electric generator.

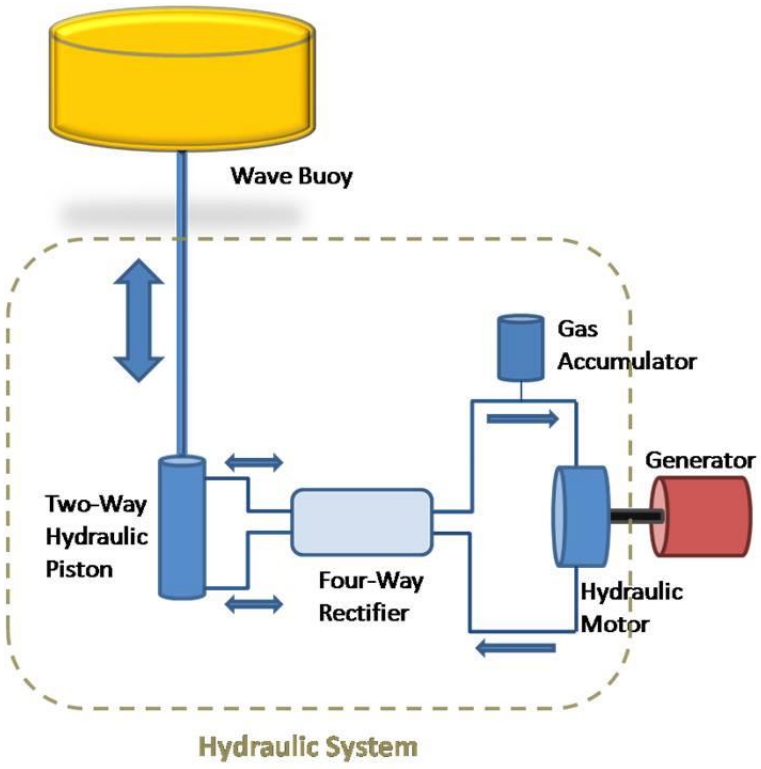

Figure 2-1: A Wave Buoy, one of the many Wave Energy Technologies (University L. , n.d.)

The ability to effectively extract power from waves is limited to some extent by the variability in energy between consecutive waves and the general variability in wave energy as a function of the weather and seasons throughout the year. As a result, the assessment of a wave energy resource is a prerequisite for the strategic planning of wave energy installations and the design of a wave device to harvest energy. The height, frequency, and seasonal variations of waves are assessed in potential installation sites. (Falcao, 2010)

Wave energy is particularly applicable to areas of world where waves are consistent in height and strength. Such places can be found on the northwestern coast of the United States and select coasts of Europe. In Norway, two full-sized shoreline prototypes were constructed near Bergen, and in 1991 the European Commission decided to "include wave energy in their research and development program on renewable energies, enabling vast advancements in wave power technologies in Europe". (Falcao, 2010)

2.2.2 Tidal Energy

Tides are formed by the gravitational pull of the moon. The lunar orbit dictates the tidal cycle as tides are pulled towards the moon wherever the moon may be in orbit (Alternative Energy Tutorials, n.d.). The effect of this gravitational pull can be seen in Figure 2-2. The tidal changes observed on the coastlines are due to the bodies of water following the ebb and flow caused by the moon's gravitational pull.

Tides dissipate approximately two and a half terawatts of energy when on an underwater shelf. (Shields, 2011) The simplest generation system for tidal plants involves a dam, known as a 'tidal barrage', constructed across a river or inlet. The basic design of a tidal energy generation system can be seen in Figure 2-3: The Basic Design of Tidal Energy Generation Systems .

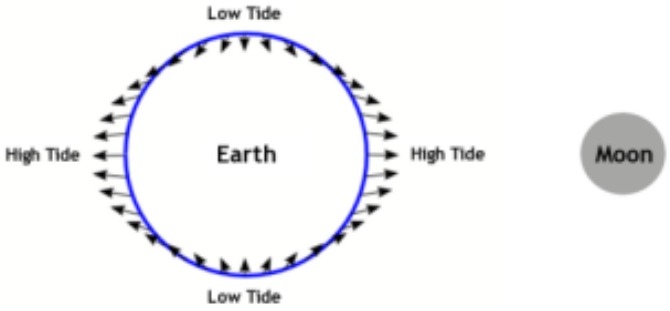

Figure 2-2: Depiction of How Tides are Created (Foundation, 2015)

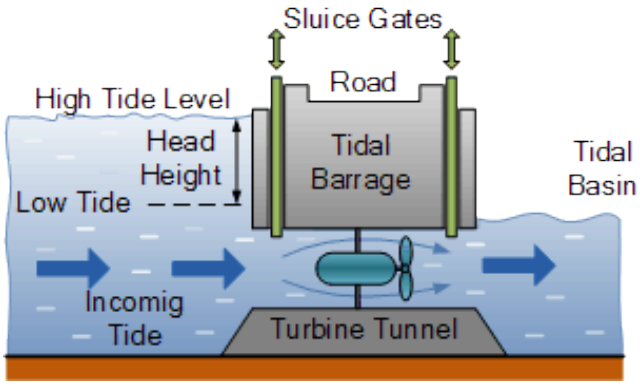

Figure 2-3: The Basic Design of Tidal Energy Generation Systems (Tidal Barrage Generation, 2015)

The loss of energy through dissipation primarily occurs when water runs up on a continental shelf or between landmasses. Because tidal energy devices are most efficient and easiest to design when there are large tidal shifts, the areas best suited to tidal energy are those with geographic pinch-points. In areas with pinch-points, water flow is forced together causing an increase in speed and thusly a rise in height. By comparison, the amplitude of a tide wave is very small in the open ocean; roughly fifty centimeters. However this height can increase dramatically when a tidal wave encounters an underwater shelf.

Tidal energy is a unique renewable resource and security and predictability gives this form of renewable energy value in a future electricity market. The tidal resources in our coastal waters could be used to raise the amount of energy generated by environmentally safe methods. (Johnstone, 2013)

2.3 Marine Energy Challenges

2.3.1 Environmental Challenges

The challenges of extracting energy from the marine environment include designing a system to fit into a given location while ensuring the sanctity of the marine environment. When a tidal current turbine power generator extracts energy from a stream, the flow speed of the stream is reduced. In designing a device that captures energy from water, it is therefore necessary to include the potential sedimentary shifts in the developmental studies, as marine life could be negatively impacted should the seascape change. (Neill, 2009) The health of the seabed must be a main concern of the developers, as a major ecological impact could originate from a small design change. (Gill, 2005)

2.3.2 Economic Development and Site Challenges

Regardless of the specific marine energy extraction system proposed, an installation must address challenges related to economic feasibility and safety. Technologies to harvest energy from marine applications must be evaluated for key economic factors such as the ability of the local electrical grid to absorb the power generated, and the ability of the system to fit into the local environment. (Leijon, 2010) Potential sites are often evaluated through estimates of the energy that can be generated for a particular

site. In general, a multitude of complex factors are used to determine the economic feasibility of a proposed site. (Leijon, 2010)

For many water energy technologies, intermittency caused by stagnant water flow or drought causes a lull in energy production. Because tides are linked to cycles of the moon, tidal technologies provide a predictable way to generate energy. The disadvantage of tidal power is the varying strength of the tides between spring tides and neap tides, which are those occurring after the first or third quarter of the lunar cycle when the height difference between high and low tides is the smallest. Since tidal height difference leads to a wide variation in rates of energy generation tidal energy extraction technologies must be capable of operating at optimal efficiency during a potentially large range of flow rates. (Denny, 2009)

Another concern of alternative energy technologies is total cost. Such factors as development and maintenance that impact overall cost are essential when considering the effectiveness of a technology. A company will be most interested in a technology that can generate the most watt-hours for the lowest capital investment and operating costs. (Leijon, 2010)

2.4 State of the Art Hydro Energy Generation

In 2013, roughly 15% of the world's electricity came from hydroelectric sources, and in 2015 that number rose to 21%. (Perlman, 2015) Small installations, those which generate up to 10MW, (Small Hydro, n.d.) comprise roughly 10% of the world's total power, while large scale technologies, such as hydropower plants, comprise roughly 11%. (Gadonneix, 2013)

2.4.1 Tidal Current Power

In the United States, there is potentially 50GW of power to be harvested from tidal streams. (Haas, 2011) Resources such as a tidal current farms can be a viable option since tidal current farms have a more environmentally friendly technology than a technology such as a turbine with spinning blades. (Walters, 2013) The 50GW potential for development can be approximated from the ambient flow, although it is acknowledged that this estimate is no longer valid if the flow is perturbed. (Walters, 2013)

Designs such as axial-flow and cross-flow turbines have been proposed to harvest tidal energy and the energy of streams. (Energy, U.S) One example of this technology is the AR1000 from Atlantis Resources. The AR1000 is a horizontal axis turbine with a 1MW rated capacity, and is undergoing testing in the Pentland Firth in Scotland. The cut-in angles of the blades can be changed during operation, ensuring that the blades meet the optimum cut-in angle for any given water current. This optimization allows the turbine to operate at a higher efficiency than a conventional design. (Resources, AR1000, 2015) An updated model, the AR1500, seen in Figure 2-4, is designed to withstand the harsh environmental conditions found in the Pentland Firth in Scotland and the Bay of Fundy in Canada. The two locations boast some of the highest tides in the world, making the bays optimal for testing tidal current energy harvesting devices. The design of the AR1500 was completed in 2014 by Lockheed Martin Corporation and the first unit was due for pre-delivery for on-shore acceptance testing at the end of 2015, however there is no record of this information as of early 2016. (Resources, AR1500, 2015)

Figure 2-4: The AR1500 – With an 18 Meter Rotor, this is the Next Generation AR1000, Currently Undergoing Tests in Scotland (Resources, AR1500, 2015)

2.4.2 On-Shore Wave Power

Yoshio Masuda is considered to be the first person to perform in-depth research concerning the use of modern wave technology. He started studying the use of wave energy in the 1940s (Falcao, A). Since Masuda, wave technology has grown into many different types of wave energy harvesting technologies. One technology in the Oscillating Wave Column family (OWC), developed by the Queen's University and Wavegen, is undergoing testing in Scotland. The official title of this technology is the Land and Marine Power Energy Transmitter (LIMPET), seen in Figure 2-5. The device has an average output of 200 kW. (Boake, 2002) The LIMPET has been reliably producing power for the national grid since 2000. (Admin, 2012)

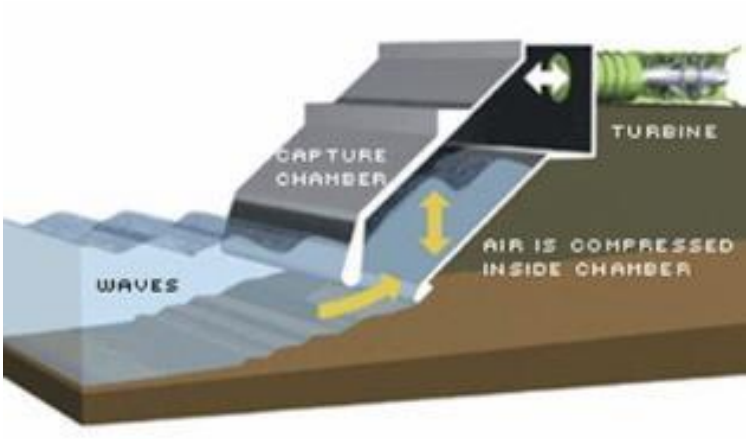

Figure 2-5: The LIMPET Energy Harvester (Seed, n.d.)

As shown in Figure 2-5, an OWC is a device that uses air pressures to generate electricity. Typically, a large enclosure will sit submerged in the water and the only exit or entrance for air is through a turbine. As the water changes heights with the incoming waves, the air pressure inside the enclosure is forced in and out of a sole opening in the enclosure. This opening consists of two turbines, one of which operates if air is

being forced one way, and the other operates if the reverse is true. The OWC system is the first wave generator to supply power to a commercial grid, and is the longest running wave power generator. (Boake, 2002)

Another onshore wave energy generator is the Oyster 800 by Aquamarine Power, seen in Figure 2-6. Testing began in 2012, with successful electricity production to the grid completed soon after. This technology has a maximum generating capacity of 800kW and the machine measures 26 meters wide. The Oyster 800 can be installed at depths of roughly 13 meters and can be sited as far as 500 meters from shore. The machine is currently installed at the European Marine Energy Centre in Orkney. (Power, 2012)

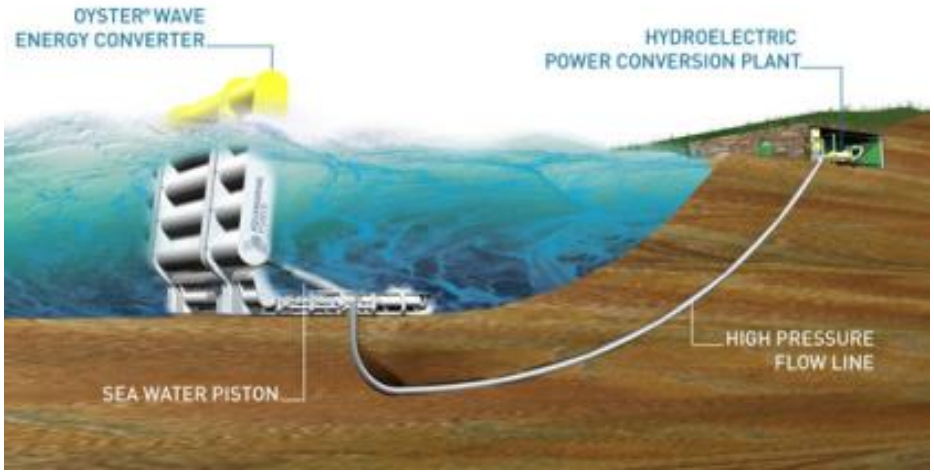

Figure 2-6: The Oyster 800 (Singh, 2011)

2.4.3 Off-Shore Wave Power

Some recent advances in wave power harvesting include the OWC, discussed earlier, as well as the Point Absorber and the Line Attenuator. The two latter technologies have been undergoing testing in the recent decade, and have shown promise on a large scale.

The Point Absorber is a cylindrical structure that floats on the surface of the waves. The device operates as a piston where the cylinder moves in and out as the weighted base of the device rises and falls with ocean currents. This vertical motion of the buoy is utilized to alternate the compression of a gas or liquid in some form of container, converted into rotational movement of the power generator, or converted in other similar ways. (Voorhis, 2012)

The PowerBuoy, shown in Figure 2-7, is an 11.5 meter long buoy built by Ocean Power Technologies (OPT). This buoy is a point absorber with the hydraulic system attached to the top. The Mark 3 version was deployed in 2011, and boasts an impressive energy production rating of 866kW. (OPT, 2015)

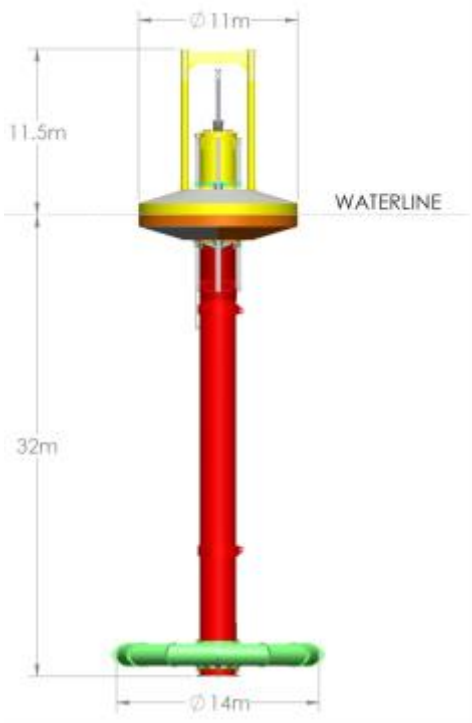

Figure 2-7: Mark 3 PowerBuoy (OPT, 2015)

The line attenuator is a device that lays on top of the ocean's surface. The entire device is built in segments and the total length can be up to 140m long. The segments move up and down with the waves. The motion between the segments is captured through the movement of hydraulic fluid as the fluid is forced through generators, producing electricity. Line attenuators are able to produce larger quantities of electricity compared to other off-shore wave devices, as miniscule movements can be captured and utilized. (Stansell, 2013)

The Pelamis Wave system, seen in Figure 2-8 and Figure 2-9, is a line attenuator that is currently implemented in an energy farm in Agucaduora, Portugal. Each device measure 140m long, and energy is generated as each of its five segments moves independently. (Carcas) The peak energy generation rating is 750kW, however potential problems may arise as the device ages and constant movement stresses the joints. (Kaiser, 2015) The movement of the segments of the Pelamis Wave system pressurizes a hydraulic system. Pressurized fluid turns hydraulic motors, which generate electricity. The system is capable of generating electricity from the low-speed, high-energy movement of the segments.

Figure 2-8: The Pelamis Wave system, Moored (Pelamis Wave Power, n.d.)

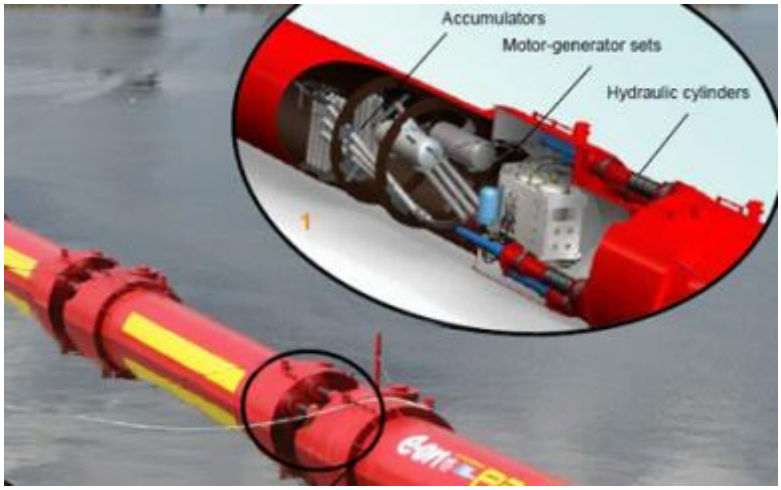

Figure 2-9: Internal mechanism of the Pelamis Wave system (Pelamis Wave Power, n.d.)

2.4.4 Small Hydroelectric

Small hydroelectric devices are those that capture the energy in flowing water and convert it to useable energy, while producing up to 10MW. (Small Hydro, n.d.) According to the World Small Hydropower Report in 2013, only one third of the small hydro potential in the world has begun to undergo development. (Liu, 2013) Small hydro is in most cases 'run-of-river', meaning little or no water has to be stored to create a head of water for a turbine use. As such, small hydro installations do not have the same kind of adverse effects on the local environment as a large, dam based hydro-electric system. Dam based hydro power alters the natural landscape because water has to be stored behind a dam wall. This alters a riverside's natural landscape, potentially harming the plants and wildlife living in the immediate vicinity of the river.

Hydropower, large and small, remains the most important 'renewable' for electrical power production, (Paish, 2002) and several countries with a large portion of the population living in rural areas have begun to exploit the benefits of small hydro. In the UK, 'roughly 100MW of the existing small hydro capacity operating from 120 sites, and at least 400MW of unexploited potential'. (Paish, 2002)

2.5 Previous Propagating Wave Turbine Project Work

The Propagating Wave Turbine project began in the 2014-2015 academic year and continued to the fall of 2015. The original project team designed, manufactured, and tested three prototypes that investigated ribbon fin configuration and mechanical powertrain design. The team successfully turned kinetic energy in flowing water into mechanical energy in a rotating shaft with an efficiency of 11%. Three prototype iterations were completed by the end of summer 2015. Additionally, a test assembly was developed to enable testing of the propagating wave turbine prototypes in a pool of standing water. (Costanzo, 2015)

The ribbon fin design idea was proposed and worked on by Ian Costanzo, Alden Kelsey, Fiona Ogren, and David Wians, with Professor Brian Savilonis as the advisor. A CAD model of the second prototype can be seen in Figure 2-10. Two arrows, seen in blue, show the side-to-side motion of the fin.

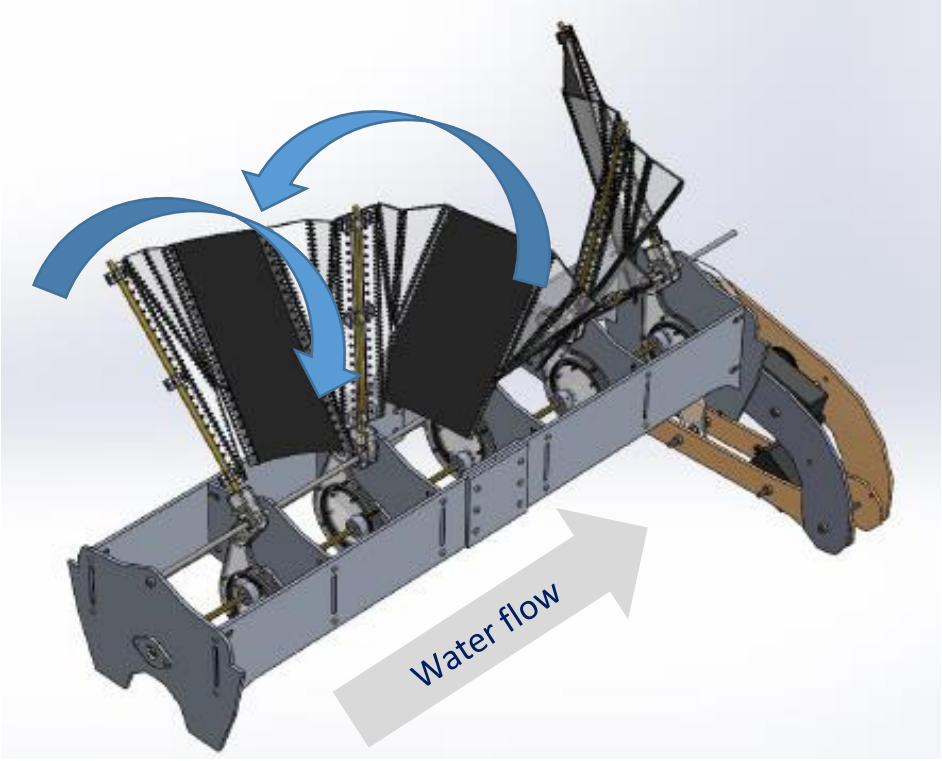

Figure 2-10: The CAD Drawing of the Propagating Wave Turbine at the end of the 2015 Academic Year (Costanzo, 2015)

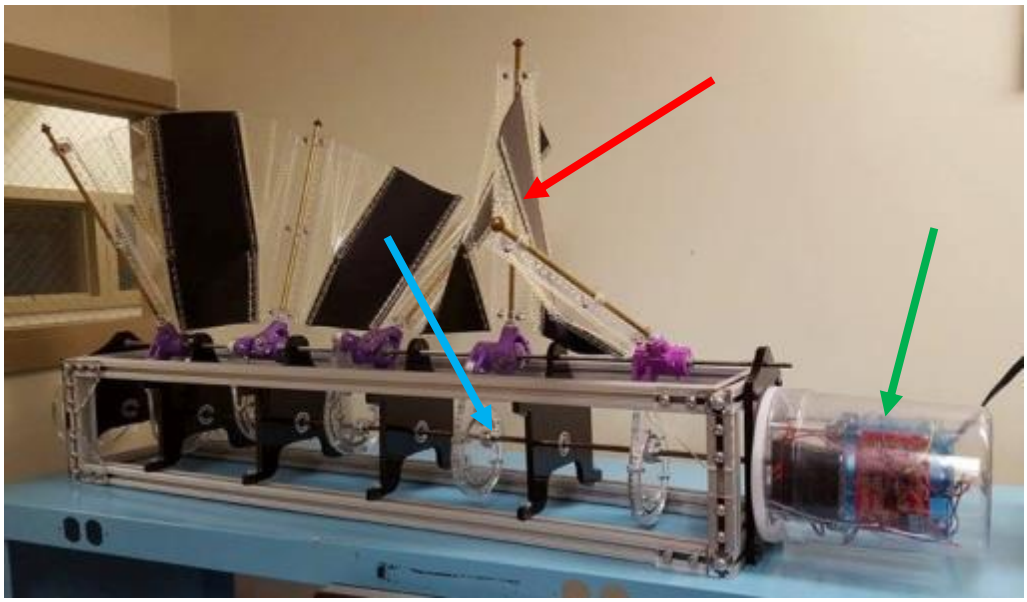

Figure 2-11: The Propagating Wave Turbine as of Fall 2015 (Tomko, 2015)

The project team made three prototypes, one of which was tested in the Donahue Rowing Center. The testing facility is seen in Figure 2-12. The first prototype was an exploration of the mechanism necessary to create the ribbon fin motion. The prototype translated the wave motion of masts into rotational shaft motion via cams. The second prototype had a longer, more rigid frame and was sized for the available testing space in WPI's Donahue Rowing Center. The prototype featured eccentric cams with bearings and a wooden frame. All three iterations had five masts each to create one complete wave along the length of each of the prototype. The second prototype, seen in Figure 2-11, was tested in the Rowing Center and produced a maximum power of 3.6 watts at an efficiency of 11%. The fin (Red arrow) was attached to a rotating shaft (Light blue arrow). The location of the energy conversion module is shown by the green arrow.

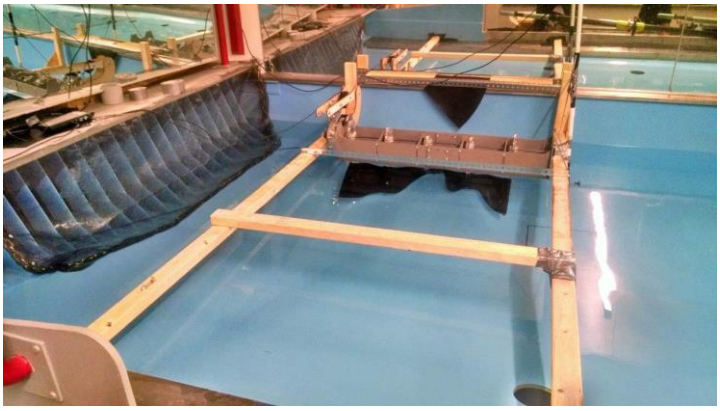

Figure 2-12: Last Year's Prototype, in the Donahue Rowing Tank (Costanzo, 2015)

Two fin types were tested. The first fin was made of neoprene between the masts. The second had plates of acrylic and sections of neoprene sewn together. Many parameters determine the effectiveness of the fin including swept area, height, material flexibility, and areas of holes. Fins can be evaluated through extensive testing.

The prototype iteration that was completed over the summer of 2015 had a metal frame and significantly lower friction in the powertrain compared to the previous prototype. A raft was created to float the wave turbine in a pool of water with the device frame above the water and the fin under the water surface. A winch was made to draw the raft across water at a constant velocity. The winch speed and distance were controllable. The raft and winch enabled the use of standing bodies of water for testing. This setup can test devices that are much larger than what the Donahue Rowing Center tank will allow. Data was not collected for the third device iteration, but the test equipment will be useful for future prototypes.

2.6 Design of the Fin

Examples of ribbon fins used in nature include the long fin belonging to eels or the Black Knifefish, seen in Figure 2-13. Long fins, which run the length of the body, display the undulating effect the fin was striving to achieve. Biomimetic, or biologically inspired, robots have been in development for some time for varying applications. The design proposed by last year's team focused on drawing from existing biomimetic designs as well as existing propulsion systems. The design featuring the 'ribbon fin' was also inspired by Theo Jansen, the Norwegian artist behind the Strandbeests seen in Figure 2-14.

Figure 2-13: The Black Knifefish (YouTube, 2013)

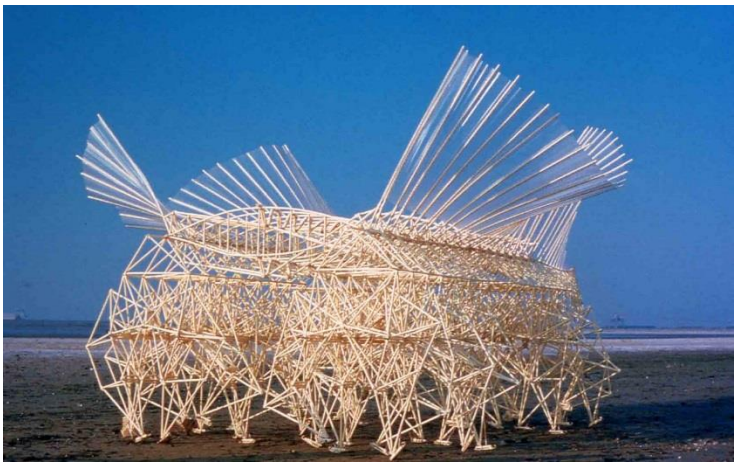

Figure 2-14: One of Theo Jansen's Strandbeests (Underplayground News, 2015)

The ribbon fin shape entailed planar geometry, forming an arc section with a width equal to the height, and the length of the top and bottom defining the curvature. (Costanzo, 2015) For the desirable material characteristics, neoprene was used for the fin material. The second version of the fin, a hybrid (See Figure 2-15), was developed with both acrylic plates and neoprene. The neoprene panels are located by the green arrow, the acrylic plating by the blue arrow, and the mast by the red arrow. A balance between stiffness and flexibility was determined to be optimal. (Costanzo, 2015) The fin was designed to be removable for easy testing, and environmentally friendly as well as efficient. Therefore, the fin design chosen dictates smooth and friendly interactions with the installation site and marine life.

Figure 2-15: The Hybrid Fin (Costanzo, 2015)

Another inspiration for the original development of the fin design was the Ghostbot (Seen in Figure 2-16), a robotic representation of the Black Knifefish. This robot is not designed for energy generation, but for propulsion and exploration. The ribbon fin design in use by this robot is undulatory, being very long and not deep. This is to mimic the design of the Black Knifefish. (University N. , 2011) The fish is known for being extremely maneuverable, with precise movements including pinpoint turning.

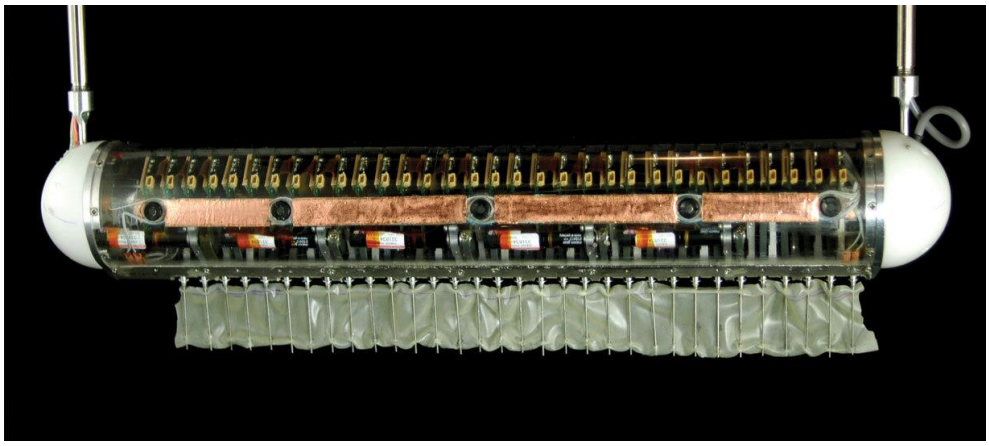

Figure 2-16: The Ghostbot Robot (HDT Global, 2016)

The Sepios robot was developed by students at the Swiss Federal Institute of Technology. Based on a four finned cuttlefish design, Sepios is designed for high maneuverability and omni-directionality and is shown in Figure 2-17. The fish-like appearance makes this robot the ideal device for filming and photographing marine wildlife, and is applicable to the propagating wave turbine due to the fin and nacelle design. The fin is made of a very fluid material, appearing similar to fabric. There are many masts throughout the fin. Each mast has a bevel gear on the end that meshes at a differential. The drive gears, mounted on individual shafts, can be fully controlled individually. This means that the fin, while normally in a sine wave status, can represent a horizontal plane. (Sepios, 2015) Each shaft is controlled by a servo, so instead of having a fixed frequency and amplitude, each fin has two hundred and seventy degrees of motion. (Ackerman, 2014)

Figure 2-17: The Sepios Robot (Sepios, 2015)

2.7 Summary

This section discussed the current large scale and small scale technologies for energy generation from water. Current methods of electricity generation and challenges for a new water energy harvesting device were explored. An overview of the propagating wave turbine and the reasoning behind previous design choices were presented. This history is described as the information relates to the modules and work yet to be implemented.

3. Design Methodology

3.1 Introduction

This section discusses the reasons behind the design of the system and outlines the constraints for parts of the system. A discussion of how the modules will be constructed is given, as well as the steps taken to optimize the overall propagating wave turbine design.

3.2 System Overview

Figure 3-1 depicts the system layout of the project as a functional diagram. The basic generator system is composed of two sub systems; a mechanical system that extracts energy from moving water and transforms that energy into rotational energy, and a power generation system that transforms the rotational energy into electrical energy. As shown in this figure, a nacelle structure contains the electrical power system composed of sensors, embedded computer systems, power electronics, and energy generation modules.

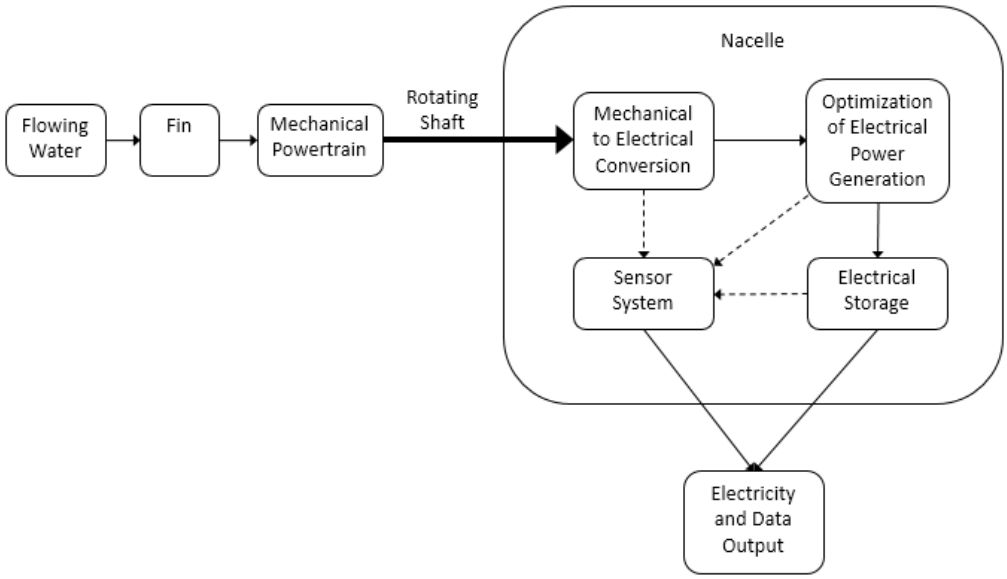

Figure 3-1: Functional Block Diagram

3.3 Design of the Fin and Mechanical Powertrain

The mechanical subsystem fin design was inspired by fins on a fish and previously developed mobile robots. The 2015-2016 ME project team was responsible for the design and development of the fin and mechanical powertrain. The ME team kept their design parameters close to the previous iteration of the propagating wave turbine. With a flow speed of 2m/s, their team expected to generate up to 10W of power. In turn, the 10W power level dictated the design of our team's power electronics and the design of the frame for their mechanical powertrain influenced the design of the nacelle.

3.4 Design of Power Electronics

A generator module and corresponding electronics control system was necessary to convert mechanical energy from the powertrain to electrical energy. The system was designed to use maximum power point tracking (MPPT) to dynamically change the load seen by the generator, enabling the generator to maximize power production at a given torque and RPM. MPPT technology is commonly used to optimize the power from solar panels. (Sun N. A., 2015)

The electrical energy generated from the system was used to power the onboard microprocessor and sensors. Additional energy was also stored in an onboard battery that could also provide backup power to the microprocessor and sensors when the generator was not producing sufficient power. Connections to the battery were accessible outside the nacelle so the energy produced by the propagating wave turbine could be used for external applications.

3.5 Design of Sensor Systems

It was necessary to monitor the performance of an energy extraction and conversion system and understand environmental conditions in order to validate the wave energy machine design. Multiple sensors were used to track generated power and provide data during testing. Sensors tracked water flow rate, generator shaft speed, voltage and electrical current before and after power optimization. Implementation of sensors for water temperature and detection of water in the nacelle gave a more complete understanding of testing conditions.

All the electronics for the energy extraction and conversion system could be tested in a lab environment, as testing the system only required a rotating shaft from which to extract energy. The ME team working on the fin and mechanical powertrain required the energy extraction and conversion system to be operational on the frame during testing in moving water. The energy extraction and conversion system was designed to function in this test environment.

3.6 Nacelle Purpose and Design

Hydropower equipment is constantly in contact with untreated and turbulent water and such systems must be robust to stay operational. The nacelle on the Propagating Wave Turbine was designed to keep harsh environmental conditions from damaging mechanical and electrical components. Mechanical power in the form of a rotating shaft provides input power to the electronics power conversion system contained within the nacelle. The electrical generator, power optimization circuitry, electrical storage, and sensor systems were all housed and protected in the waterproof nacelle. Sensor data and electrical power were the nacelle system outputs.

The design of the nacelle was based on the frame made by the ME team. It was decided in the Preliminary Design Review that the nacelle would take the form of a round ‘end cap’ for the box frame holding the mechanical powertrain. The materials used had to protect the internal components during testing, but did not need to match durability of production-level marine energy harvesters.

3.7 Timeline

Propagating wave turbine system development was comprised of two teams working together. One team was responsible for redesigning the original wave energy mechanical prototype to optimize the efficiency of the mechanical designs, and one team responsible for the design of the electromechanical systems to convert the mechanical energy generated by the mechanical ribbon fin system into electricity. Throughout the design and fabrication of the new wave turbine, both teams collaborated to ensure the final device was effectively extracting power from water, converting mechanical energy into electricity, and outputting usable energy. The objectives of this project were focused on in the following order:

A-Term:

a. Design of system modules.
b. Development of the Introduction, Background, System Design

End of A-Term:

c. Preliminary Design Review on 13 October 2015

B-Term:

d. Complete preliminary design of energy conversion system, including parts specifications, calculations of all critical power, energy, voltage and current values, and specifications of all digital/measurement interfaces including sensors and other test components.
e. Critical Design Review on 19 November 2015.
f. Develop Design Methodology section.
g. Construction of electricity generation module.
h. Construction of sensor and power transmission systems.

Second half of B-Term:

i. Construction of nacelle.

End of B-Term:

j. Submission of system design and draft detailed design documents

C-Term:

k. Test and evaluation of system and circuit designs
l. Construction of mounting solution for nacelle that interfaces with the frame of the ME team's powertrain.
m. Complete energy generation system and complete bench testing
n. Completion of Detailed Design, Results and Analysis, and Conclusion sections of the project report.

3.8 Summary

This section provided an overall description of the reasoning behind the design decisions made by the project team and the ME project team. The design methodology of the system was made clear, and the implementation strategy of the modules was given.

4. System Design

4.1 Introduction

This chapter presents system design constraints, design decisions and processes, and procedures for testing. Also presented are justifications for design and development choices, and an outline as to how modules must interface to achieve the goal of a successful propagating wave turbine.

4.2 System Overview

The generator for the system produced three-phase DC power, which was sent through a three-phase bridge rectifier to create single-phase DC. Energy was then optimized using a MPPT integrated circuit. The MPPT IC had an integrated charge controller, which was used to charge a 3.7V LiPo battery. The battery then was used with a boost converter to produce a regulated 5V output. This output was used to power the Teensy 3.2, a few onboard sensors, and an external sensor The Teensy 3.2's regulated 3.3V pin was additionally used to power onboard sensors.

Figure 4-1 depicts the system layout as a functional block diagram. The nacelle structure contains the sensors, embedded computer systems, power electronics, and energy generation modules needed for this project. The rotational velocity of the mechanical powertrain's shaft was geared up to meet the input range for the generator. The rotating shaft of the generator was used to generate AC power, which would pass through a three-phase bridge rectifier in order to transform the power into DC. This DC power was sent directly to the MPPT, to be optimized. The MPPT also featured a charge controller capable of charging an onboard 3.7V LiPo battery, in order to keep the system self-sustaining. To power the microprocessor and sensors, the 3.7V voltage from the battery was sent through a boost converter, which output regulated 5V. Onboard and offboard sensors were powered using either the regulated 3.3V pin form the microprocessor or the regulated 5V from the boost converter. The output from all the sensors was processed by the microprocessor, and the resulting information was used in the code to perform calculations such as RPM and current. In order to read how the system was performing, the microprocessor's USB port was connected to an external laptop, in order to stream the data in real-time.

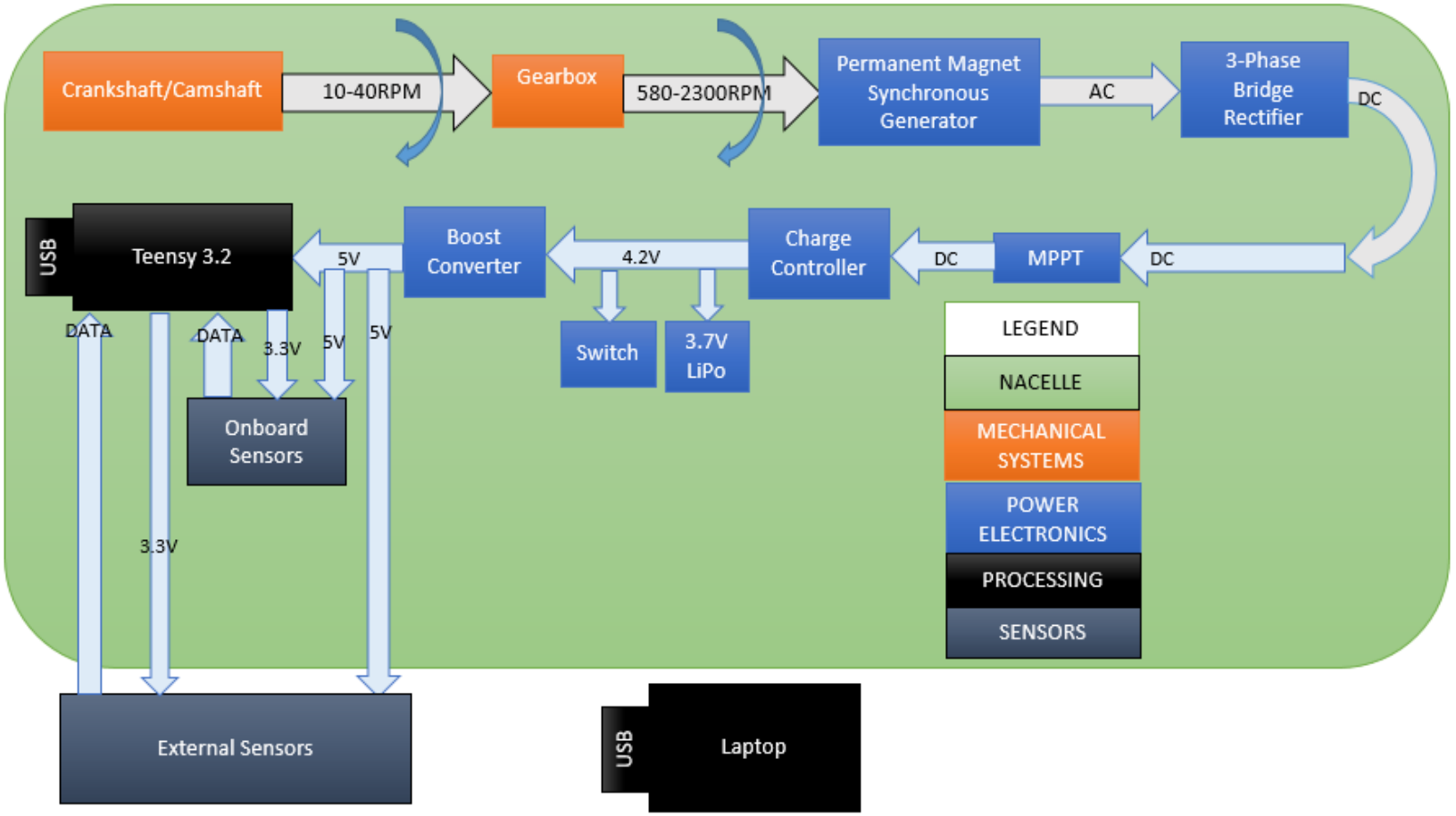

Figure 4-1: Electromechanical Power Conversion System Functional Block Diagram

Figure 4-2 shows the transfer of data and generated energy throughout the system, as well as the respective inputs and outputs and datatypes of the system. It was estimated that the average water flow velocity of water passing by the ribbon fin was 0.5m/s to 2m/s. This flow velocity would force the ribbon fin to move in a sinusoidal motion, thus rotating the shaft. The RPM of the shaft was geared up to match the optimal RPM range of the generator. A shaft encoder was used to detect shaft rotations, from which RPM was calculated. This information was stored in four bits of data. Using the 16-bit ADC on the Teensy 3.2, voltage and current values were measured before and after optimization through the MPPT chip. Two moisture sensors, constructed using two probes, and a pressure (force) sensor were also measured using the Teensy's ADC.

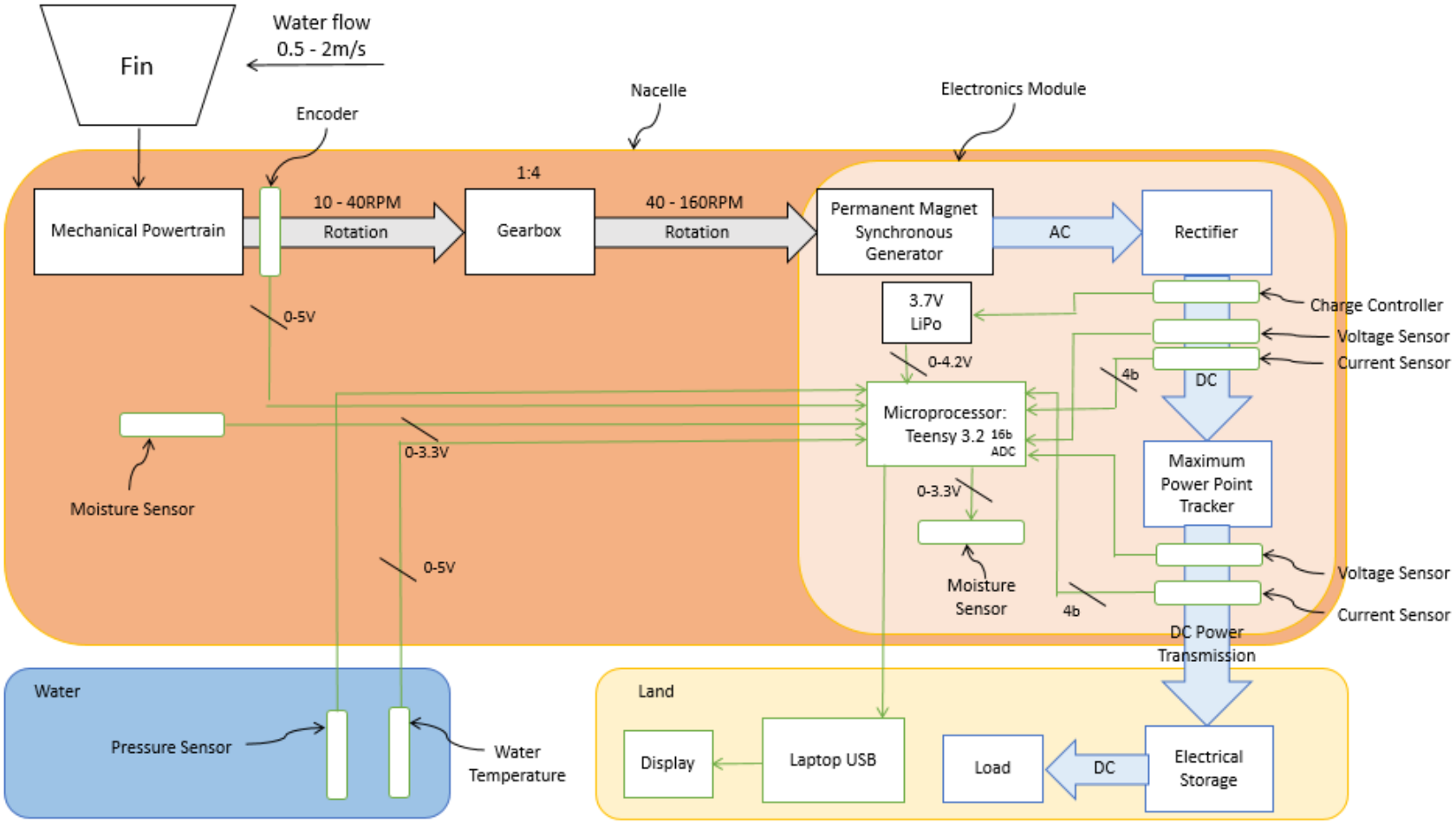

Figure 4-2: Data Flow Diagram, Showing Locations of System Components

The nacelle frame, shown in Figure 4-3, was constructed from laser cut acrylic sheets of 0.236”. The electronics module (green arrow) and the generator module (yellow arrow) can be seen in the Figure. The electronics module served to provide a waterproof compartment where all the electronics of the system were held. The generator module contained the generator, and photointerrupter.

The blue arrow in Figure 4-3 also shows the location of the frame with the fin and mechanical powertrain. The generator module, indicated with the yellow arrow, is connected to the mechanical powertrain though a waterproof bearing and two gears. The electronics are contained in the electronics module, indicated with the green arrow. All modules and sensors are attached with the nacelle frame, indicated by the red arrow.

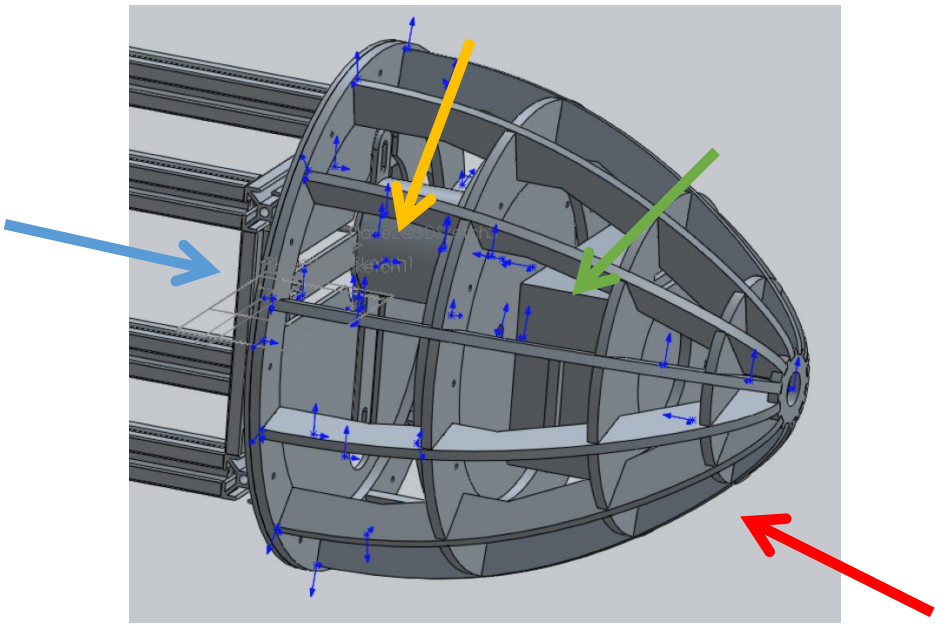

Figure 4-3: Nacelle Overview

4.3 Energy Extraction from Moving Water

The calculations below represent the average power that the electric generator must be able to convert to electricity. With a flow velocity of 1m/s, the maximum power that can be developed, ideally, is roughly 33W, which translates to a net production of 11W when incorporating an efficiency rate of 33%. This value dictated the design of the power electronics, sensor circuits, and electro-mechanical design choice

v = fluid flow velocity
ρ = fluid density
a = swept frontal area of fin
θ = swept angle

Water density:

$$\rho := 1000 \frac{kg}{m^3}$$

Set variables:

$$h := 0.2921m \qquad v := 1 \frac{m}{s} \qquad \theta := 90$$

$$a := \pi \cdot \frac{\theta}{360} \cdot h^2 \qquad a = 0.067\,m^2$$

$$P_{flow} := \left(\frac{1}{2}\right) \cdot a \cdot \rho \cdot \left(v^3\right) \qquad P_{flow} = 33.506\,W$$

Total energy from fluid is from kinetic and pressure, since water is incompressible.

Calculations for energy that can be extracted from moving water were outlined in the previous propagating wave turbine report. (Costanzo, 2015) The frontal area of the volume swept by the fin (a, above) was calculated from the length of the masts (h, above) and the swept angle (Θ, above). The kinetic energy in the water (P_{flow}) was calculated based on the water flow volume and velocity. At the given flow velocity of 1 m/s, it was calculated that ~33.506W could be extracted from the water. Since 100% efficiency cannot be achieved in any power conversion system, (Betz's law for wind turbines states that it is impossible to capture 100% of the wind's energy due to the physical limits of the structure and mechanisms and the necessity of the continuation of fluid flow) it was estimated that perhaps 1/3 or less of the potential waste power could be extracted and converted to electrical power.

4.4 Mechanical Powertrain

The constraints for the mechanical powertrain, much like fin design, were established by the ME project team. Because the ME project team utilized a camshaft the previous year, the group constructed both a crankshaft and a camshaft for a comparison to determine which powertrain was the better design. The ME team tested their newly designed fin on a camshaft designed to replicate the previous groups' camshaft as well as a crankshaft. The prototyped powertrain will have an output shaft for mechanical power that will interface with our team's gearbox and electric generator. The powertrain prototype will be contained within the frame built by the previous year's project team.

The two project teams interfaced where the gearing system from the ME project team met the generator used for generating electricity. The RPM of the mechanical powertrain is dependent on water flow rate and mechanical load. RPMs were determined via testing. The RPM values were used to select a gear ratio to turn the high-torque, low-RPM from the powertrain into low-torque, high-RPM for the electrical generator. The gear ratio was selected with the RPM/Volt rating of the chosen generator so the necessary voltage would be produced for the operation of the power electronics. Figure 4-4 and Figure 4-5 depict the mechanical powertrains of the ME project team. Figure 4-4 shows the camshaft, and Figure 4-5 shows the crankshaft.

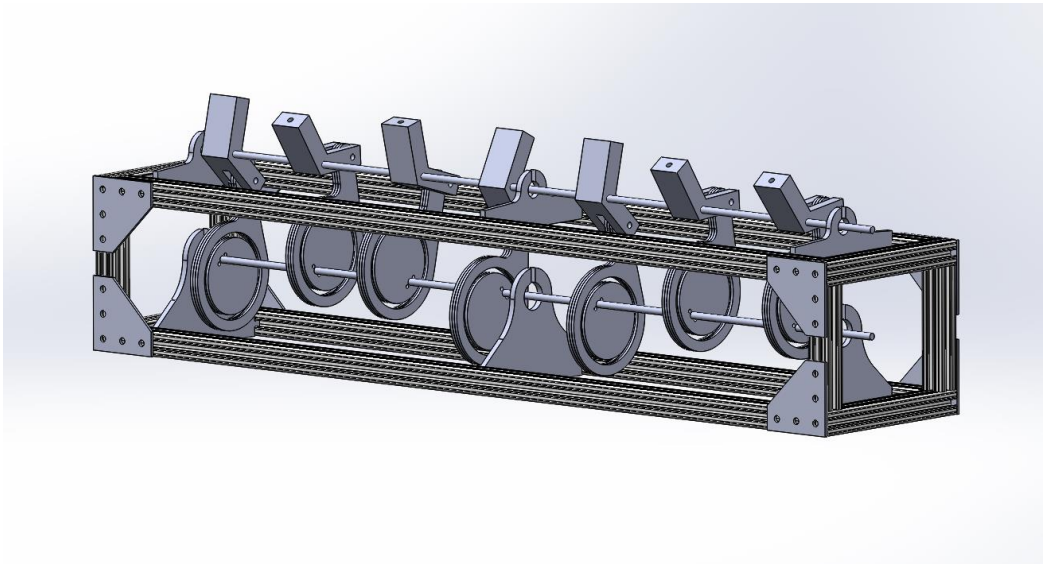

Figure 4-4: CAD of Cams from WPI ME MQP Team

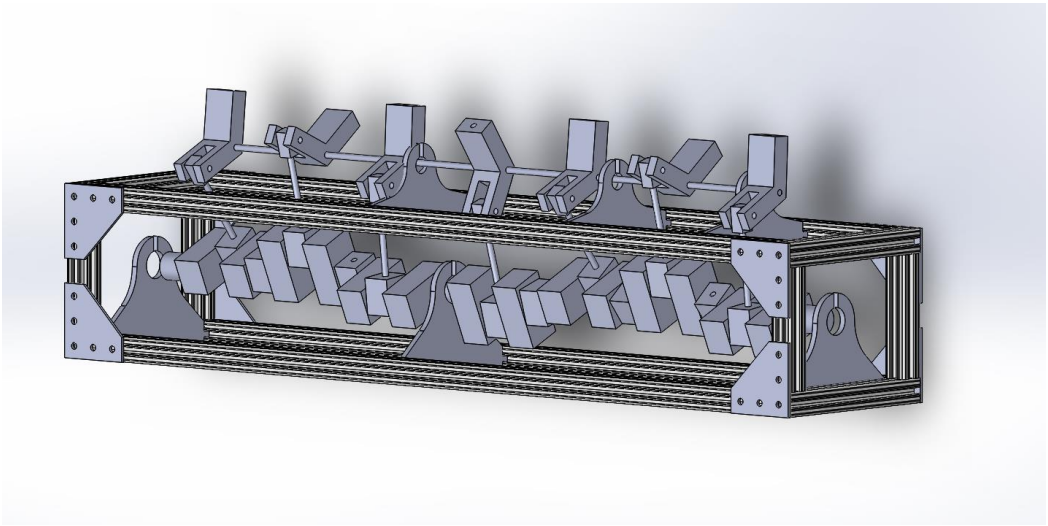

Figure 4-5: CAD of Cranks from WPI ME MQP Team

Figures 4-4 and 4-5 have mechanical systems for converting mechanical power in the fin to rotating shaft power. In each design, cranks above the box frame connect to masts on the fin (fin not shown). The masts oscillate and move the cranks, which then move the cams (Figure 4-4) or move the cranks (Figure 4-5), rotating the shaft. The nacelle and energy conversion system created by this project team was designed to be bolted to one end of the box frame shown in Figures 4-4 and 4-5. The interface required specifications for bolt and shaft placement.

4.5 Electrical Power Generation

4.5.1 Method of Energy Generation

Electricity generation will be accomplished through the use of a DC motor. Brushless DC outrunners were chosen because brushless DC outrunners have a low starting torque. The chosen motor was effective at generating lower levels of power. The three-phase DC output was converted to single-phase DC in order to perform maximum power point tracking. The motor chosen to act as the generator can be seen on the testing rig in Figure 4-6, surrounded by a red square. The motor used to drive the rotating shaft used for testing can be seen inside the blue square. The yellow arrow is pointing to the encoder wheel, used to determine the RPM of the shaft during testing.

The fin and mechanical powertrain produced energy in the form of a shaft rotating at low RPM with high torque. This had to be converted into shaft power that was high RPM and lower corresponding torque, since generators produce higher voltage at higher RPM. The generated voltage had to be high enough to be in the operational range of the MPPT.

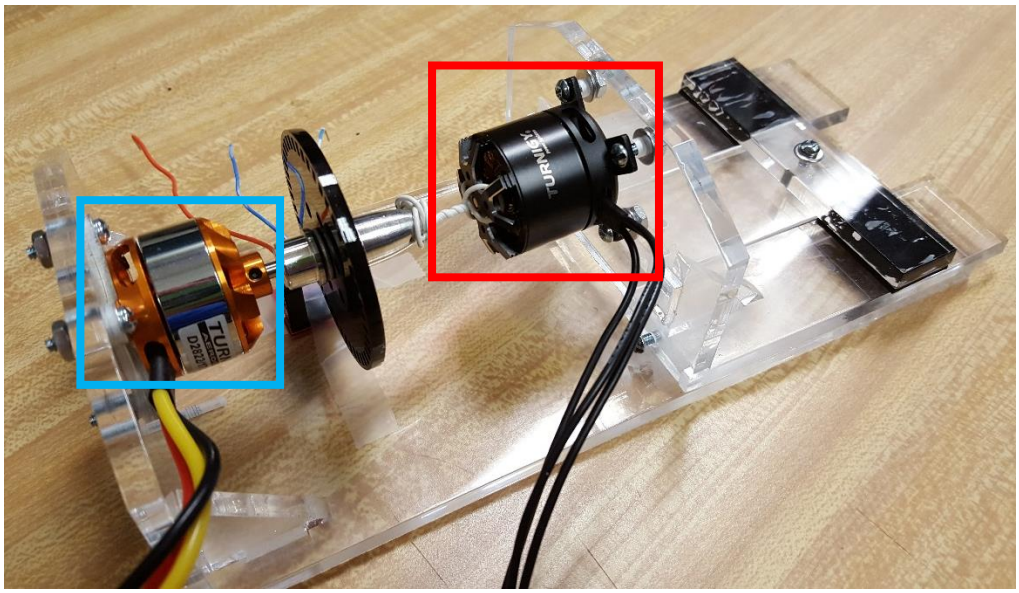

Figure 4-6: The Gimbal Motor in the Test Rig

Figure 4-6 shows the motor test rig. A motor, shown in the blue box, spins a motor under test, shown in the red box. The motor in the red box acts as a generator. The shaft between the motors has an encoder to measure revolutions per minute. The voltage and amperage of the generated electricity is recorded with corresponding RPM values to characterize the performance of the motor as a generator.

Table 4-1: Generator Motors

Generator Motor	Poles Weight	KV (RPM/V) Weight	Internal Resistance (Ohms) Weight	Score
Turnigy HD2212 (King, Turnigy HD2212, n.d.)	12N14P 2	72 5	15.6 2	9
2804-210Kv (King, 2804 - 210Kv, n.d.)	12N14P 2	210 2	10.4 3	7
Multistar 1807 (King, Multistar 1807, n.d.)	12N14P 2	340 1	10 3	6
Quantum 2208 (King, Qantum 2208, n.d.)	14N12P 2	114 3	23 1	6

Brushless three-phase DC outrunners normally sold as motors for gimbals were considered for the generator application. The motors feature three bi-directional outputs, controlled by an internal logic circuit. (Panels, n.d.) The motors in Table 4-1 have lower RPM/V ratings that motors used for thrust applications and are preferable because voltages high enough to be in the input range for the MPPT can be achieved at low RPMs. Additionally, the motors have low starting torque. The Turnigy HD2212 was selected because it had the lowest value for RPM/V.

The energy generation portion of the propagating wave turbine was closely integrated with the sensors and power transmission aspect of this project. Power generation was monitored via sensors at the output of the generator and at the end of the MPPT, enabling an examination of the effectiveness of the MPPT in this system. The power generated by this device was utilized in charging an onboard LiPo battery used to power the microprocessor and transmitted externally to display the power generated.

4.5.2 Optimization of Electricity Generation

Maximum Power Point Tracking allows the generator to operate at peak efficiency over a range of input RPM. An MPPT serves to optimize the match between the power being generated and the battery bank. (Sun, 2016) This technology was necessary because the generator output changed depending on the water flow velocity. To enable the MPPT, a specially integrated circuit (IC) is needed to manage the load

on the generator. When the generator voltage fell, the IC adjusted the IC output current and conversion voltage to operate the motor at the maximum power transfer voltage/current. The visualization of this characteristic curve can be seen in Figure 4-7. Given two input points on an I-V curve, the MPPT chip calculates the resulting power point on the curve.

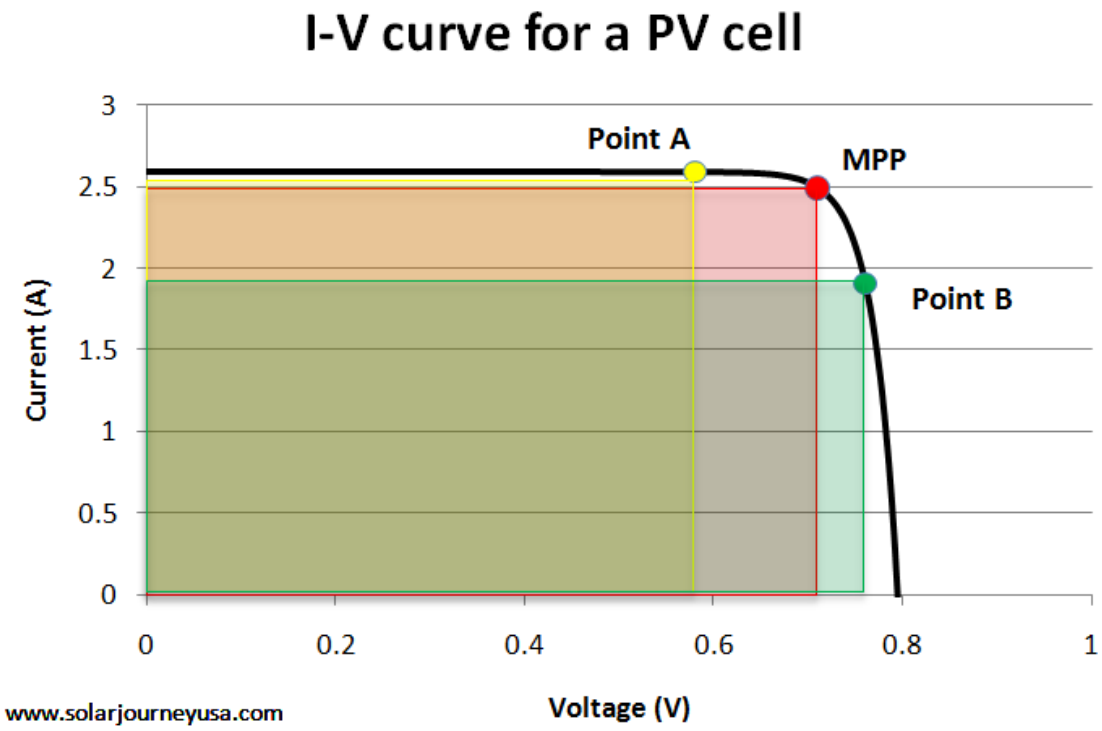

Figure 4-7: The MPPT Point, for two Input I-V Points (Journey, 2015)

Table 4-2: MPPT ICs

MPPT IC	Voltage Range In *Weight*	Voltage Range Out *Weight*	Integrated Battery Charger *Weight*	Score
SPV1020 **STMicroelectronics (STMicroelectronics, SPV1020, 2016)**	**6.5 – 45V** 5	**10 – 45V** 2	**No** 0	7
SPV1040 **STMicroelectronics (STMicroelectronics, SPV1040, 2016)**	**0.3 – 5.5V** 3	**2 – 5.2V** 5	**No** 0	8
LT3652 **Linear Technologies (Linear Technology, n.d.)**	**4.95 – 32V** 5	**3.3 – 14.4V** 5	**Yes** 5	15

The selected MPPT, the LT3652, had an input voltage range of 4.95V to 32V. The expected output of the generator falls within this range. The integrated battery charger meant that an additional battery charging IC was not necessary. The chip was capable of charging a single cell lithium polymer battery.

4.5.3 Energy Storage and Transmission

Energy generated from the propagating wave turbine was stored in the nacelle using a 3.7V LiPo battery. This is a high energy density battery with a voltage lower than the nominal voltage produced by the generator. Chargers for this type of battery are common, and the MPPT chip used has a built-in charger for a 3.7V LiPo battery. This battery was chosen because documentation was plentiful and the battery provided the preferred voltage input to the boost converter. The battery was charged by the generator, using the charge controller built into the MPPT. The energy stored in the battery was then provided to the outside world through a cable. Also, the microcontroller and sensors were powered by the battery and a charge status indicator from the MPPT was displayed outside of the nacelle.

Power transfer is a key component in the development of an energy harvester. Since the maximum load power shall be obtained when the resistance of the load is equal to the internal resistance of the voltage source, efficiency will be optimal when the motor used to generate power has the correct value of internal resistance.

Successful power transmission occurs when the majority of the electricity generated travels from the origin of generation to either an electricity storage facility or, in some large cases, the Grid. The preferred method of power transference is high capacity power lines, able to carry large quantities of electricity long-distance. On a small scale level energy harvester, power transference can occur through large diameter wires or cables. In aquatic cases, wires and the points of attachment must be completely waterproof.

4.5.4 Testing

The electricity generation module served as a testing module for various parts of this project and was tested through mathematical models and data collection. Generation capabilities of motors were tested and the optimal type was chosen, determined through internal resistance, size, and cost. When the project was fully assembled, final testing will occurred in the WPI Sports and Recreation Center swimming pool.

4.6 Microprocessors

The microprocessors needed for the propagating wave turbine had to meet the following criteria:

1. Low cost. The microprocessor needed to be $20.00 or less for budgetary reasons.
2. Low power consumption. The microprocessor, due to the small energy harvester status of the project, needed to use as little energy generated as possible. This means, ideally, that the microprocessor will consume 20mA of current at most when running.
3. Small Size. The size of most launch pads is close to two by four inches, and the propagating wave turbine needed something in the one by two inch range because the team had a two by three space to work with, and needed space for wires to run.
4. Modular components were desirable. While an individual processor chip could be purchased as well as the components needed to construct a microcontroller, it saved construction time to buy a commercially available board (COTS).
5. At least 128kB of Flash memory because the program size was estimated to be roughly fifty kB.
6. At least ten ADC pins, because the sensors used in the project required nine.
7. At least one digital I/O pin because the team had one sensor that required it.
8. 5V compliant because that's what the boost converter would need to output for some of the sensors.

The microprocessor would serve to receive the data collected from all the onboard sensors. A USB would be used to connect the microprocessor to an external laptop, so real-time data streaming of the propagating wave turbine's operation could be monitored.

While many microprocessors fit the above requirements, the deciding factor fell into two categories: Whether or not the board was pre-assembled (COTS), and the overall size of the component itself. The microprocessor chosen for control this project was priced at less than thirty dollars.

Table 4-3: Trade Study for Microprocessors

Microprocessor	Analog Pins *Weight*	Size (mm) *Weight*	Cost *Weight*	Current Consumption *Weight*	Memory *Weight*	COTS? *Weight*	Score
Arduino MEGA 2560 Launchpad (Sparkfun, Arduino Mega 2560, n.d.)	**16** *3*	**100x53** *1*	**$45.95** *1*	**50mA** *1*	**256kB** *5*	**Yes** *5*	*20*
ATmega2560 (Atmel, ATmega2560, n.d.)	**16** *3*	**17x16** *5*	**$16.54** *2*	**50mA** *1*	**256kB** *5*	**No** *1*	*17*
Arduino Uno Launchpad (UNO, n.d.)	**6** *0*	**68x53** *3*	**$24.95** *2*	**50mA** *1*	**32kB** *1*	**Yes** *5*	*12*
ATmega328P (Atmel, ATmega328, n.d.)	**6** *0*	**9x9** *5*	**$1.93** *5*	**50mA** *1*	**32kB** *1*	**No** *1*	*13*
MSP430G2 Launchpad (TI, MSP430, n.d.)	**8** *2*	**68x51** *3*	**$9.99** *4*	**220uA** *5*	**32kB** *1*	**Yes** *5*	*20*
MSP430G2552 (Texas Instruments, 2015)	**8** *2*	**4.8x4.8** *4*	**$2.80** *5*	**220uA** *5*	**32kB** *1*	**No** *1*	*18*
MSP432 Launchpad (TI, MSP432, n.d.)	**24** *2*	**95x57.5** *2*	**$12.99** *4*	**90uA** *5*	**256kB** *5*	**Yes** *5*	*23*
MSP432P401R (Texas Instruments, 2015)	**24** *2*	**15.2x15.2** *4*	**$7.60** *5*	**90uA** *5*	**256kB** *5*	**No** *1*	*22*
Teensy 3.2 Launchpad (Sparkfun, Teensy 3.2, n.d.)	**12** *5*	**35x18** *4*	**$19.95** *3*	**6mA** *4*	**256kB** *5*	**Yes** *5*	*26*
MK20DX256VLH7 (Digi-Key, n.d.)	**12** *5*	**13x13** *5*	**$7.07** *4*	**6mA** *3*	**256kB** *5*	**No** *1*	*23*

Table 4-3 depicts the trade study between ten different microprocessors. Ultimately, the project team decided to choose the Teensy 3.2 microprocessor over the other options because it had the highest score in a trade study. This high score resulted because the Teensy 3.2 boasts a large amount of memory, relatively small current draw, a very small size for a pre-assembled board, and enough analog I/O pins for the necessary sensors. Additionally, the Teensy 3.2 is COTS, so the team does not have to construct the microprocessor circuit for a processor chip. The Teensy 3.2 can be seen in Figure 4-8.

Figure 4-8: The Teensy 3.2 (Sparkfun, Teensy 3.2, n.d.)

4.7 Sensors

The system sensors enable data to be collected concerning the operation of the propagating wave turbine and help during testing to determine system performance and, ultimately, power output. The sensors needed for our system were as follows.

1. Water Temperature: To monitor the external health of the installation site.
2. Voltage Sensor: to calculate power before and after the MPPT along with the current sensor.
3. Current Sensor: to calculate power before and after the MPPT along with the voltage sensor. This sensor must be capable of measuring small measurements such as 10mA.
4. Generator Shaft Rotational Speed: allowed the fin speed to be compared to the optimal energy generated to determine the most efficient working speed.
5. Water Velocity: Velocity of the water, to determine the optimal working conditions.
6. Water Detection: Detect any water inside the nacelle, so the team can ensure the device is watertight.

4.7.1 Temperature

The temperature sensor used for this project was the TMP36, by Analog Devices. (ADI, 2016) This sensor was chosen because it was linear in nature (output test graph results shown in Figure 4-9), small in size,

easily available, and inexpensive. The physical sensor can be seen in Figure 4-10, and was powered by the five volt regulated output by the boost converter. The TMP36 communicated directly with the Teensy 3.2 through an ADC pin to provide a reliable and simple means of measuring temperature.

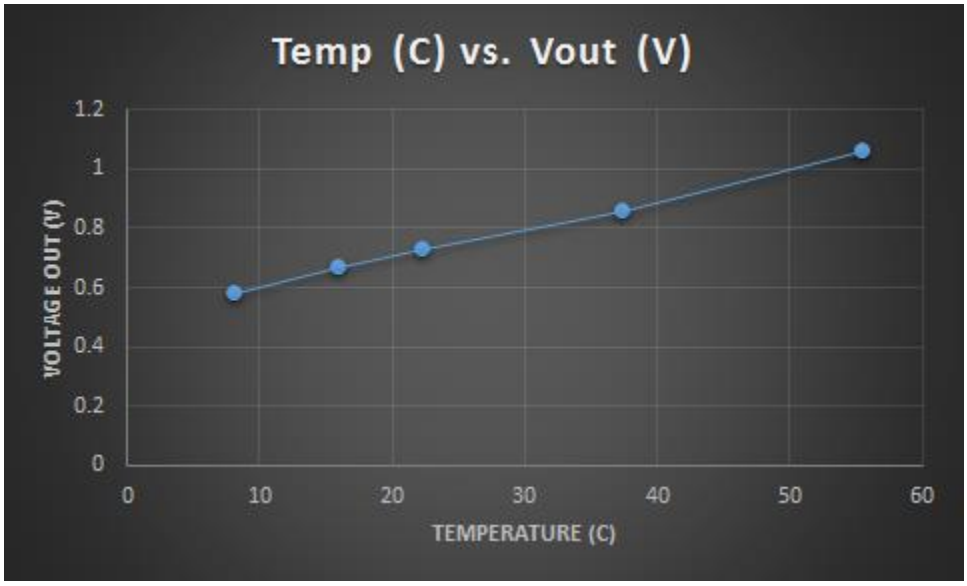

Figure 4-9: The TMP36 Analog Output

Figure 4-10: The TMP36 (ADI, 2016)

4.7.2 Voltage and Current

The voltage of the single-phase DC directly after the generator and three-phase rectifier and the voltage of the battery directly after the MPPT chip were detected. This was used to determine the effectiveness of the MPPT.

The current measurements expected to be measured by this sensor ranged between 10mA and 200mA. This meant that sensors already on the market could not be used, as the sensor was not sensitive enough.

The hall-effect sensor, ideal for this low power application because it required no losses in the system, was not applicable due to its sensitivity of 185mA.

To accurately measure current in this application, a current sensor using a shunt resistor was designed. While this meant the resistor would drop 5mV, it was found to be accurate within 0.5mA. Using Ohm's law, the voltage drop across the known shunt resistor value was used to calculate the current in that section of the circuit. A simple schematic of this circuit can be seen in Figure 4-11.

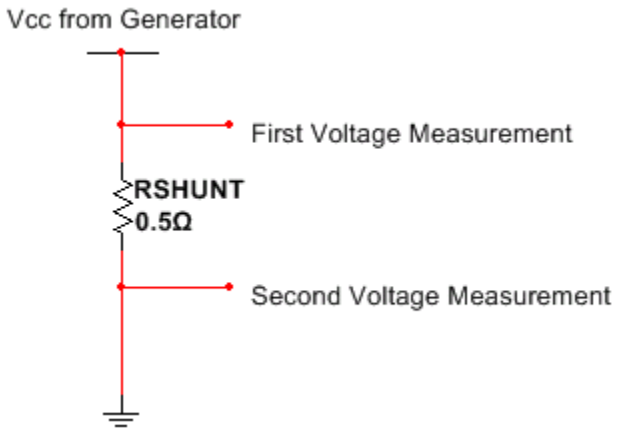

Figure 4-11: Shunt Resistor Current Sensor

4.7.3 Photointerrupter

The project team decided to use a pre-built photo-interrupter to act as the shaft encoder for the generator. The photo-interrupter, seen in Figure 4-12, consists of an LED and a photocell positioned across from one another. The photocell registers when an object passes in between the arms of the sensor, and the data is stored inside the code. A disc was fit onto the generator shaft, which had one hole cut around the perimeter. This meant that the photo-interrupter could register ten LED ticks as one revolution of the generator shaft. This value was compared with the built in timer of the Teensy 3.2, to determine the RPM of the generator. Since the photo-interrupter was set to operate on interrupts in the code, the sensor used the digital I/O pin of the Teensy along with the five volt power from the boost converter.

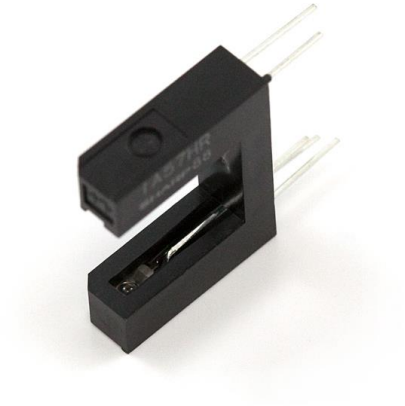

Figure 4-12: The COTS Photo-interrupter (Sparkfun, Photointerrupter, n.d.)

4.7.4 Force Sensors

To determine the velocity of the water flowing by the nacelle in the installation environment, the project team decided to use a force sensor mounted parallel to the water flow. When the water hit the flat surface of the sensor head, seen in Figure 4-13, the sensor registered a force pressing against it. As the velocity of the water increased, the pressure the sensor read would increase accordingly. The sensor was calibrated in the pool, using the known speed of the winch against the collected pressure readings.

Figure 4-13: The Force Sensitive Resistor (Sparkfun, FSR 0.5", n.d.)

Since the force sensor is effectively a variable resistor (Figure 4-14 below), we decided to use an impedance buffer circuit to measure the sensor output. This circuit was chosen because no matter output voltage of the sensor, the force sensitive resistor would not experience interference from other circuitry. The suggested circuit from SparkFun was used, as the behavior was sensitive and largely linear within the expected range. To determine the output voltage range of the sensor for the expected pressure range, the sensor was tested by placing it into a plastic bag and held under running water from a tap. Under low

velocity water flow, the voltage output of the circuit correlated to roughly seventy grams of pressure. Under high velocity water flow, the voltage output correlated to a pressure of roughly one hundred and seventy grams. An impedance buffer circuit was used because the expected usage range of the sensor was determined to be less than two hundred grams and this range was linear in nature and held a steep slope. The behavior of the sensor output can be seen in Figure 4-15, with the impedance amplifier plot in yellow. The log amplifier, while the behavior is closer to linear in nature than the impedance amplifier, did not yield a sensitive range under two hundred grams.

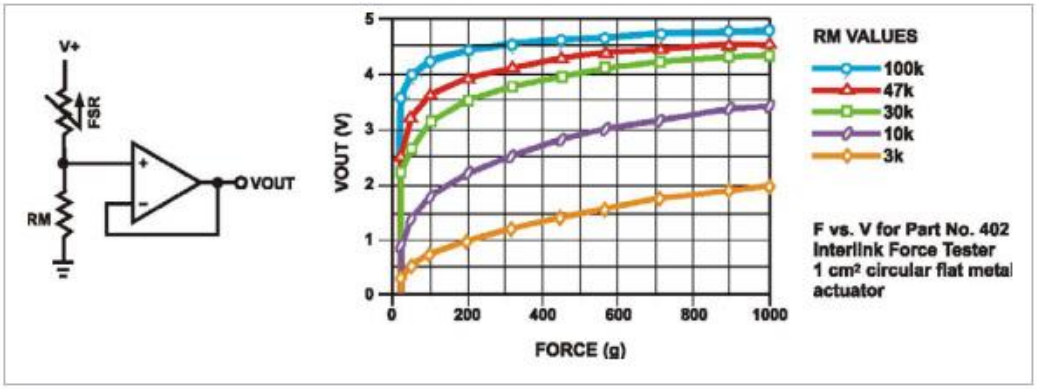

Figure 4-14: The Impedance Buffer Circuit (FSR, n.d.)

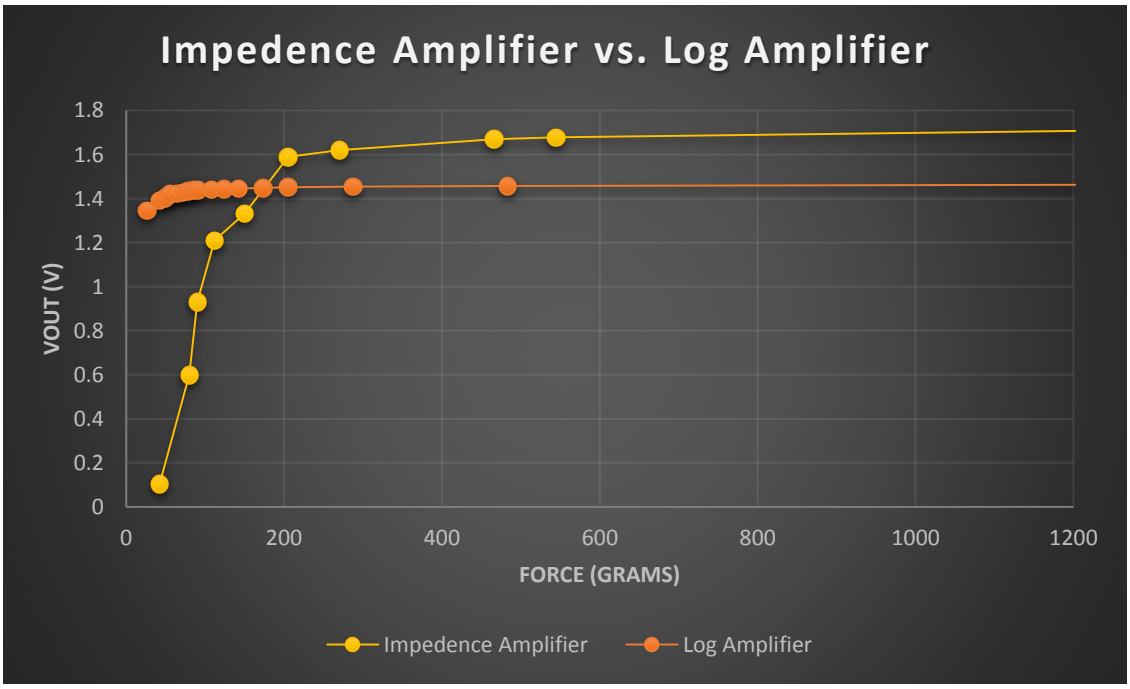

Figure 4-15: Comparison of Circuit Types

4.7.5 Water Detection

To detect water inside the device, a voltage divider circuit using two probes was used. The two probes, under water-free operating conditions, would effectively measure a resistance of infinite ohms between them. If there was any water inside the nacelle or electronics module that could pool at the bottom, the water would bridge the two probes and current would flow throughout the circuit. An ADC input pin on the Teensy is used to receive the signal from this circuit. If a voltage of effectively zero volts is measured, the code calculates that there has not been water detected inside the compartment. If the ADC is receiving a value close to 3.3V, the code calculates that there is a leak. The diagram of this simple circuit can be seen in Figure 4-16. For readily available liquids such as tap water, the current at the ADC measurement point was calculated to be approximately 3.3mA. Other liquids, such as deionized water, were not tested as the project team did not expect the propagating wave turbine to be operating under such conditions. Chlorine enhanced the conductivity of the water, (Stewart, 2012) so the water detection sensor was found to be effective in pool conditions.

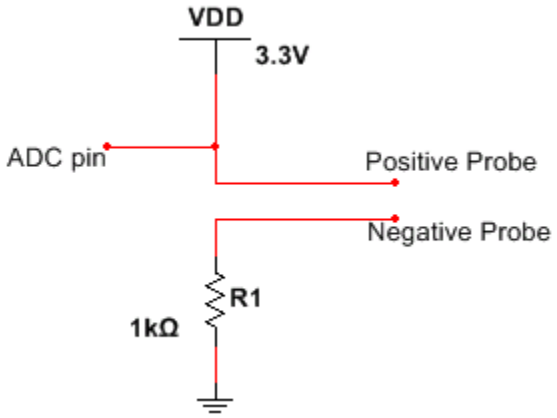

Figure 4-16: The Water Detection Circuit

4.7.6 Sensor Testing

After circuits for the sensors were designed, and calibrated, code written to comply with the values received (The code can be seen in Appendix A). Tests on land concluded of the sensors operate as expected with the system completely built, and in-water testing ensured the device could supply the correct data, as discussed in the following chapter. The majority of testing for the sensors occurred in a lab environment where conditions in an installation environment could be replicated.

4.8 Nacelle

4.8.1 Constraints

The nacelle was a housing for the generator, electronics module, and sensors. The nacelle was attached to one end of the frame holding the fin and mechanical powertrain. The nacelle was a rounded shape converging in a tip similar to that of a zeppelin. The primary purpose was to protect modules, such as sensitive electronics, from water contact. The CAD model of the nacelle can be seen in Figure 4-17. Constraints for the nacelle are listed below:

1. The nacelle must contain all the electronics.
2. The nacelle must interface with the frame and mechanical powertrain designed by the ME team.
3. The nacelle must be internally waterproof.
4. The nacelle must be able to aid the propagating wave turbine in achieving neutral buoyancy.

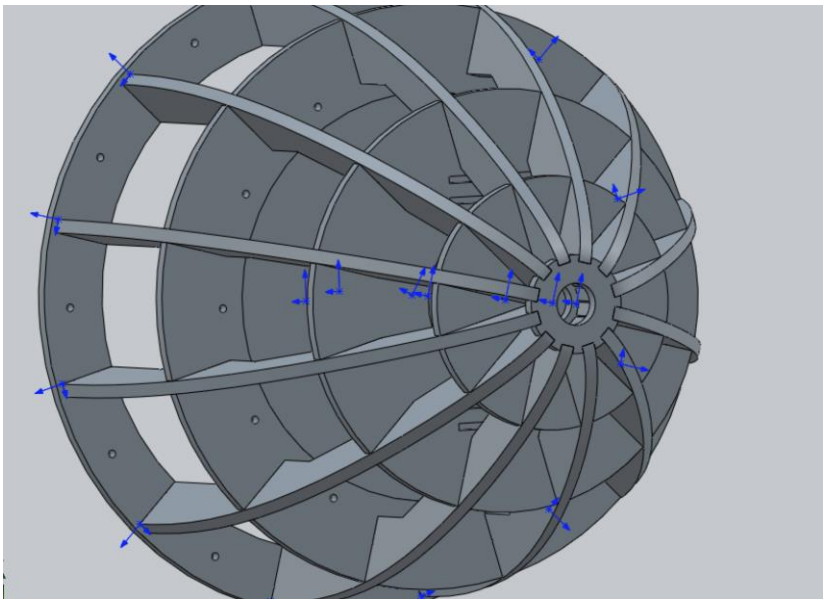

Figure 4-17: CAD Model of the Nacelle

4.8.2 Frame Design

The nacelle frame was designed with interlocking pieces of flat material. This enabled the manufacture of the nacelle with a laser cutter. The design provided rigid support for attaching the generator, electronics module, and sensors to the main propagating wave turbine frame. Rigidity was critical, as any flex in the frame could break a waterproof seal.

The nacelle frame was constructed from clear acrylic, because acrylic sheets were inexpensive, durable, and able to be laser cut. The acrylic sheets measured 0.236” thick, enabling the frame to be strong yet lightweight. Wood was not chosen because thin wood sheets were prone to warping when exposed to humid environments, making this material less than ideal for a water energy harvester.

4.8.2 Shell Construction

Another aspect of the nacelle design was the outer shell. The purpose of the shell was to provide protection to the components inside the nacelle, as well as enable water to move around it cleanly with minimal turbulence. The shell needed to be able to seal against water, weight between one and five pounds, be durable, simple to work with by hand, and cost under $30.00.

Several materials were considered to form the nacelle shell:

1. ThermoMorph, a malleable plastic that, when heated, becomes pliable and hardens as it cools.
2. ABS plastic, a hard plastic sheet that can become slightly moldable when heated uniformly.
3. Fiberglass fabric with a resin, which is extremely moldable and durable, and used in boat hull construction.
4. Fosshape, a plastic felt-like material that shrunk when heated.

To determine which material was best suited to the nacelle shell, a trade study was conducted, which can be seen in Table 4-4. Higher scores indicate preferred options.

Table 4-4: The Trade Study of Nacelle Shell Materials

Material	Ability to Seal *Weight*	Weight *Weight*	Durability *Weight*	Price *Weight*	Ease of Use *Weight*	Score
ThermoMorph	4	3	3	5	1	16
ABS Plastic	2	2	2	3	1	10
Fiberglass	5	2	5	3	2	17
Fosshape	1	5	1	5	2	14

Fiberglass fabric with a resin was chosen as the material of choice. This is because it was simple to work with, the team had prior experience, it was very durable, and was able to seal against water well. Since fiberglass is used professionally by boat manufactures, it led to a professional, streamlined appearance.

A device installed in the ocean would use a costly metal shell for a nacelle. This is out of the scope and budget for this project, and use of weaker materials would lead to lower durability. However, the nacelle for this prototype should still serve its purpose and keep components dry and protected. This module must be checked for leaks.

The nacelle, generator module, and electronics module were sealed at the seams with caulk. The generator shaft had to have a waterproof bearing to keep water away from the encoder and generator. The electronics module was contained in a pre-made, waterproof Pelican case (Amazon, 2016), as seen in Figure 4-18. As a result, the case only needed waterproofing around the through-hole where wires were run. This was accomplished by sealing the hole with silicone caulking.

Figure 4-18: The Waterproof Pelican Case (Amazon, 2016)

The generator module was constructed out of multiple materials, with two holes in the housing. The first, containing a waterproof bearing, allowed the mechanical powertrain's shaft to enter the generator module. The second hole served to let wires pass from the generator module to the electronics module. This hole was sealed with silicone caulking. The CAD model of the generator module can be seen in Figure 4-19. The shaft to the left of the module represents the shaft from the mechanical powertrain.

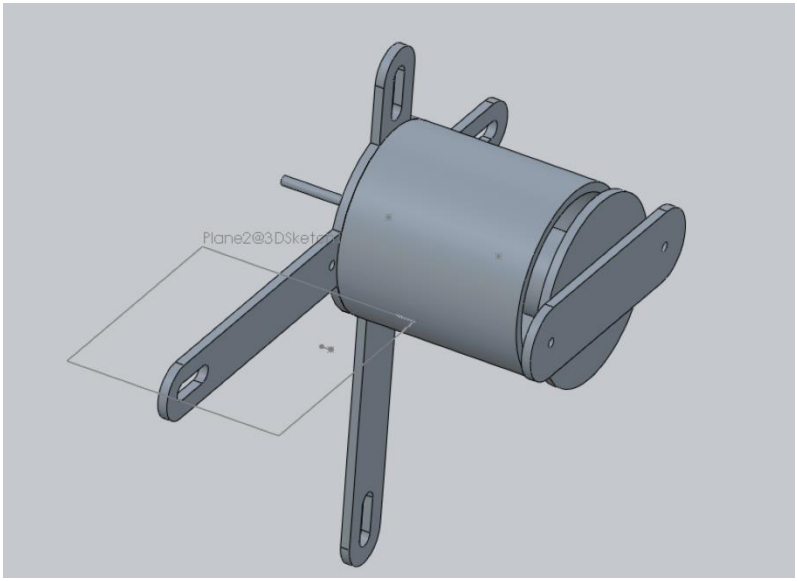

Figure 4-19: The Generator Module

4.8.3 Collaborating on the Nacelle

The most complex task in module integration between the two project teams was the interface where the fin and the powertrain connect. This interface was situated on the front end of the device, so as to not interfere with the motion and operation of the mechanical powertrain or fin movement. The project team focused on the construction of the nacelle near the end of development when the ME project team had completed their mechanical design.

4.8.4 Testing

Complete testing of the nacelle demonstrates capability of the design to generate power from the propagating wave turbine. This includes proper fin and drivetrain integration, output of electricity relative to input power, a successful mounting solution, operational sensors, and a watertight seal.

4.8.5 Mounting and Installation

The areas in which we can test limit the exploration of mounting. The project team is looking for a proof of concept and will not require installing a prototype in an aquatic environment for long periods. The modules of the project will be tested for validation, not durability.

4.9 Summary

This section discussed the design decisions that took place in order to start the project. A careful analysis of how this project will progress and the reasoning was explained. The purpose of the design methodology has been to allow the reader to understand the methods that have gone into any of the design developments as well as show a comparison of why decisions were made.

5. Detailed Design

5.1 Introduction

This section discusses in detail the decisions that went into circuit designs and mechanical designs, and discusses any equations used to determine parameters and component values necessary for the project. Detailed designs, tools used, and construction issues are discussed.

5.2 Generator

5.2.1 Interfacing with the ME Project Team

The ME project team was responsible for the design of the fin and the mechanical powertrain of this project. The two teams interfaced at the gearing system used to transfer rotation from the mechanical powertrain to the generator shaft. Gearing was required to convert the low RPM, high torque power from the mechanical powertrain into the high RPM, low torque power needed by the generator to produce voltages in the range of the MPPT IC.

5.2.2 Power Electronics Circuitry

Three-phase DC from the generator was converted to DC through a three-phase rectifier (upper left, Figure 5-1). The charge controller in the integrated circuit charged the 3.7V lithium polymer battery. The PCB (Printed Circuit Board) containing the power electronics circuitry is seen in Figure 5-1.

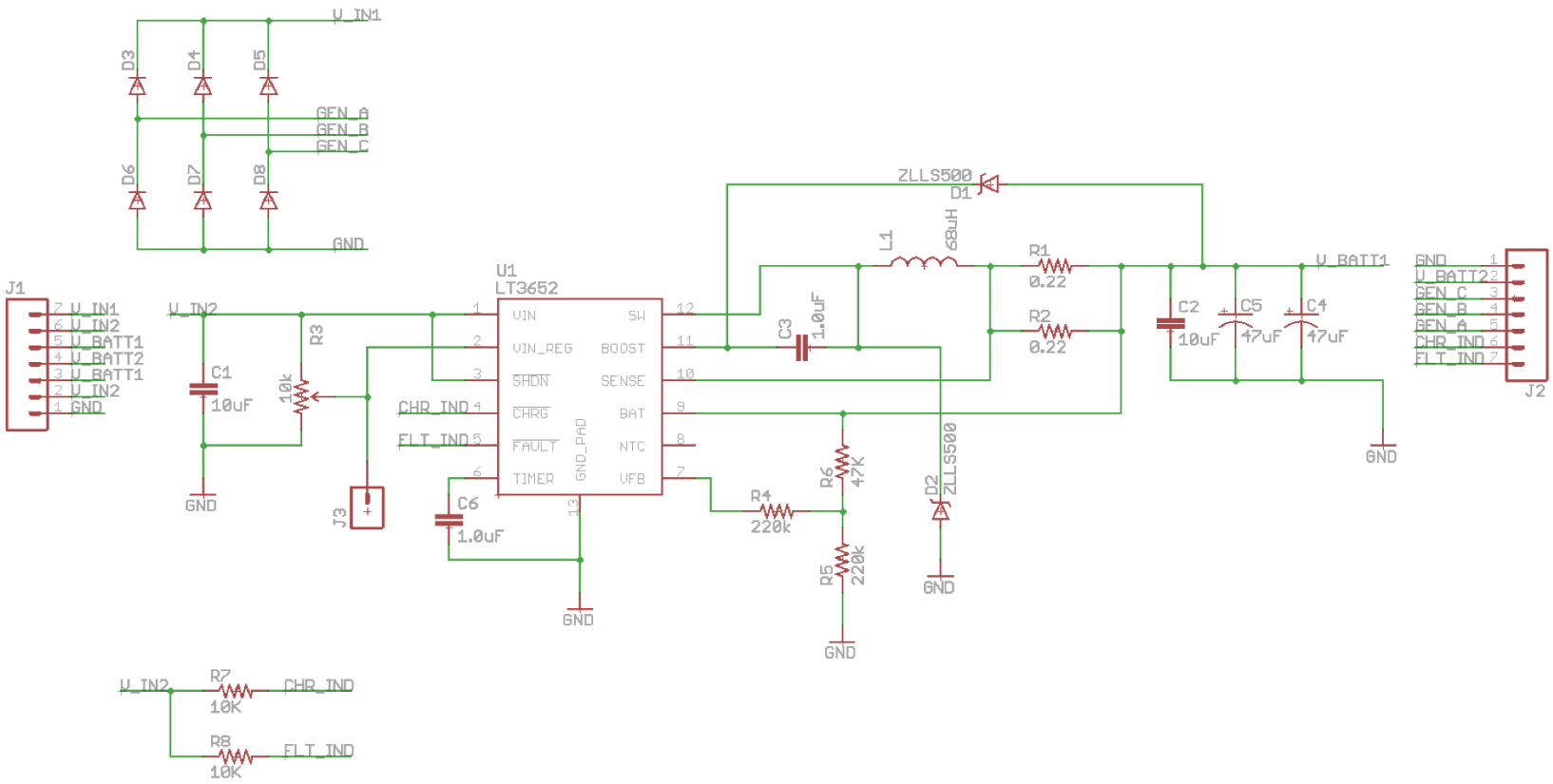

Figure 5-1: The Power PCB Schematic

5.3 Sensors and Data Processing

5.3.1 Temperature

The temperature sensor was one of two sensors that measured environmental conditions outside of the propagating wave turbine. The TMP36 temperature sensor was a simple IC that returned a voltage proportional to the temperature sensed. The schematic for this sensor's circuit can be seen in Figure 5-2.

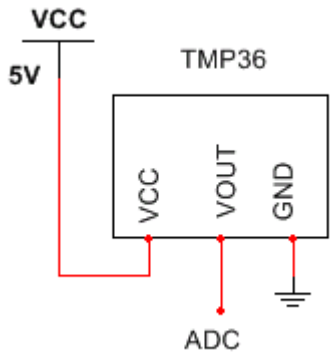

Figure 5-2: The Schematic of the Temperature Sensor

This sensor output was read with the Teensy 3.2's 16-bit ADC. Temperature from this sensor was calculated using Eq. 1. This equation used the ADC value, which ranged between 0 and 1023, and determined the corresponding voltage between 0V and 3.3V. The equation then used the voltage value to calculate the temperature in real-time.

Eq. 1

$$Celsius = \left(\left(\left(\frac{ADCread}{1023}\right) * Vcc\right) - 0.5\right) * 100$$

This sensor did not require calibration. During testing the temperature calculated in Celsius was compared to two other temperature sensors to ensure accuracy. When compared to an infrared (IR) thermometer, it was found that the TMP36 was within 1.2 degrees Celsius of the IR thermometer's value and was considered accurate enough for the conditions of this project.

5.3.2 Voltage and Current

Voltage was measured at two points in the power conversion system: between the three-phase rectifier and the MPPT, and between the MPPT and the battery, such that a comparison could be made as to how efficient the MPPT functioned in the project. Eq. 2 was used to take the ADC value read from the measurement point and map it to a corresponding voltage between 0V and 3.3V. The schematic representation of this sensor can be seen in Figure 5-3. Because this sensor needed to detect voltages between 0V and 8V, it was necessary to step down the voltage from the circuit for the measurement

because the Teensy 3.2's ADC was not capable of measuring over 3.3V. The circuit used to accomplish this, a voltage divider, can be seen in Figure 5-3 below.

Eq. 1

$$Voltage = \left(\frac{3.3V}{1023}\right) * ADCread$$

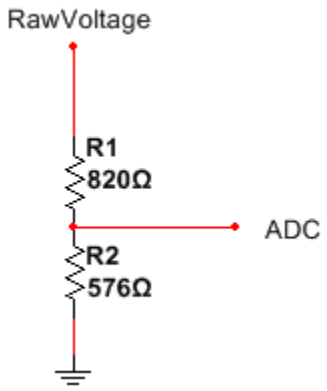

Figure 5-3: Voltage Sensing in the Circuit

Eq. 3 was used to calculate the necessary resistor ratio in the voltage divider. Two circuits were needed because two ranges were expected. The first voltage measurement was of the voltage directly after the three-phase bridge rectifier and before the MPPT. This voltage was expected to reach 15V, so the 3.3V source voltage was mapped to 15V using a multiplier of 0.22. The second point of measurement was the battery charging voltage, which was expected to reach 6V. A range of 8V was set in place using a multiplier of 0.41.

Eq. 2

$$V_{out} = V_{in}\left(\frac{R2}{R2 + R1}\right)$$

The current sensor used was a custom sensor utilizing a shunt resistor. A custom sensor was chosen because it was found through generator testing that the expected current range was 10mA to 300mA. Since sensitivity of the other current sensors tested, such as the hall-effect current sensor, was 185mA/V, this sensor was not found to be accurate enough for the project: a level of accuracy down to 10mA was needed. The custom current sensor was found to be accurate within 2mA of the actual measured current. Using a 0.5 Ohm resistor, the voltage drop was 5mV per sensor. This sensor operated on the principle of Ohm's Law, seen below in Eq. 4. The voltage drop, divided by the known resistance, equates to the current value.

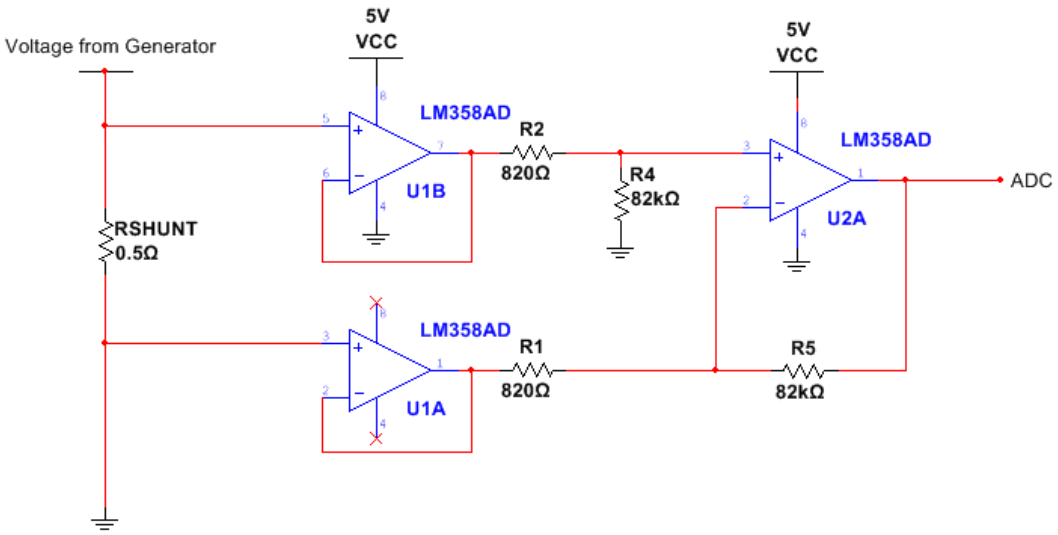

Figure 5-4: Schematic of the COTS Current Sensor (SparkFun, 2016)

A difference amplifier, shown in Figure 5-4, was used to amplify the difference in voltage across the sense resistor and produce a voltage output proportional to current.

To calibrate the sensor, a simple series circuit lighting an LED was setup. The shunt resistor was placed in line with the LED. An ammeter was used to take a current measurement at this point in the circuit, to verity the result and ensure the sensor was operating correctly. It was estimated that the gain needed in the circuit was roughly one hundred. The gain for the difference amplifier was set using an 822 Ohm resistor was R2, and an 81k Ohm resistor as R1 (See Eq. 5). This gave an expected gain of 98. The voltage output of the difference amplifier was lower than expected (See Eq. 7), with an actual gain of 72.6 for the first current sensor (Figure 5-5), and an actual gain of 62.5 for the second sensor (Figure 5-6). This difference is attributed to losses from the components, resistor tolerances, LM358AD tolerances, and manufacturing imperfections. With the differences in gain accounted for in the code, the difference in current measured between the two sensors was 0.16mA.

Eq. 4

$$I = \frac{V}{R}$$

Eq. 5

$$Gain = \left(\frac{R2}{R1}\right)$$

Eq. 6

$$V_{out} = V_{in}$$

Eq. 7

$$V_{out} = (V2 - V1)\left(\frac{R2}{R1}\right)$$

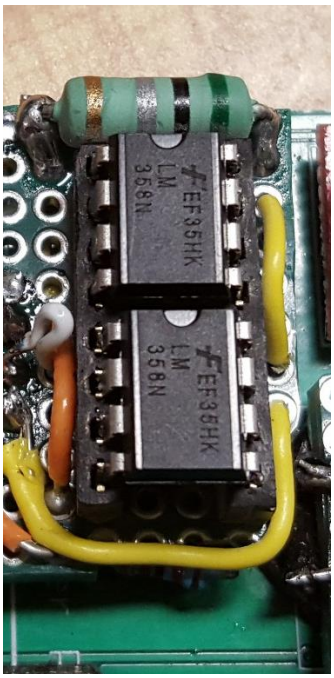

Figure 5-5: Current Sensor #1

Figure 5-6: Current Sensor #2

The completed current sensor perfboards can be seen in Figure 5-5 and Figure 5-6. Figure 5-5 depicts the first current sensor, which detects the current between the three-phase bridge rectifier and the MPPT chip. This sensor utilized sockets for the LM358AD ICs, to allow the chips to be replaced if need be.

Figure 5-6 shows the second current sensor, which was used to detect current directly after the MPPT chip and before the battery. This sensor also utilized sockets for the LM358 ICs. The 0.5 Ohm resistor was mounted on top of the perfboard, to enable the perfboard to be compact and within the perimeter of the perfboard.

5.3.3 Encoder

A COTS photointerrupter was used to detect rotations of the generator shaft. A laser cut disc was mounted on the shaft of the generator, and the disc was situated such that the edge passed between the two arms of the photointerrupter. A visualization of the internal workings of a photointerrupter can be seen in Figure 5-7.

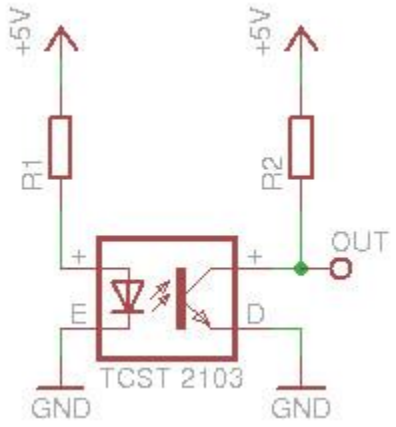

Figure 5-7: Schematic of the Internals of a Photointerrupter (MIT, 2013)

In the code for the project, a timer driven interrupt would trigger every second. Upon triggering, the number of ticks the photocell had detected in that second was passed to a function that calculated the revolutions per second of the generator shaft. This equation (Eq. 6) can be seen below. To transform RPS into RPM, RPS was multiplied by sixty using Eq. 7. Another representation of the schematic can be seen in Figure 5-8.

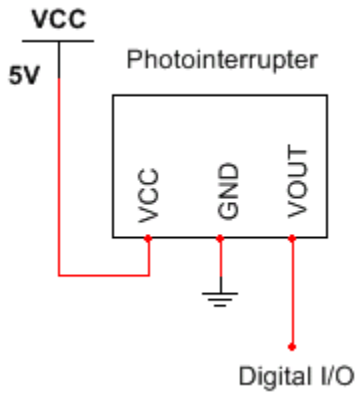

Figure 5-8: Schematic of the Encoder Circuit

Eq. 3

$$RPS = \left(\frac{Pulses}{PulsesPerTurn}\right)$$

Eq. 7

$$RPM = RPS * 60$$

5.3.4 Force

One force sensitive resistor (FSR) was used in this project, although two circuits were implemented in the PCB should the project team decide to utilize two. The schematic for the circuits can be seen in Figure 5-9. The force sensitive resistor was used to detect the pressure of the water as it hit the front of the nacelle. This pressure correlated to the water speed, and a lookup table could be implemented in the code to allow quick results. An LM358AD was selected as the operational amplifier chip because it is readily available and did not need a negative voltage input.

An impedance amplifier circuit was chosen because it prevented the output circuit from placing a load on the circuit attached to the non-inverting input pin. Because this is simply a buffer circuit, there is no gain, which means the input and output voltage relationship can be seen in Eq. 7. The FSR resistors can be seen in the schematic as R3 and R4. The resistors make up one half of a voltage divider, with *Vout* of the voltage divider being the input to the op-amp. A resistance value of fifteen kilo-ohms was chosen for R1 and R2 because this value gave an op-amp output voltage around 60% of 3.3V for two-hundred grams of pressure. This correlation can be seen below in Figure 5-10.

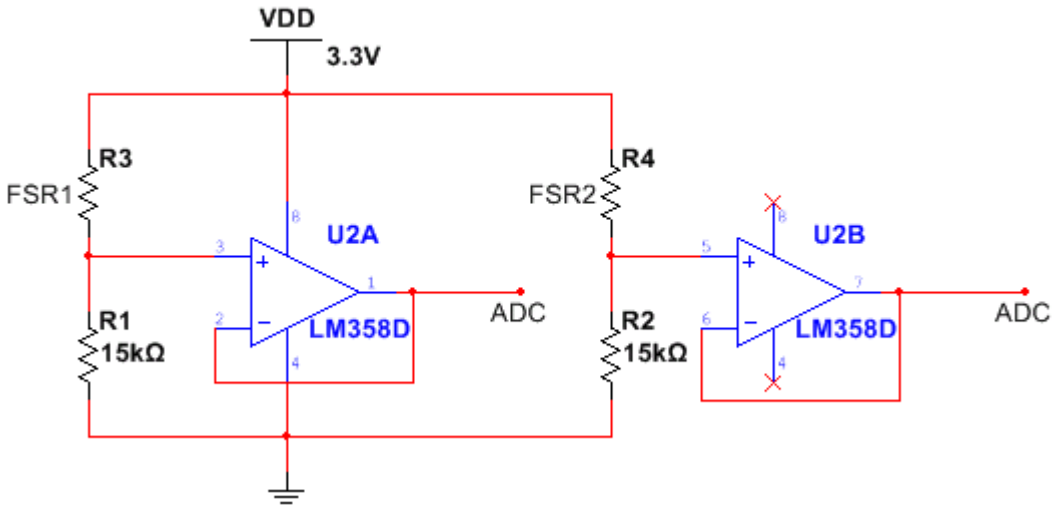

Figure 5-9: Schematic of the FSR Circuit

Eq. 4

$$V_{in} = V_{out}$$

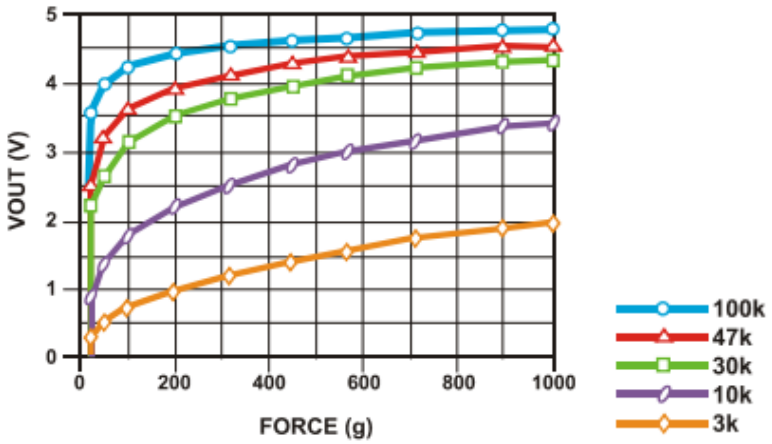

Figure 5-10: The Output Voltage Curve for 5V (FSR, n.d.)

5.3.5 Water Detection

To detect the presence of water inside the nacelle and the electronics module, a simple two-probe circuit setup was used. The schematic can be seen in Figure 5-11. The circuit remains "broken", and cannot pass current, if the probes are not connected – i.e., if no water has been detected between them. If the probes are connected and a voltage value higher than a residual number is detected by the ADC, the code will print a statement informing the user that water is inside one of the chambers of the nacelle. A one kilo-ohm resistor was chosen for R1.

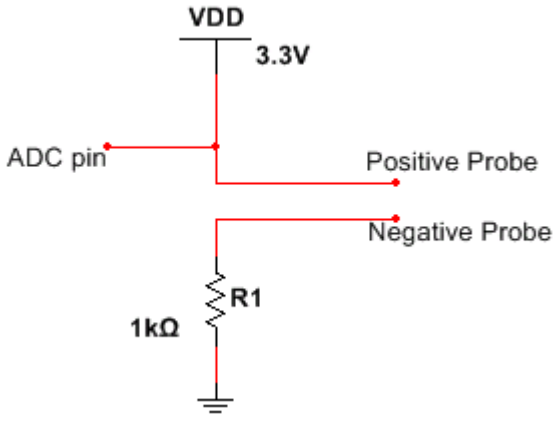

Figure 5-11: The Schematic of the Water Detection Circuit

One of the circuits for detecting water inside the nacelle was situated in the bottom of the shell. This was because if water were present in the chamber, it would pool at the bottom of the nacelle shell. To detect water inside the electronics module, the two probes were fixed to the bottom of the rubber lining of the Pelican case.

5.4 PCB Design

5.4.1 Powering the PCB

The power conversion control and instrumentation system circuits were powered through the use of a single 3.7V LiPo battery. The battery was directly connected to the external power switch, allowing the system to be turned on and off from outside the nacelle. A TPS61200 boost converter was used to raise the voltage of 3.7V up to 5V, in order to power the Teensy 3.2, the encoder, the TMP36, and the two LM358AD current sensors. The boost converter chip purchased was part of a COTS module, thus the team was saved assembly time. The schematic of the COTS board can be seen in Figure 5-12.

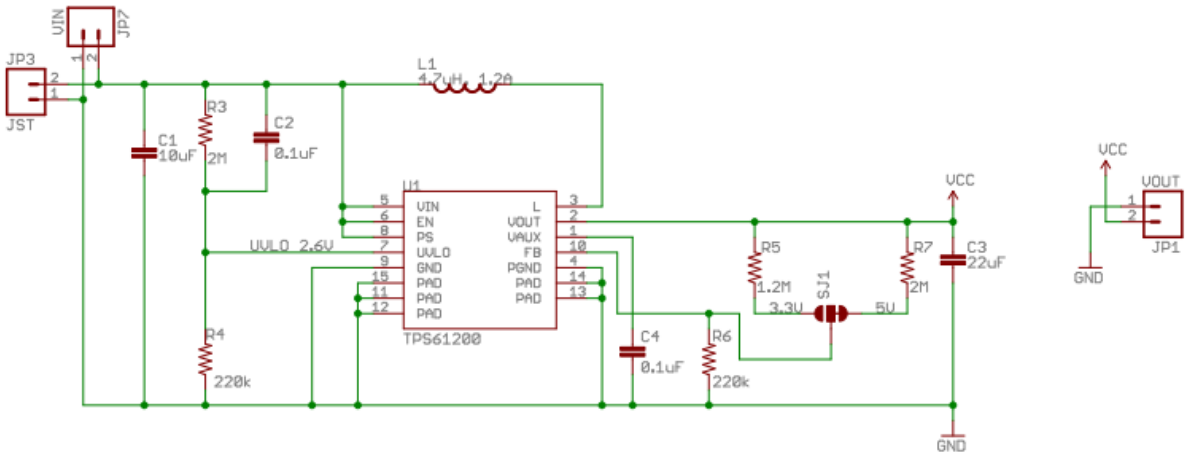

Figure 5-12: The COTS Boost Converter Schematic,

Designed by O. Mazurov and A. Weiss (Mazarov, 2014)

In order to ensure the energy conversion and monitoring system could power itself, the MPPT chip chosen also featured battery charging capabilities. This allowed the MPPT IC to charge the onboard battery when the system was operating. The charge level of the battery was determined by two indicators from the MPPT chip: a charge level indicator and fault indicator, both of which extended outside the nacelle. The charge indicator showed, via an LED, if the battery was being charged, or if the battery already retained a full charge. The fault indicator served to monitor the charging of the battery and indicate if something in the system had gone wrong, such as an unexpected power surge to the battery. Both the fault indicator and the charge indicator were built into the MPPT chip.

5.4.2 Power Electronics PCB

The power PCB contained the three-phase bridge rectifier and the MPPT chip circuitry and was mounted on the sensor PCB. All circuits and signals external to the PCB assembly connected to the sensor and data processing PCB (S&D PCB). Headers were used to connect the generator, battery, charge and fault indicators, and voltage and current sensors to the power PCB. The schematic for this PCB is shown above in Figure 5-1.

5.4.3 Sensor and Data Processing PCB

The S&D PCB, seen in Figure 5-13, was situated in the pelican case, resting on the bottom. This PCB held the battery plug, the Teensy 3.2, two current sensors, the TPS61200 boost converter, the two water detection circuits, and the two FSR circuits using one LM358AD op-amp. The PCB also included two sets of headers, and a large connector for handling all onboard to offboard wires. The two headers, seen in the Figure 5-13 as “From_Power_Header” one and two, are for the second PCB to mount onto. The power PCB, roughly one third the size of the S&D PCB. The project team chose to stack the two PCBs in order to save space inside the Pelican case.

The headers that connected the two boards together handled the three phases of the generator, charging capability for the battery from the charge controller, the charge and fault indicators, and the two voltage measurement sensors. Additionally, the two current sensors required the circuit to be broken at two points for measuring purposes, so the traces routed down through the headers to the S&D PCB and across the two shunt resistors.

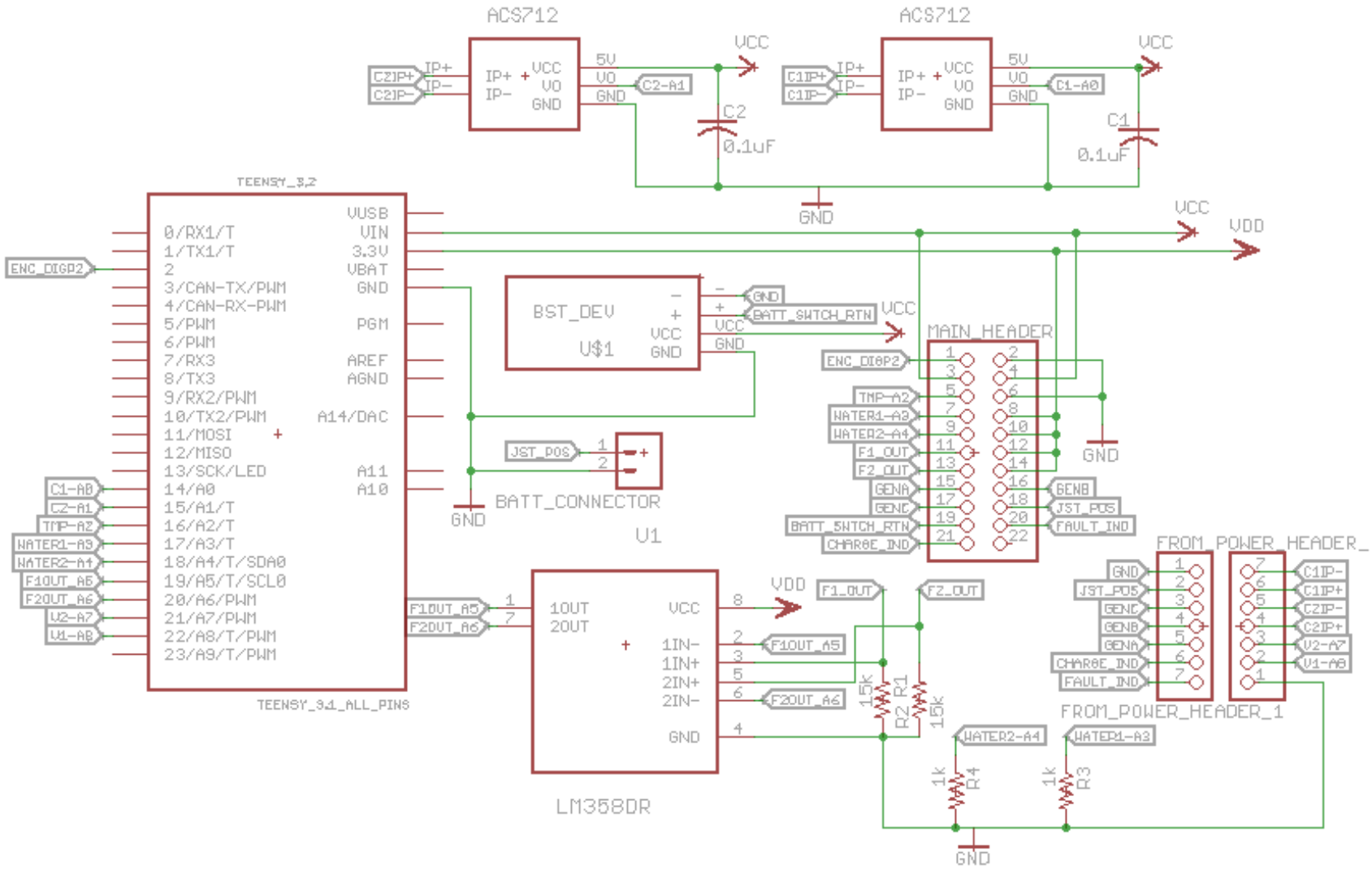

Figure 5-13: Schematic of the Sensor PCB

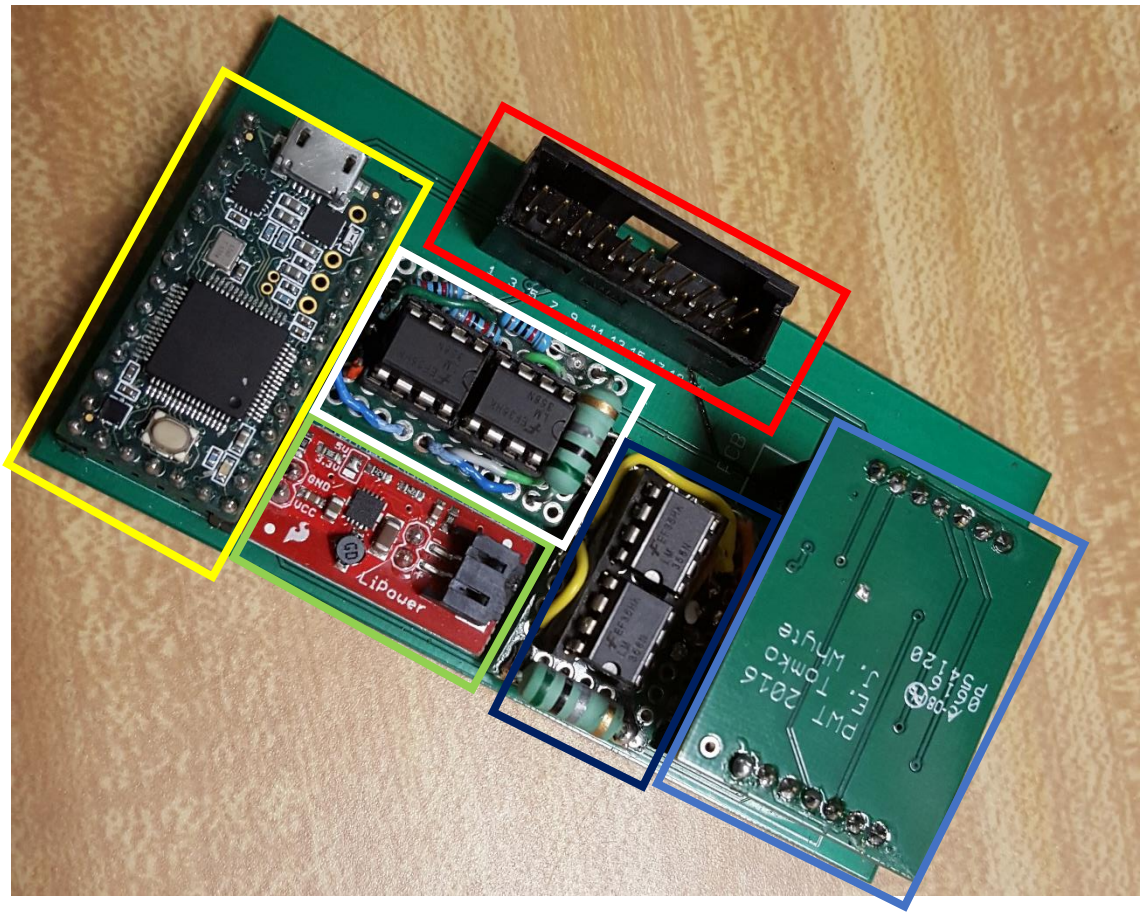

Figure 5-14: The Complete Sensor and Data Processing PCB

The completed S&D PCB can be seen above in Figure 5-14. This PCB mounted inside the Pelican case. On this PCB was mounted the Teensy 3.2 (yellow box), the boost converter (green box), the first current sensor (dark blue box), and the second current sensor (white box). Additionally, the force detection circuits and water detection circuits also had components mounted underneath the Teensy 3.2. The circuit board connector, seen inside the red box, handled all the onboard and offboard wires through the Pelican case, except for the USB connection to the Teensy 3.2. The Power PCB mounted on the two rows of headers seen above and below the current sensor inside the dark blue box. An outline of the Power PCB's footprint can be seen as silkscreen on the S&D PCB board. Additionally, the white battery connector can be seen to the far right of the PCB. The power PCB can also be seen in Figure 5-15. Figure 5-16 displays what's underneath the power PCB. The two voltage dividers can be seen in the yellow square.

Figure 5-15: The Power PCB Mounted – Component View

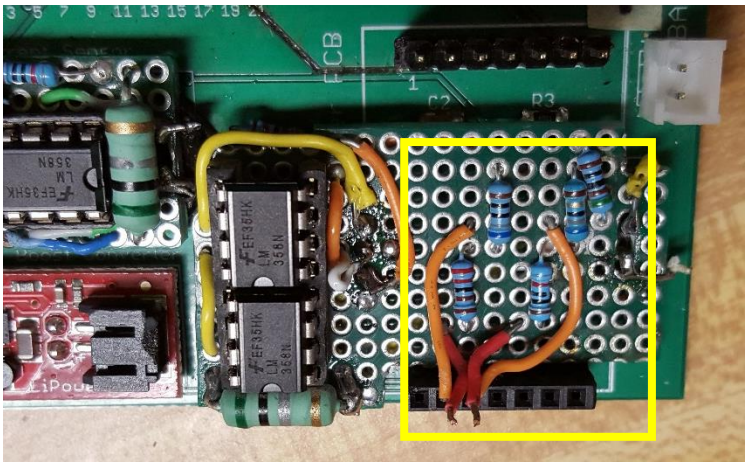

Figure 5-16: The Voltage Dividers

The S&D PCB was mounted inside the electronics module: the Pelican case discussed in Chapter 4. The power PCB was mounted on top, and the battery sat alongside the two PCBs. The enclosed Pelican case, strapped into the nacelle frame using a Velcro strap, can be seen in Figure 5-17.

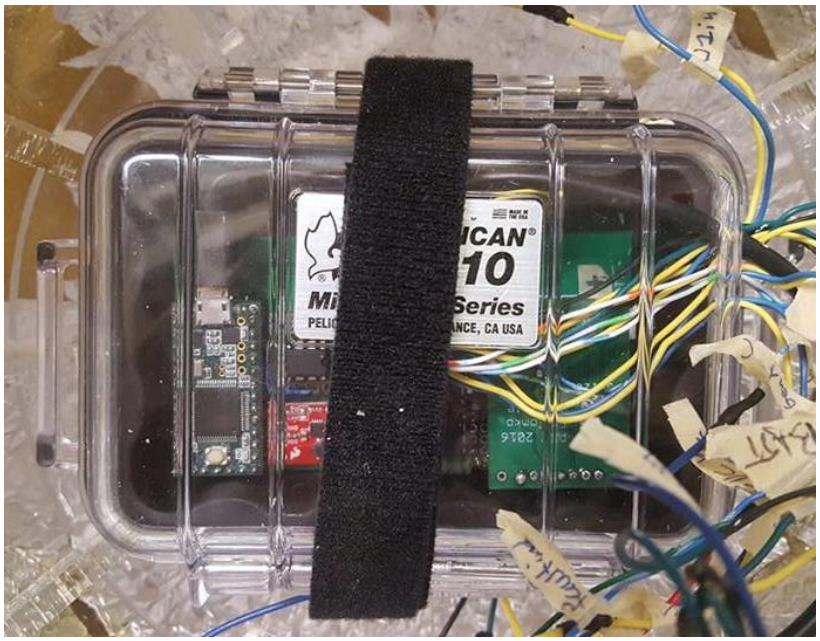

Figure 5-17: The Enclosed Electronics Module

5.5 Nacelle

5.5.1 Frame Construction

The nacelle frame served to provide a sturdy structure for the outer shell as well as ensure the protection of the components and generator inside. The nacelle frame was constructed from laser cut acrylic sheets. The circular spans, seen in Figure 5-18, were vertical when the nacelle was assembled. The ribs, also seen in Figure 5-18, were laid in place around the circular spans. When the pieces were glued together, the resulting structure was string and rigid, creating a frame that could protect parts inside. The circular parts of the frame served to provide structure to the ribs, and served as walls between separate sections of the nacelle.

The largest frame ring measured 11.5” in diameter, and from tip to tail the nacelle measured 10.236”. The constructed nacelle frame can be seen below in Figure 5-19.

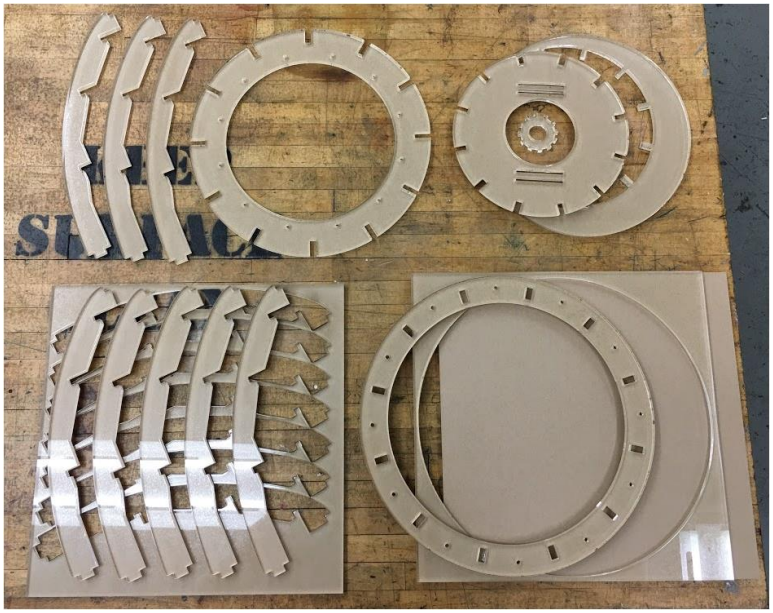

Figure 5-18: Laser Cut Nacelle Frame Pieces

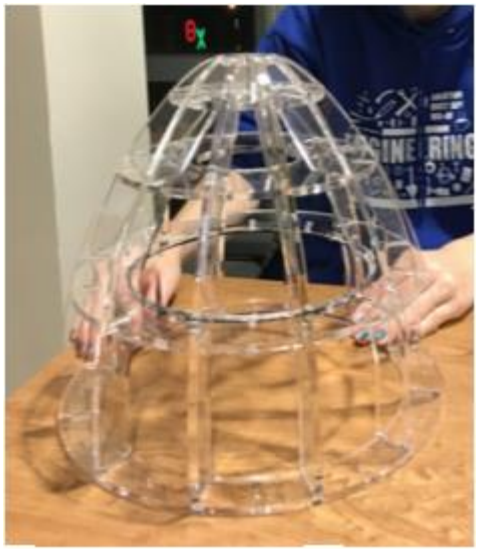

Figure 5-19: The Assembled Nacelle Frame

5.5.2 Mechanical Modeling of Nacelle Design

The nacelle frame was designed to have a waterproof compartment where the Pelican case containing the PCBs would be located. This space can be seen represented in Figure 5-20, between the blue and pink arrows. To hold the Pelican case in place, two sets of horizontal slits were added to the design, where Velcro straps could be threaded. The straps would serve to ensure the Pelican case did not move

from its mounted position. The horizontal slits can be seen in the CAD model in Figure 5-22. A CAD model of the nacelle frame, when covered with fiberglass, can be seen in Figure 5-23.

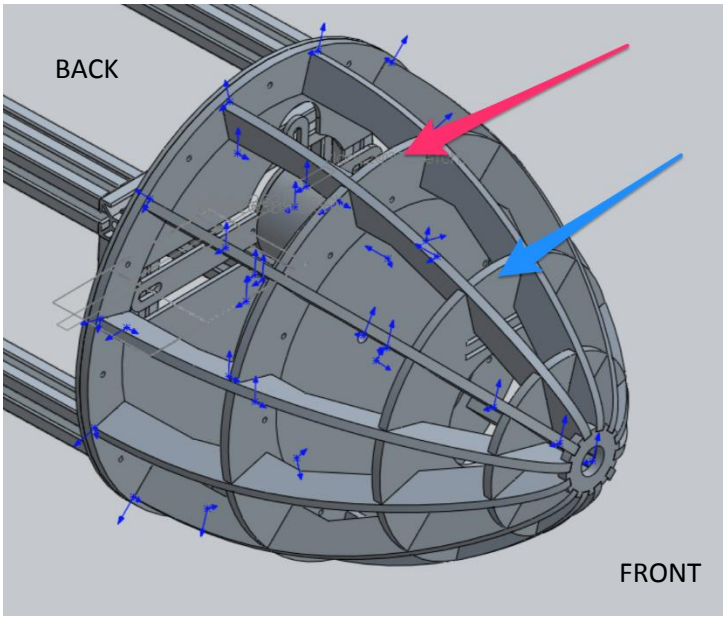

Figure 5-20: The Nacelle Design

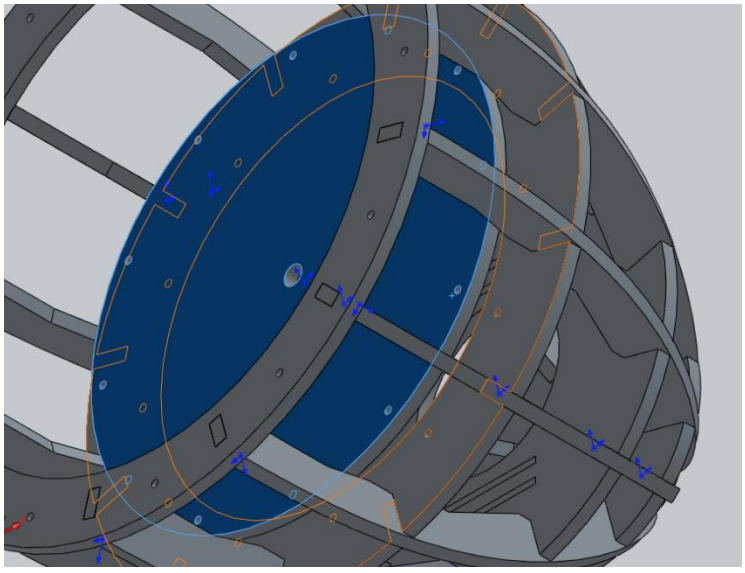

Figure 5-21: The Panel Providing Extra Sealing to the Electronics Module Chamber

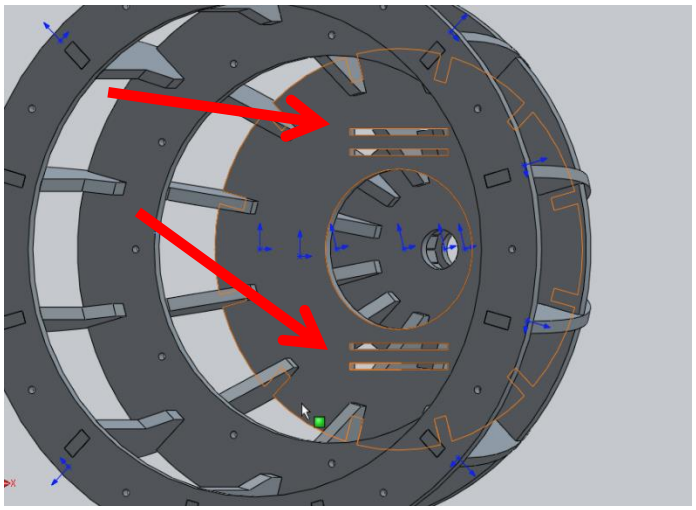

Figure 5-22: The Mounting Holes for the Pelican Case

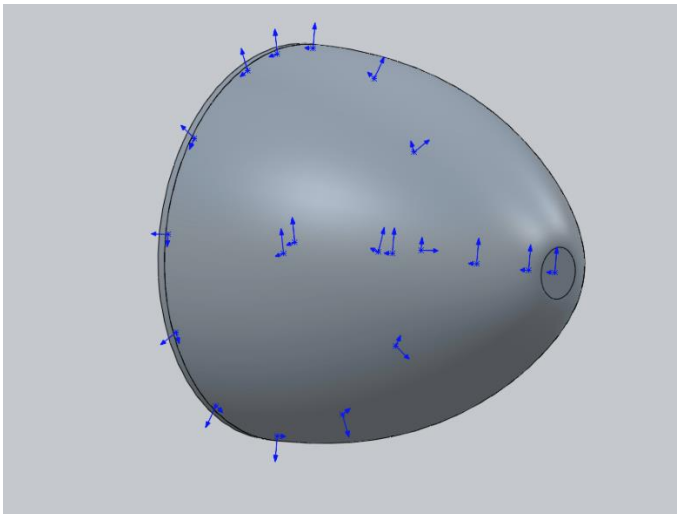

Figure 5-23: Nacelle Frame with Cover

There were two waterproof modules inside the nacelle. The first, containing the Pelican case, was situated in the midsection of the nacelle and held in place with Velcro straps. The second, housing the generator and photointerrupter, was situated at the back of the nacelle, where the metal frame attached to the nacelle frame. The generator module was constructed from multiple materials, with two holes in the housing. One hole allowed a waterproof bearing to be fixed in place, through which the mechanical powertrain's shaft would travel. This allowed the gears to be kept in a waterproof compartment. The second hole was for wires, enabling the generated energy to pass from the generator module to the electronics module. This hole was sealed with silicone caulking to ensure no water could leak through.

Because the ME project team was creating a system in which a crankshaft and camshaft could be switched out for one another, the project team decided it was necessary to allow for slight variations in the

mechanical powertrain's shaft positioning. To accomplish this, the generator module was able to mount separately from the nacelle. In Figure 5-29, the small circular generator module can be seen, mounted on a "cross" shape of acrylic. The four legs of this cross have oblong slots cut in the ends, allowing the module to be moved up to ¼" in two dimensions perpendicular to the powertrain shaft when being mounted.

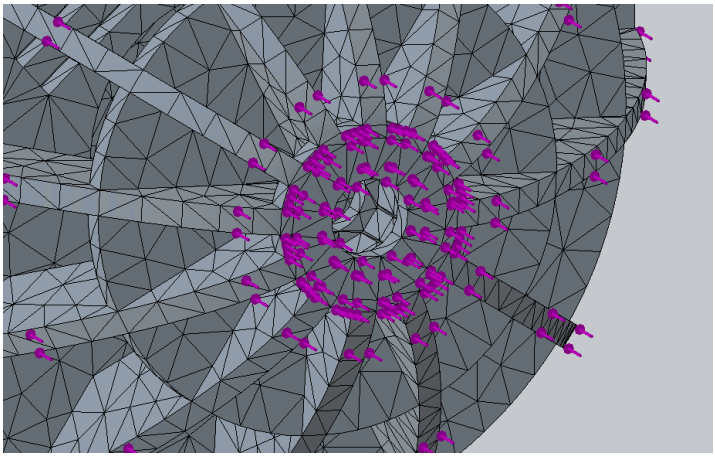

Figure 5-24: Mesh and Force on the Frame

A finite element analysis was performed on the frame to assess the frame's performance under mechanical load. A digital mesh was wrapped over the frame elements, and the frame was subjected to a simulated force.

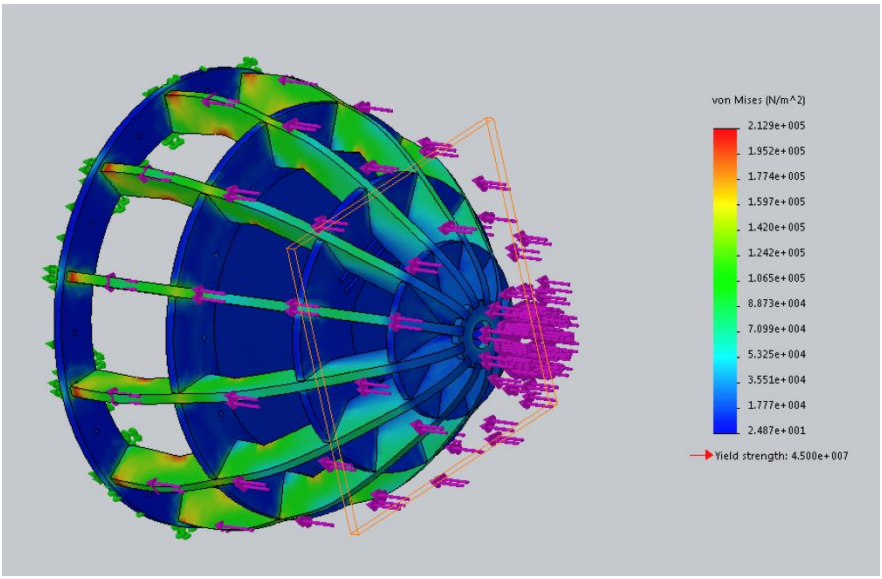

Figure 5-25: Simulation of Stress on Frame with 268.4N Force

The first simulation was of a 268.4N force (See Figure 5-25) over the frontal area of the frame. Stresses are represented by a color gradient. This force corresponds to water flowing at 2m/s past the nacelle. Careful examination of the figure shows bending of the frame ribs. The ribs would not actually deform in this way; it is an exaggerated demonstration by the simulation software to show the areas of deformation.

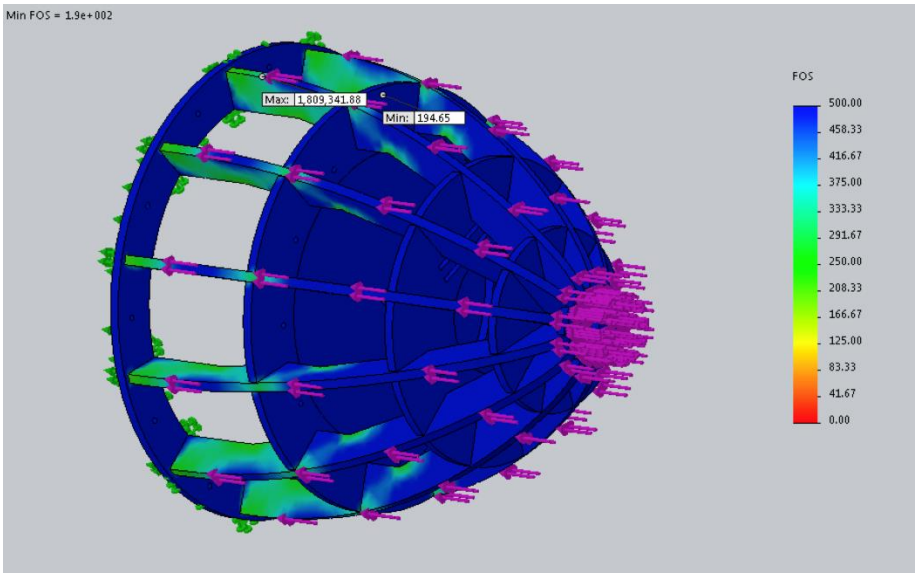

Figure 5-26: Simulation of Safety Factor of Frame with 268.4N Force

To explain the effect of the forces on the frame, a simulation was run to calculate safety factors. The lowest safety factor is 194.65, indicating that the acrylic material is sufficient for this application. The simulation of the safety factor can be seen in Figure 5-26.

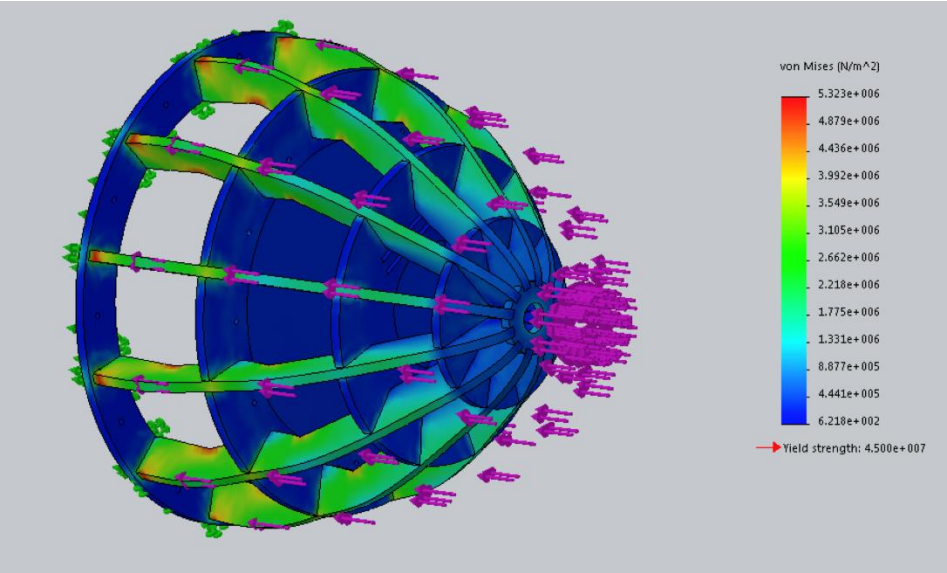

Figure 5-27: Simulation of Stress on Frame with 6710N Force

The stress simulation shown in Figure 5-25 corresponds to a water flow speed of 2m/s. This was at the high end of the flow speed necessary for device performance, but it there was a chance the device could be subjected to higher flow speeds. Another stress simulation was run, this time for a force of 6710N, corresponding to a water flow speed of 10m/s. This is shown in Figure 5-27.

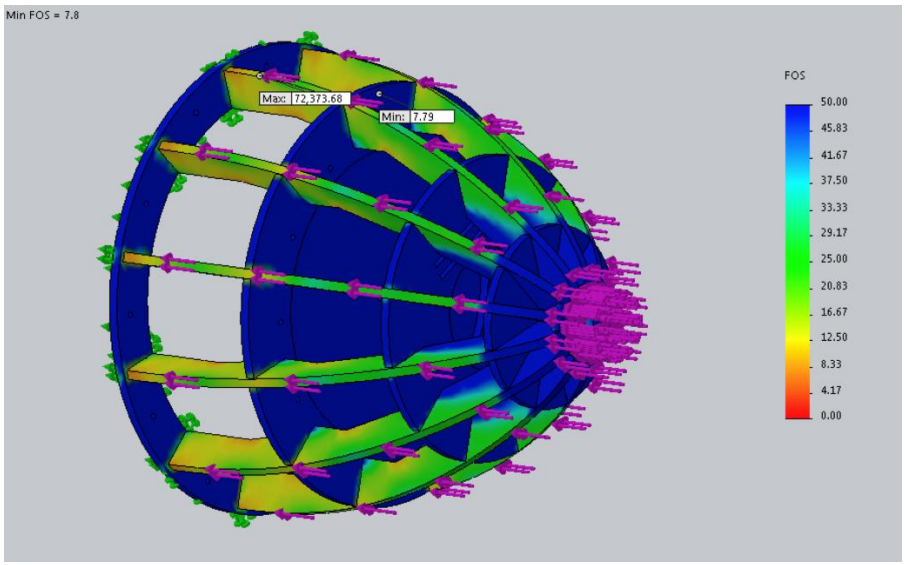

Figure 5-28: Simulation of Safety Factor of Frame with 6710N Force

A new safety factor gradient, shown in Figure 5-28, was calculated for the force of 6710N. The new minimum safety factor is 7.79. A safety factor of 7.79 indicates that the frame is capable of surviving water flow speeds much higher than would be seen in a test.

5.5.3 Generator Construction

The CAD model of the generator was updated to reflect the physical components used in the generator assembly.

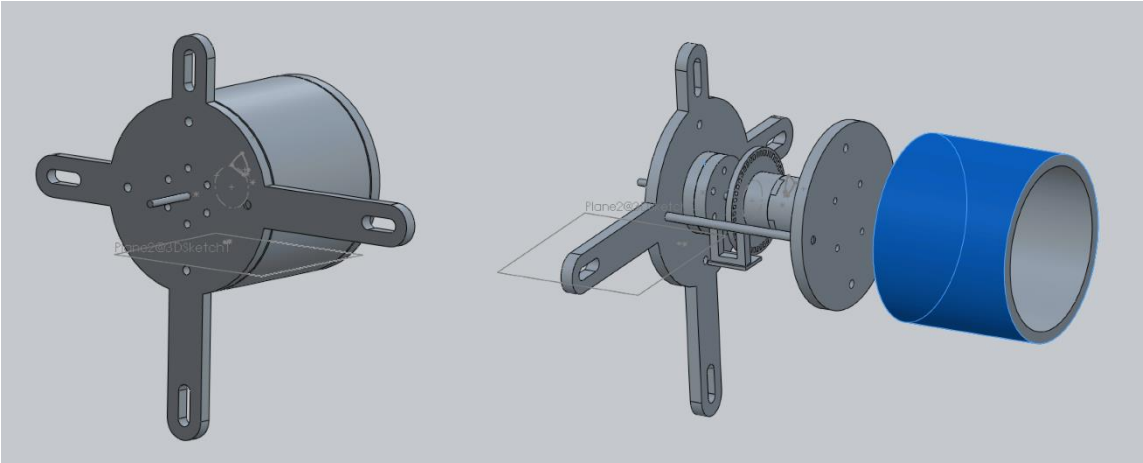

Figure 5-29: The Generator Module

Figure 5-29 shows the model of the generator as assembled, with the cover on and the cover removed. The shaft passes through a waterproof bearing and encoder wheel, and then connects to the electromechanical generator.

The assembled generator module can be seen in Figure 5-30. The encoder wheel (See the yellow arrow) can be seen inside the module. The gimbal motor, acting as the generator for the power generation system, is mounted on the clear acrylic plate on the near side of the module (See the blue arrow). Figure 5-31 shows the side of the generator module that faces outside of the nacelle: note the shaft extending from the housing (See the red arrow). This shaft must be rotated for the system to generate power.

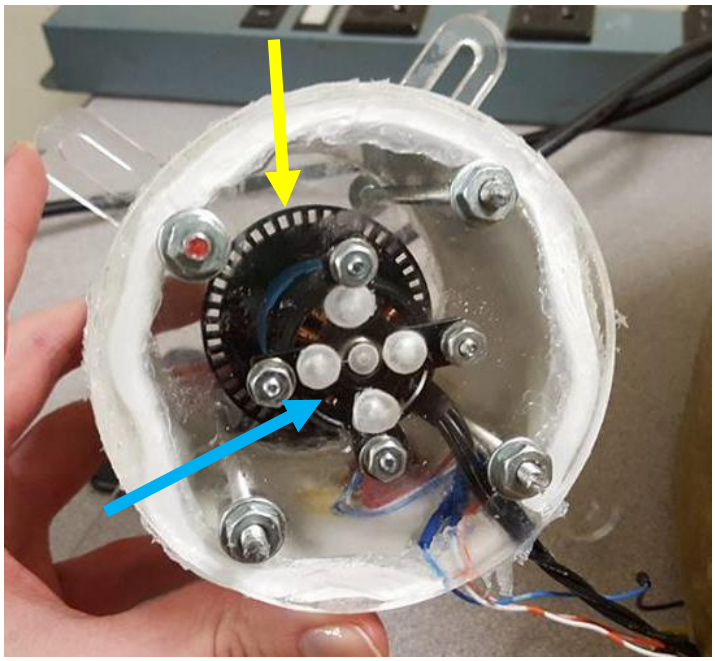

Figure 5-30: The Assembled Generator Module

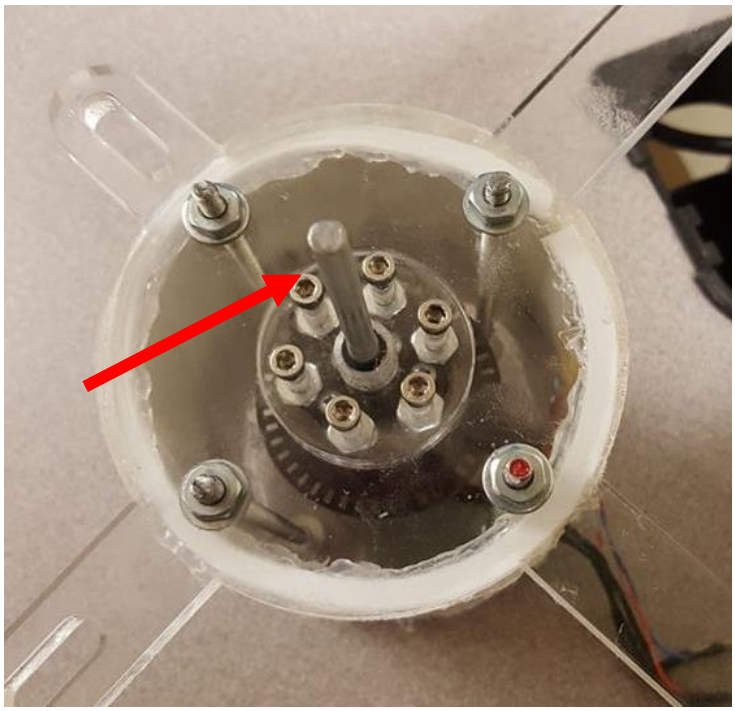

Figure 5-31: The Assembled Generator Module: External Shaft Side

5.5.4 Shell Construction

The nacelle shell was built from fiberglass mat sheets surrounding an acrylic housing. Fiberglass mat was chosen instead of cloth because mat allows for various shapes to be torn and fit together, and due to the circular nature of the nacelle frame, the ideal material found was the workable mat. To mold the shape out of fiberglass mat and resin, a foam mold (Seen in Figure 5-32) was used to obtain the conical shape of the frame. The foam block was sculpted using the dimensions of the CAD model of the nacelle. The mold was covered in aluminum foil, because resin does not adhere to this product. With the mold covered, fiberglass sheets were placed on top and covered with resin. After one thick layer of fiberglass mat was placed, the mold was left to dry in a well-ventilated space. Once the shell had dried, it was removed from the foam mold. The hardened nacelle shell can be seen in Figure 5-33. The hardened nacelle shell was fixed onto the nacelle frame. Figure *5-34* depicts a close up of the shell nose, with the FSR and temperature glued externally.

Figure 5-32: The Foam Mold

Figure 5-33: The Formed Fiberglass Nacelle Shell

Figure 5-34*: The Nose of the Nacelle Shell, with the FSR and TMP36 Visible*

5.6 Summary

This section gave a detailed description as to the design choices concerning schematic and circuit design, nacelle frame design, construction of power electronics as well as how the generator was incorporated into the system, and a description of how the nacelle was created. The details of the system were made clear, and the interfaces between the components as well as the implementation of circuits was discussed.

6. Testing and Results

6.1 Introduction

This section presents the results from different tests in the system. A detailed look at effects of RPM, current, and voltage on the generated power is discussed. To test the energy generation system in a lab environment, the generator was spun using a motor. For each test, the motor spun the generator through a range of RPMs. The motor speed was increased from the minimum to the maximum for each range and RPM and electrical performance data were recorded. Voltage and amperage produced by the generator, and voltage and amperage output by the battery charger were recorded with RPM. Three gear ratios were used between the motor and generator, producing data over a range of about 50RPM to about 1500RPM at the generator. Three data sets were taken with each gear ratio to collect data under repeated conditions. The data sets are represented by 'Run 1,' 'Run 2,' and 'Run 3' in each graph. Graphs of the voltage, amperage and power between the generator and the maximum power point tracker are presented to show the performance of the generator. Graphs of the voltage, amperage and power between the battery charger included in the maximum power point tracker and the battery are also presented to show the performance of the MPPT chip.

6.2 5-to-1 Gear Ratio

A gear ratio of 5-to-1 was chosen to rotate the generator close to 50RPM. This was the low end of the tested RPM range of the power conversion system. Data was recorded on three runs using this gear ratio, and the resulting graph of generator voltage as a function of RPM can be seen in Figure 6-1. The graph shows the three sets of data points overlapping, showing that the system is operating consistently. As expected, voltage output and RPM have a direct relationship: when one increases, the other does as well. Figure 6-2 shows the plot of generator amperage vs. RPM, with amperage along the y-axis and RPM along the x-axis. This plot shows the current reaching an average of 13mA. In the RPM range shown in Figure 6-1 and 6-2, the voltage produced by the generator was not enough to activate the MPPT.

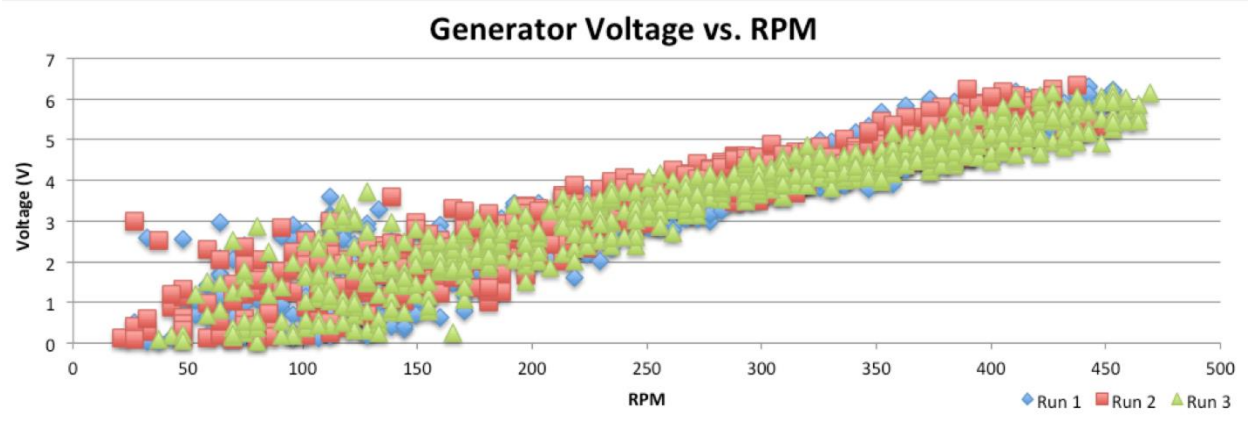

Figure 6-1: Generator Voltage vs. RPM, for the 5-to-1 Ratio

The graphs shown are generated from the data points recorded by the sensor system. Every quarter second, the system records values for RPM, voltage and amperage produced by the generator, and voltage and amperage output by the MPPT's battery charger. The RPM of the generator was increased as data points were recorded. The data collected was not without noise, so scatter plots were made to show the position of each data point. Each color on a graph represents data from a separate run.

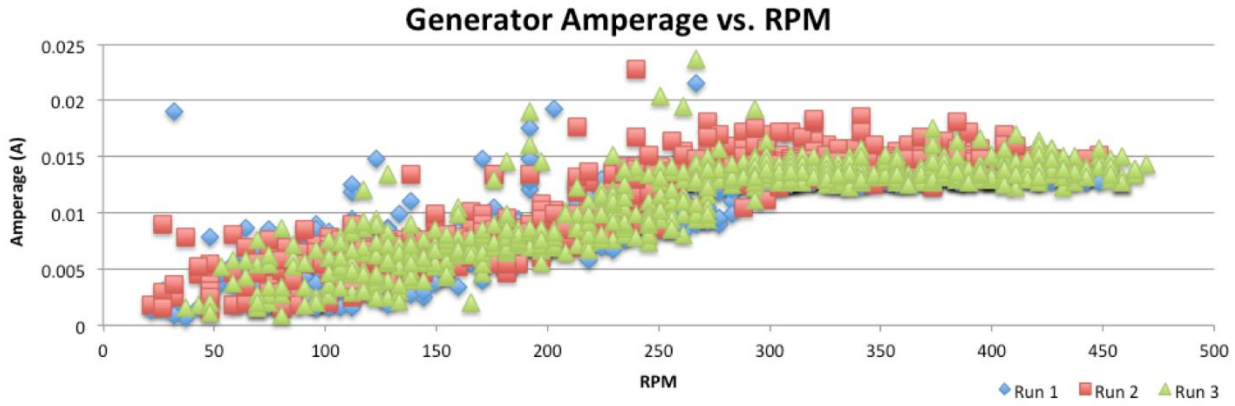

Figure 6-2: Generator Amperage vs. RPM, for the 5-to-1 Ratio

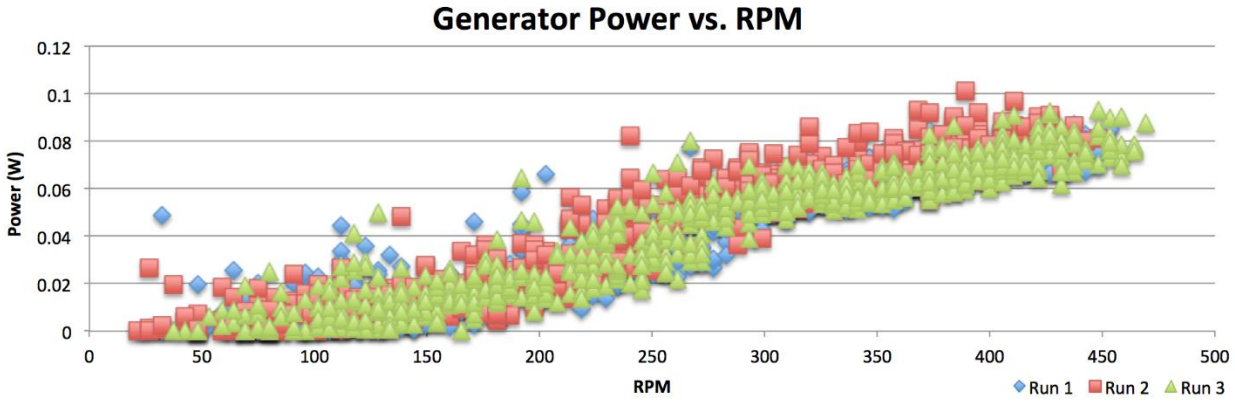

Figure 6-3: Generator Power vs. RPM, for the 5-to-1 Ratio

6.3 1.667-to-1 Gear Ratio

A gear ratio of 1.667-to-1 was used between the motor and the generator to gather data from roughly 100 RPM to 700 RPM. As seen in the curve in Figure 6-4, the voltage was not consistent for RPM values below 400. The gimbal motor produced more consistent voltage and amperage at RPMs above 400. The amperage curve of the 1.667-to-1 gearing, seen in Figure 6-5, depicts similar behavior to the amperage curve for the gear ratio of 5-to-1. It can be noted that the behavior follows the same trend: A steady

increase in amperage, with more consistent values above 350RPM. The gimbal motor was designed to be operated at low RPMs, and as RPM increased, the permanent magnets in the generator may not have been of sufficient strength to generate greater amperages.

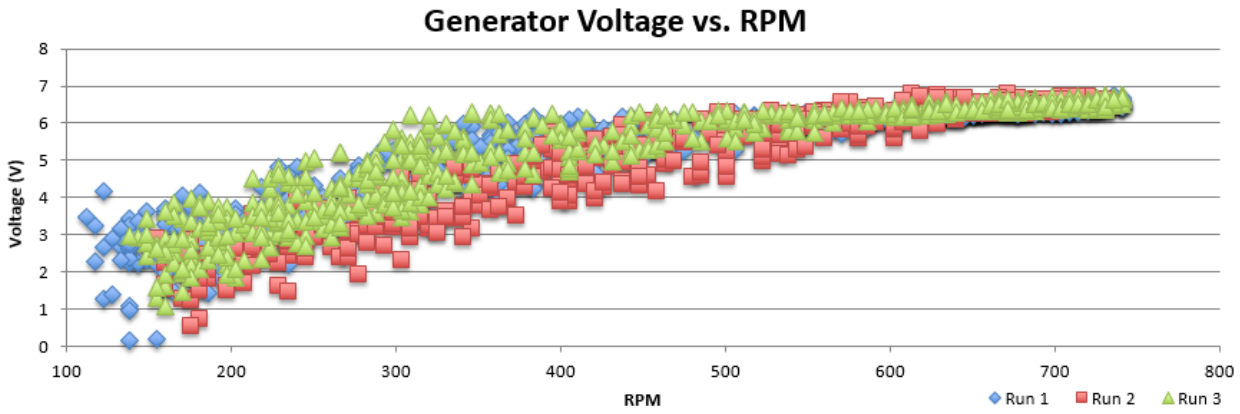

Figure 6-4: Generator Voltage vs. RPM, for the 1.667-to-1 Ratio

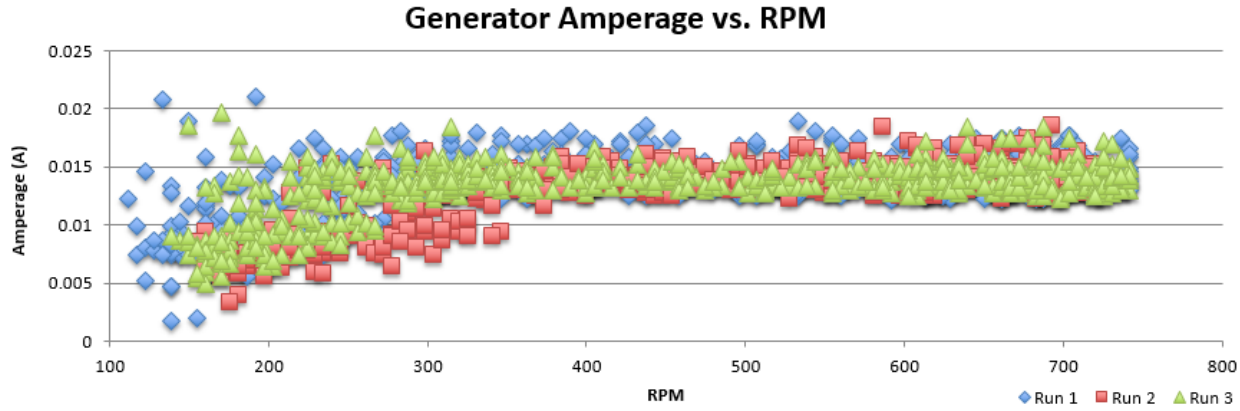

Figure 6-5: Generator Amperage vs. RPM, for the 1.667-to-1 Ratio

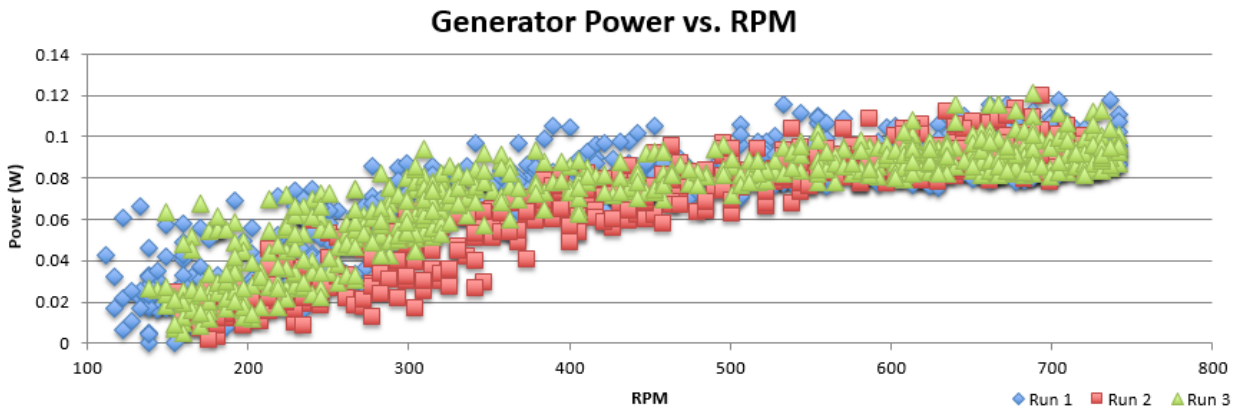

Figure 6-6: Generator Power vs. RPM, for the 1.667-to-1 Ratio

6.4 1-to-1 Gear Ratio

Data was recorded with the motor shaft connected directly to the generator. Tests were run with the voltage sensor on the output of the generator set to read up to 8V. Then, tests were run with the same voltage sensor set to read up to 14V. The ability to read a greater maximum voltage corresponded to a decrease in the accuracy of the sensor. Data was recorded up to 8V for three runs, and up to 14V for three more runs.

6.4.1 Generator Output Below 8V

Data less than and including a generator output voltage of 8V was recorded for three runs. Data for RPMs over 800 required the sensor to measure over 8V. Figure 6-8 shows the amperage generated when using a gear ratio of 1-to-1. There is no apparent increase in amperage over the range of roughly 300 to 900RPM. Most data points are within a range of 4mA. The current sensor was accurate within 2mA; not sufficient to accurately capture the current data points. However, the current data is accurate enough to calculate power produced by the generator, shown in Figure 6-9.

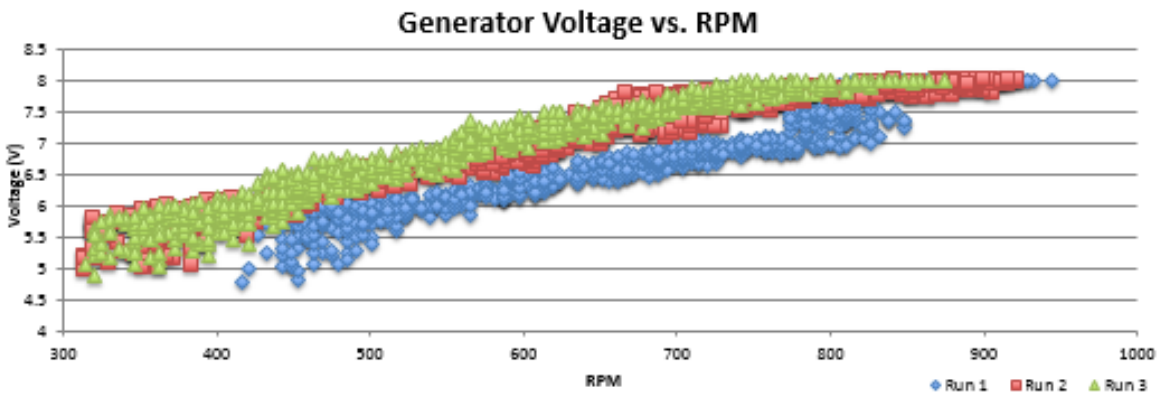

Figure 6-7: Generator Voltage vs. RPM, for the 1-to-1 Ratio

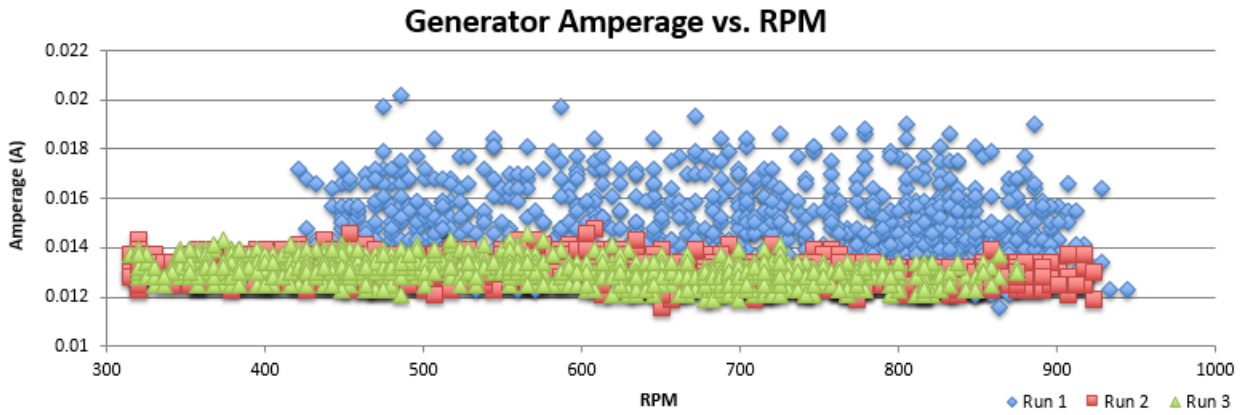

Figure 6-8: Generator Amperage vs. RPM, for the 1-to-1 Ratio

The power generated by the system with a gear ratio of 1-to-1 can be seen in Figure 6-9. The curve retained a variance of roughly 0.03W and the power was found to steadily increase as RPM increased. Since amperage stayed constant over the RPM range, this increase in power is caused by an increase in generated voltage.

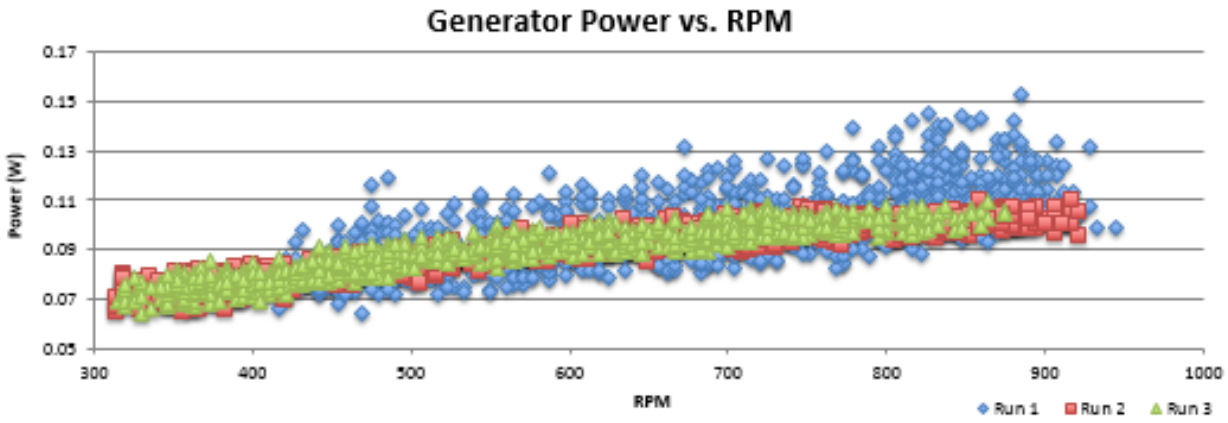

Figure 6-9: Generator Power vs. RPM, for the 1-to-1 Ratio

6.4.2 Generator Output Below 14V

Recording data at generator voltages above 8V enabled the observation of the behavior of the circuit above 900RPM. The voltage generated as a function of RPM, seen in Figure 6-10, is noisy at RPMs below 650, and stable at RPMs above 650. The change from noisy to stead values indicated the point where the MPPT chip began operation. The chip required a minimum turn-on voltage, which was achieved at 650RPM.

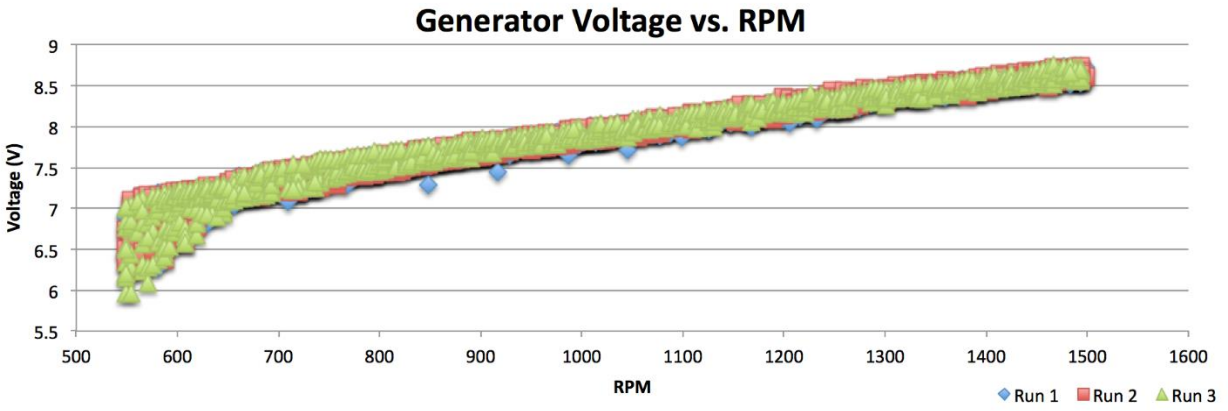

Figure 6-10: Generator Voltage vs. RPM for the 1-to-1 Ratio

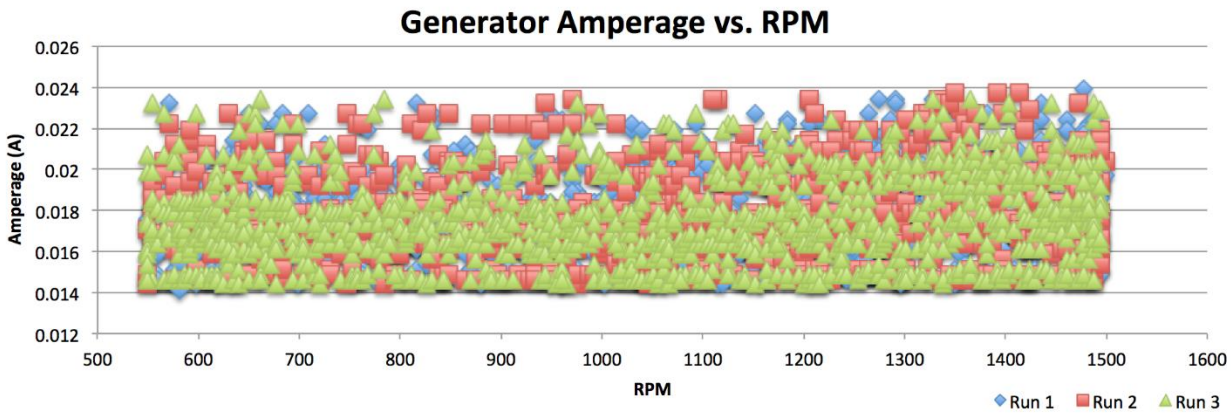

Figure 6-11: Generator Amperage vs. RPM for the 1-to 1-Ratio

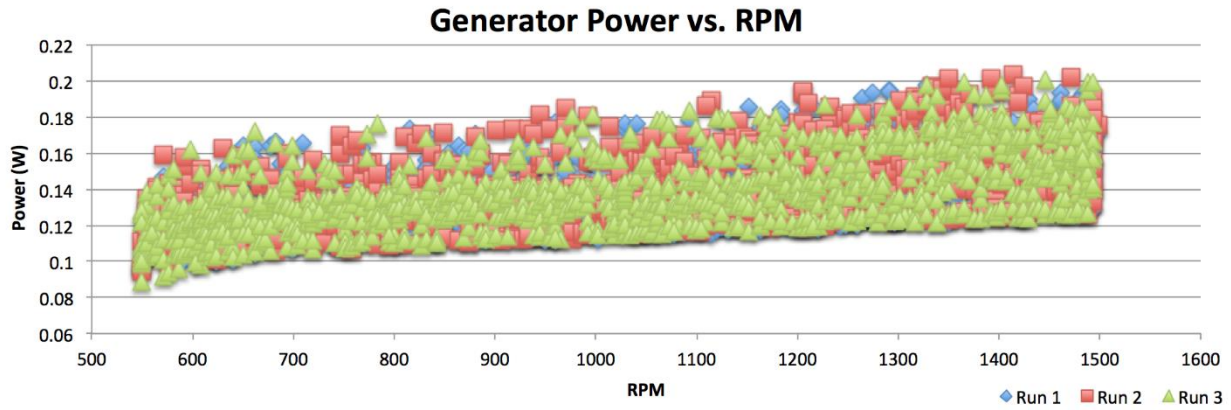

Figure 6-12: Generator Power vs. RPM for the 1-to-1 Ratio

As electricity was produced by the generator, the LiPo charge controller in the MPPT charged the battery. The charger created an output voltage above the battery voltage. The charger kept charging current constant while increasing the charging voltage as generator RPM and generated voltage increased.

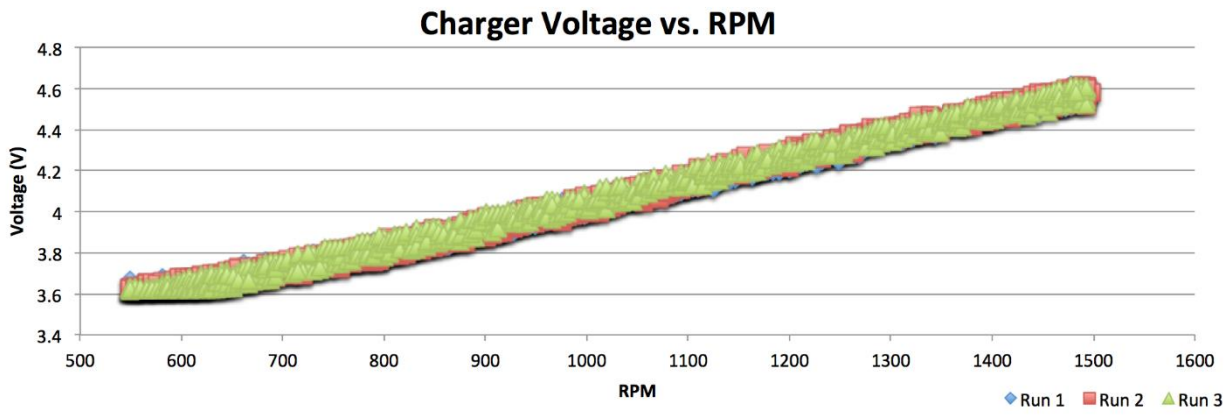

Figure 6-13: Charger Voltage vs. RPM, for the 1-to-1 Ratio

Figure 6-14 shows the charging current of the system. This graph displays a noisy data between 600 and 800RPM, caused by the inaccuracies of the current sensors used. The current generated by the system ranged between 10mA and 25mA during the generator tests, as measured with a handheld multimeter. Inaccuracy in current measurement translated to noise in the graph of charger power as a function of RPM. The charger power vs. RPM is shown in Figure 6-15.

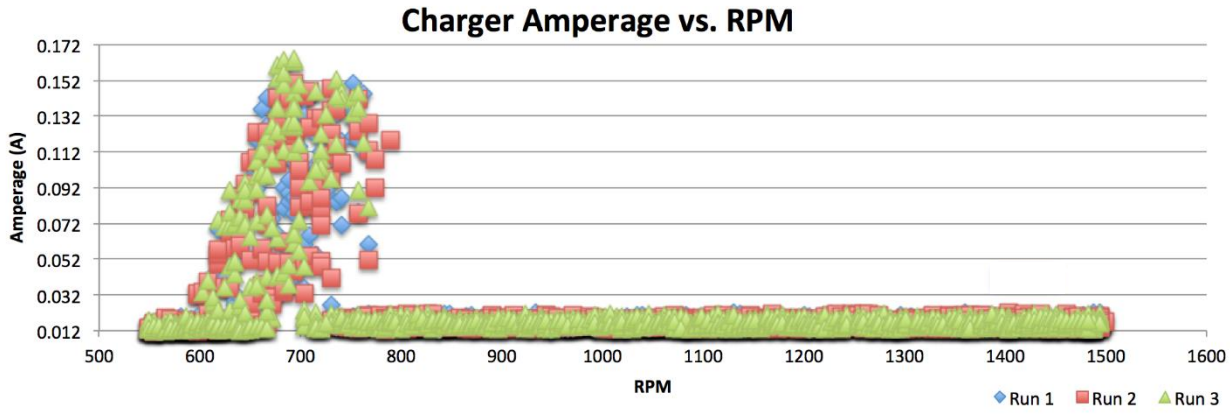

Figure 6-14: Charger Amperage vs. RPM for the 1-to-1 Ratio

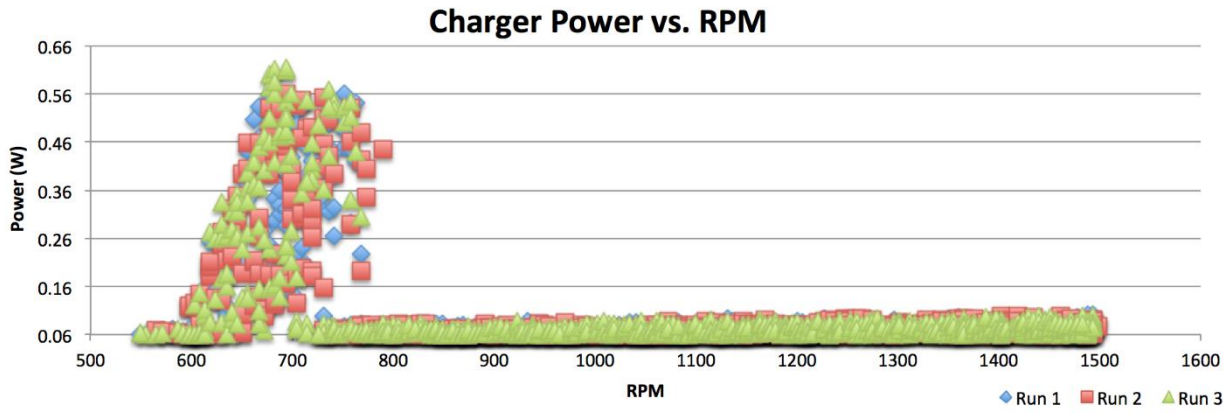

Figure 6-15: Charger Power vs. RPM for the 1-to-1 Ratio

6.5 Summary

This section explored the results collected in recorded data sets for the project. The three sets of data points per gear ratio were plotted in each graph. Three different gear ratios were explored and compared in order to characterize the operation of the generator and charger. The following characteristics are noted:

- Between 50RPM and 500RPM, the voltage generated from the system ranged between 0V to 5.5V, which was not high enough to turn on the MPPT. As a result, the graphs of this data (Section 6.2) displayed significant noise.
- Between 500 and 700RPM, the noise reduced and the resulting graphs became less noisy. Note the turn-on voltage for the MPPT occurred at 650RPM. Over 650RPM, when the turn-on voltage for the MPPT was reached, the voltage output graphs displayed a clean, linear nature.
- Before the turn-on voltage of the MPPT, the generated amperage values display significant noise. When the turn-on voltage was reached, the resulting generated amperage remained steady. It was noted that the MPPT chose to optimize the match between the voltage generated and the battery, and not the amperage. This is possibly due to low-strength permanent magnets in the generator.
- The graphs of voltage, amperage, and power are all steady after the turn-on voltage for the MPPT is reached.

The performance of the generator, MPPT, and charger were used to evaluate the effectiveness and operation of the system in operating with the mechanical system of the propagating wave turbine. An examination of the compatibility with the propagating wave turbine is included in Chapter 7.

7. Summary and Conclusions

7.1 Introduction

This section provides closure to the project report and discuss future work that that could be considered to further advance the power generation system.

7.2 Summary and Observations

The goal of the project was to utilize the ribbon fin design proposed and tested by a previous project team and devise an efficient method of low-power electrical energy generation. To accomplish this goal, the project team designed a power generation system. The system included a maximum power point tracker in order to produce an optimized power output curve. Additionally, a sensor system was designed and built to track the generated electricity and a nacelle was designed and built to house and not protect the generator and sensor system. The nacelle was designed to connect to the mechanical powertrain of the propagating wave turbine.

Sensors used to monitor the system included voltage, current, external temperature, water speed, and generator shaft RPM. Measured output voltage values from the sensors were recorded through the use of an onboard microprocessor. This enabled the team to monitor the system in real-time. To monitor the energy generation system, two voltage and two current sensors were used. One of each was placed directly before the MPPT, in order to monitor the voltage and current directly after the three-phase bridge rectifier, and one of each was placed directly after the MPPT in order to monitor the charging voltage and current of the onboard battery.

Since the system generated less than 1 watt, the project team encountered difficulties concerning energy generation and monitoring. Difficulties included:

- The MPPT chip had a minimum turn on voltage that was not met by the generator below a shaft speed of 650RPM.
- The propagating wave turbine mechanical powertrain did not turn at a high enough RPM to generate a useful generator output voltage.
- Gearing between the crank or camshaft of the mechanical powertrain and the generator resulted in a significant energy loss.
- The resolution of the Arduino ADC was only 3mv from a 10bit converter and was not sufficient for detecting and voltage changes when 3mV or less.

The end result of this project was a success in that a system was created that could utilize an incoming shaft RPM and generate electricity, provided the shaft was rotating fast enough. Unfortunately, the mechanical shaft rotation speed from the wave turbine fin was simply too low for reasonable power generation from the electromechanical generator and MPPT system.

7.3 Future Work

In the school year following this project, new projects will be conducted that stem from the physical limitations of the equipment utilized in the propagating wave turbine. The projects, when completed, could serve to improve the effectiveness and efficiency of the propagating wave turbine.

It is necessary to use a more efficient MPPT designed to operate from a wide range of input voltages, and particularly voltages as low as 3V. Because the propagating wave turbine generated less than 1 watt, it was difficult for the project team to find a MPPT chip that could match the system's output power. An MPPT chip capable of working in a range of 0 to 10W would be an ideal candidate for the propagating wave turbine system.

It would be valuable to investigate the use of a linear motor with the propagating wave turbine system. This type of motor is an ideal candidate for the propagating wave turbine because it eliminates the need for the wave turbine to be designed to generate a rotational output. Further, if the linear motor is designed to optimally operate at relatively low linear speeds, then it will be better matched to the output of the fin power generation system. Ultimately, improvements to the propagating wave turbine center on the optimization of energy harvesting components, specifically the motor generator and MPPT.

In addition to the power generation system, the mechanical fin design of the propagating wave turbine has yet to be optimized through the use of modeling and simulations. If the propagating wave turbine were to incorporate the changes discussed in this subsection, the project team has confidence that the end result would be superior to the project discussed in this report.

7.4 Conclusion

The propagating wave turbine project was completed over the span of one year, from its conception to the submission of this document. Due to time constraints, a complete submersible propagating wave turbine was not completed, but with additional project research, the project team expects this to become a reality. With the completion of this project and the results to prove that a system such as the one discussed in this report can generate power, the project team hopes that expansion projects can continue to refine the technology. Ultimately, the system was able to produce 0.13 Watts of power during demonstrations, sufficient to power a string of small LEDs.

8. References

Ackerman, E. (2014, December 31). *Sepios: ETH Zurich's Robot Cuttlefish*. Retrieved from IEEE Spectrum: http://spectrum.ieee.org/automaton/robotics/robotics-hardware/sepios-eth-zurichs-robot-cuttlefish

ADI. (2016). *TMP36 Datasheet and Info*. Retrieved from Analog Devices: http://www.analog.com/en/products/analog-to-digital-converters/integrated-special-purpose-converters/integrated-temperature-sensors/tmp36.html#product-overview

Admin. (2012). *Islay LIMPET Wave Power Station*. Retrieved from Scotland's Renewable Energy Guide: http://www.scotsrenewables.com/blog/?s=lIMPET&search=Search

Alstom. (n.d.). *Tidal Power Solutions.* Alstom.

Alternative Energy Tutorials. (n.d.). *Movements of Waves*. Retrieved from Alternative Energy Tutorials: http://www.alternative-energy-tutorials.com/energy-articles/movements-of-waves.html

Amazon. (2015). *Fantasycart Fiberglass Cloth*. Retrieved from Amazon.com: http://www.amazon.com/Fantasycart-Fiberglass-Cloth-6-48oz-wide/dp/B00M188N2G/ref=sr_1_2?ie=UTF8&qid=1447388564&sr=8-2&keywords=fiberglass+cloth

Amazon. (2016). *Pelican Case 1010*. Retrieved from Amazon: http://www.amazon.com/Pelican-1010-Micro-Black-Clear/dp/B001CCZF6E/ref=sr_1_1?ie=UTF8&qid=1456014905&sr=8-1&keywords=pelican+1010

Atmel. (n.d.). *ATmega2560*. Retrieved from http://www.atmel.com/Images/Atmel-2549-8-bit-AVR-Microcontroller-ATmega640-1280-1281-2560-2561_Summary.pdf

Atmel. (n.d.). *ATmega328*. Retrieved from http://www.atmel.com/images/atmel-8271-8-bit-avr-microcontroller-atmega48a-48pa-88a-88pa-168a-168pa-328-328p_datasheet_complete.pdf

Australia, E. (n.d.). *Water Wheels*. Retrieved from For teachers for Students.

Bale, R. (2014, June 9). *Separatability of drag and thrust in undulatory animals and machines*. Retrieved from Scientific Reports: http://www.nature.com/articles/srep07329#f6

Bitowt, M. (2013). *Design of a Tidal power Park and a Wave Park with a Techno-Economical Approach.* Goteborg, Sweden: Chalmers University of Technology.

Boake, C. (2002). *Overview and Initial Operational Experience of the LIMPET Wave Energy Plant.*

Carcas, M. (n.d.). Ocean Power Delivery Ltd.

Carroll, C. B. (1999). *USA Patent No. US642079B1.*

Centre for Rural Technology, N. (2009). *Upgraded water mills in the Himalayas*.

Costanzo, I. (2015). *Design of a Novel Concept for Harnessing Tidal Stream Power.*

Demay, V. (2014, June 20). *Measure soil Moisture with Arduino - Gardening*. Retrieved from Homeautomation: http://www.homautomation.org/2014/06/20/measure-soil-moisture-with-arduino-gardening/

Denny, E. (2009). The Economics of Tidal Energy. *Energy Policy*, 1914-1924.

Digi-Key. (n.d.). *MK20DX256VLH7*. Retrieved from http://www.digikey.com/product-detail/en/MK20DX256VLH7/MK20DX256VLH7-ND/3742957?WT.srch=1

DIYTrade. (n.d.). Retrieved from DIY Trade: http://www.diytrade.com/china/pd/7402195/fiberglass_mat.html

Energia. (2015). Retrieved from Energia: http://energia.nu/

Epstein, M. (2006). *Generating Thrust with a Biologically-Inspired Robotic Ribbon Fin.*

Evolving Art. (n.d.). Retrieved from Gizmag: http://www.gizmag.com/strandbeest-beach-art/29726/pictures#11

Facts About Hydropower. (2013). Retrieved from Wisconsin Valley Improvement Company: http://www.wvic.com/Content/Facts_About_Hydropower.cfm

Falcao, A. (2010, April). Wave Energy Utilization: A Review of the Technologies. *Renewable and Sustainable Energy Reviews*, pp. 899-918.

Foundation, S.-C. C. (2015). *Depth*. Retrieved from SCCF Recon: http://recon.sccf.org/definitions/depth.shtml

FSR. (n.d.). *Datasheet*. Retrieved from https://www.sparkfun.com/datasheets/Sensors/Pressure/fsrguide.pdf

Gadonneix, P. (2013). 2013 Survey: Summary. *World Energy Resources*.

Gill, A. (2005). Offshore Renewable Energy: Ecological Implications of Generating Electricity in the Coastal Zone. *Journal of Applied Ecology*, 605-615.

Haas, D. K. (2011). *Assessment of Energy Production Potential from Tidal Streams in the United States.* Georgia Tech Research Corporation.

Hadhazy, A. (2013, July 23). *Sciense of Summer: How do Ocean Waves Form?* Retrieved from Live Science: http://www.livescience.com/38361-how-do-ocean-waves-form.html

HDT Global. (2016). *Ghostbot*. Retrieved from HDT Global: http://www.hdtglobal.com/product/ghostbot/

Hitchcox, A. (2012, January 1). *Water Hydraulics: Benefits and Limitations*. Retrieved from Hydraulics & Pneumatics: http://hydraulicspneumatics.com/200/TechZone/HydraulicFluids/Article/False/6452/TechZone-HydraulicFluids

Jacobson, P. (2011). *Mapping and Assessment of the United States Ocean Wave Energy Resource.*

Jana. (2013). *Maximum Power Transfer Theorem*. Retrieved from Learn the Basics of Electronics.

Johnstone, C. M. (2013). A Techno-Economic Analysis of Tidal Energy Technology. *Renewable Energy*, 101-106.

Journey, S. (2015). Retrieved from http://www.solarjourneyusa.com/learn-buy-equipment.php

Kaiser, K. (2015, January 7). *Pelamis Wave Power - Another ALternative Energy Bust*. Retrieved from Principia Scientific: http://www.principia-scientific.org/pelamis-wave-power-another-alternative-energy-bust.html

King, H. (n.d.). *2804 - 210Kv*. Retrieved from Hobby King: http://www.hobbyking.com/hobbyking/store/__71104__2804_210Kv_Brushless_Gimbal_Motor_Ideal_for_GoPro_to_Compact_Style_Cameras_AR_Warehouse_.html

King, H. (n.d.). *Multistar 1807*. Retrieved from Hobby King: http://www.hobbyking.com/hobbyking/store/__78319__Multistar_1807_340Kv_Brushless_Gimbal_Motor_for_Mobius_Camera_AR_Warehouse_.html

King, H. (n.d.). *Qantum 2208*. Retrieved from Hobby King: http://www.hobbyking.com/hobbyking/store/__71427__Quanum_2208_Precision_Brushless_Gimbal_Motor_GoPRO_size_100_200g_AR_Warehouse_.html

King, H. (n.d.). *Turnigy HD2212*. Retrieved from Hobby King: http://www.hobbyking.com/hobbyking/store/__71428__Turnigy_HD_2212_Brushless_Gimbal_Motor_BLDC_AR_Warehouse_.html

Leijon, M. (2010). On the Physics of Power, Energy and Economics of Renewable Electric Energy Sources-Part I. *Renewable Energy*, 1729-1734.

Linear Technology. (n.d.). *LT3652*. Retrieved from Linear Technology: http://cds.linear.com/docs/en/datasheet/3652fe.pdf

Liu, H. (2013). *World Small Hydropower Development Report 2013.* United Nations Development Organization; International Center on Small Hydro Power.

Mazarov, O. (2014, 2 6). *SparkFun*. Retrieved from Circuitsathome.com: http://cdn.sparkfun.com/datasheets/Prototyping/Li_Power_Boost_Converter.pdf

MIT. (2013). *heliosoph*. Retrieved from MIT Links: http://heliosoph.mit-links.info/photointerrupter-schematic-details/

MSP432. (n.d.). *Datasheet*. Retrieved from http://www.ti.com/lit/ds/slas826a/slas826a.pdf

Neill, S. (2009). The Impact of Tidal Stream Turbines on Large-Scale Sediment Dynamics. *Renewable Energy*, 2803-2812.

OPT. (2015). *The Power Buoy*. Retrieved from Ocean Power Technologies: http://www.oceanpowertechnologies.com/powerbuoy/

Paish, O. (2002). Small Hydro Power: Technology and Current Status. *Renewable and Sustainable Energy Reviews*, 537-556.

Panels, O. (n.d.). *OEM Panels*. Retrieved from http://www.oempanels.com/what-does-single-and-three-phase-power-mean

Pelamis Wave Power. (n.d.). Retrieved from Expo 21XX: http://www.expo21xx.com/renewable_energy/19446_st3_industrial_research_renewables/default.htm

Perlman, H. (2015, August). *Hydroelectric Power Water Use*. Retrieved from U.S. Geological Survey: http://water.usgs.gov/edu/wuhy.html

Power, A. (2012). *Projects: Oyster 800 Project, Orkney*. Retrieved from Aquamarine Power: http://www.aquamarinepower.com/projects/oyster-800-project-orkney.aspx

RC, F. (n.d.). *Arduino Conductivity Probe*. Retrieved from http://flowrc.co.uk/conductivity_probe.html

Reich, G. (2014). *Resins, Resins, Everywhere, But WHich One to Use?* Retrieved from Boats.com: http://www.boats.com/how-to/resins-resins-everywhere-one-use/

Resources, A. (2015). *AR1000*. Retrieved from Atlantis Resources: http://atlantisresourcesltd.com/turbines/ar-series/ar1000.html

Resources, A. (2015). *AR1500*. Retrieved from Atlantis Resources: http://atlantisresourcesltd.com/turbines/ar-series/ar1500series.html

Seed. (n.d.). *MIT*. Retrieved from Seed: http://learning.media.mit.edu/seed/wave%20energy.html

Sepios. (2015). *Sepios: Riding the Wave of Progress*. Retrieved from Sepios: http://sepios.org/

Shevkar, P. (2015). Tidal Energy Harvesting. *International Journal of Science, Engineering and Technology Research*.

Shields, M. (2011). Marine Renewable Energy: The Ecological Implications of Altering the Hydrodynamics of the Marine Environment. *Ocean & Coastal Management*, 2-9.

Singh, T. (2011). *Aquamarine Power Breaks Ground on Oyster Wave Energy Farm in Orkney*. Retrieved from inhabitat: http://inhabitat.com/aquamarine-power-breaks-ground-on-oyster-wave-energy-farm-in-orkney/

Small Hydro. (n.d.). *Small Scale Hydropower*. Retrieved from Small Hydro International Gateway: http://www.small-hydro.com/about/small-scale-hydrpower.aspx

Sparkfun. (2015). *Force Sensitive Resistor 0.5*". Retrieved from Soarkfun: https://www.sparkfun.com/products/9375

Sparkfun. (2015). *Soarkfun Current Sensor Breakout - INA169*. Retrieved from Sparkfun: https://www.sparkfun.com/products/12040

Sparkfun. (2015). *Temerature Sensor - Waterproof* . Retrieved from Sparkfun: https://www.sparkfun.com/products/11050

SparkFun. (2016). *ACS712 Low Curent Sensor Eagle Schematic.* Retrieved from SparkFun: http://cdn.sparkfun.com/datasheets/Sensors/Current/ACS712%20Low%20Current%20Sensor%20Board%20v14.pdf

Sparkfun. (n.d.). *ACS712 Low Current Sensor*. Retrieved from https://www.sparkfun.com/products/8883

Sparkfun. (n.d.). *Arduino Mega 2560*. Retrieved from https://www.sparkfun.com/products/11061

Sparkfun. (n.d.). *FSR 0.5"*. Retrieved from https://www.sparkfun.com/products/9375

Sparkfun. (n.d.). *Photointerrupter*. Retrieved from https://www.sparkfun.com/products/9299

Sparkfun. (n.d.). *Teensy 3.2*. Retrieved from https://www.sparkfun.com/products/13736

Stansell, P. (2013, March). Maximum Wave-Power Absorption by Attenuating Line Absorbers Under Volume Constraints. *Applied Ocean Research*, pp. 83-93.

Stewart, D. (2012). *Discovery of Chlorine*. Retrieved from Chemicool: http://www.chemicool.com/elements/chlorine.html

STMicroelectronics. (2016). *SPV1020*. Retrieved from STMicroelectronics: http://www.st.com/st-web-ui/static/active/en/resource/technical/document/datasheet/CD00275733.pdf

STMicroelectronics. (2016). *SPV1040*. Retrieved from Mouser: http://www.mouser.com/ProductDetail/STMicroelectronics/SPV1040T/?qs=sGAEpiMZZMtitjHzVIkrqUzKQwtdeIlZg22FhsgpFdc%3d

Story, A. (n.d.). *The World's First Hydroelectric Power Plant Began Operation September 30, 1882*. Retrieved from America's Story from America's Library: http://www.americaslibrary.gov/jb/gilded/jb_gilded_hydro_1.html

Sun. (2016). *What the Heck is an MPPT Charge Controller?* Retrieved from Northern Arizona: http://www.solar-electric.com/mppt-solar-charge-controllers.html/

Sun, N. A. (2015). *What the Heck is a MPPT Charge Controller?* Retrieved from Northern Arizona Wind & Sun.

Taylor, G. W. (2001). The Energy Harvesting Eel: A Small Subsurface Ocean/River Power Generator. *Journal of Oceanic Engineering*, 539-547.

Tester, J. (2005). *Sustainability Energy: Choosing Among Options.* MIT Press.

Texas Instruments. (2015). *MSP-430FR4133*. Retrieved from Texas Instruments: https://store.ti.com/msp-exp430fr4133.aspx

Texas Instruments. (2015). *MSP-EXP432P401R*. Retrieved from Texas Instruments: https://store.ti.com/msp-exp432p401r.aspx

TI. (n.d.). *MSP430*. Retrieved from http://www.mouser.com/ProductDetail/Texas-Instruments/MSP-EXP430G2/?qs=sGAEpiMZZMv1ORdfpzTN%252bMwZ3%252b5KGk2B

TI. (n.d.). *MSP432*. Retrieved from https://store.ti.com/Basket.aspx

Tidal Barrage Generation. (2015). Retrieved from Alternative Energy Tutorials: http://www.alternative-energy-tutorials.com/tidal-energy/tidal-barrage.html

Tiwari, R. (2012). IPMC as a Mechanoelectric Energy Harvester: Tailored Properties. *Smart Materials and Structures*.

Tomko, E. (2015).

Twiefel, J. (2008). Power Output Estimation and Experimental Validation for Piezoelectric Energy Harvesting Systems. *Journal of ELectroceramics*, 203-208.

Underplayground News. (2015). Wind Powered Strandbeests by Theo Jansen. *Underplayground News*, pp. http://www.upperplayground.com/blogs/news-upperplayground/tagged/strandbeest.

University, L. (n.d.). *Linear Control of Wave Energy Converters*. Retrieved from Lancaster University Renewable Energy Group: http://www.engineering.lancs.ac.uk/lureg/group_research/wave_energy_research/Linear_Control.php

University, N. (2011, January 18). *Robotic Ghost Knifefish is Born*. Retrieved from Northwestern University: http://www.northwestern.edu/newscenter/stories/2011/01/robotic-ghost-knifefish.html

UNO, A. (n.d.). Retrieved from https://www.arduino.cc/en/Main/ArduinoBoardUno

Uria-Martinez, R. (2014). 2014 Hydropower Market Report. *U.S. Department of Energy*.

Voorhis, R. (2012, July 25). *Point Absorbers: The Technology and Innovations*. Retrieved from Energy and the Environment - A Coastal Perspective: http://coastalenergyandenvironment.web.unc.edu/ocean-energy-generating-technologies/wave-energy/point-absorbers/

Walters, R. (2013). Estimation of Tidal Power Potential. *Renewble Energy*, 255-262.

William. (2010). *Hydroelectric Power* . Retrieved from Nothing Nerdy: http://nothingnerdy.wikispaces.com/HYDROELECTRIC+POWER+-+William

Wiring. (n.d.). *Sparkfun ACS712*. Retrieved from http://wiring.org.co/learning/basics/currentacs712.html

World, H. (n.d.). *HIstory of Technology*. Retrieved from History World: http://www.historyworld.net/wrldhis/PlainTextHistories.asp?ParagraphID=dol

Youngsu, C. (2015). *Physics-Based Modeling of Ionic Polymer Metal Composites for Underwater Energy Harvesting.*

YouTube. (2013). *YouTube*. Retrieved from YouTube: https://i.ytimg.com/vi/yKho1njso5I/hqdefault.jpg

9. Appendix A: Code used in the Project

Below is the code from the entire project. Constants, variables, and initializers are listed first.

```
//Current variables
const int CURRENT1_PIN = A0;
const int CURRENT2_PIN = A1;
const float gain1 = 110; //62.5
const float gain2 = 90; //
const float R1 = 0.8;
const float R2 = 0.58;

//voltage reading variables

const int VOLT_PIN1 = A8;
const int VOLT_PIN2 = A7;
double VoltRead1;
double VoltRead2;

//Temperature variables
const int TEMP_PIN = A2;
int sensorInput;
double tempC;
double voltageOut;

//Water Detection Variables
const int WATER1_PIN = A3;
const int WATER2_PIN = A4;
int water1Val;
int water2Val;
double water1Volt;
double water2Volt;
```

```
//Force Sensor variables
const int FORCE1_PIN = A5;
const int FORCE2_PIN = A6;
int force1Input;
int force2Input;
double force1VoltageOut;
double force2VoltageOut;

//Encoder Variables
unsigned long lastReading = 0;
unsigned int pulsesperturn = 45; //VERY IMPORTANT
int encoder_in = 2;

double revolutionsPerQT = 0;
double RPS = 0;
volatile unsigned int pulses = 0;

const int ledPin =  13;
int ledState = LOW;             // ledState used to set the LED
unsigned long previousMillis = 0;
unsigned long interval = 1000;

const int VOLTAGE_REF33 = 3.3;  // Reference voltage
const int numReadings = 15;

//Set up the serial
void setup() {
  // Initialize serial monitor
  Serial.begin(9600);
  Serial.println("start...");
  //attach the interrupt to pin 2, or DIG. (2)
  pinMode(encoder_in, INPUT);
```

```
  attachInterrupt(2, ISRpulses, RISING); //digital pin2
  pinMode(ledPin, OUTPUT);
}

//Looping code
void loop() {
  //digitalWrite(led, HIGH);
  unsigned long currentMillis = millis();
  if((currentMillis - previousMillis) > interval) {
    // save the last time you blinked the LED
    previousMillis = currentMillis;
    // if the LED is off turn it on and vice-versa:
    if (ledState == LOW)
      ledState = HIGH;
    else
      ledState = LOW;
    // set the LED with the ledState of the variable:
    digitalWrite(ledPin, ledState);
  }

  // read the input on the ADC pins for the current sensors:
  int currSense1 = analogRead(CURRENT1_PIN);
  int currSense2 = analogRead(CURRENT2_PIN);

  //take the amplified ADC value and make it a voltage
  float vBigCurr1 = currSense1 * (3.3 / 1023.0);
  float vBigCurr2 = currSense2 * (3.3 / 1023.0);

  //take the amplified value and make it the "actual" voltage value
  float vActual1 = vBigCurr1 / gain1;
  float vActual2 = vBigCurr2 / gain2;
```

```
//to find current use ohm's law:
float curr1 = vActual1 / R1;
float curr2 = vActual2 / R2;


//Voltage:
float stepDown1 = 5.0;
float stepDown2 = 2.42;
int voltageValue1 = analogRead(VOLT_PIN1);
int voltageValue2 = analogRead(VOLT_PIN2);
VoltRead1 = voltageValue1 * ((3.3 / 1023.0) * stepDown1);
VoltRead2 = voltageValue2 * ((3.3 / 1023.0) * stepDown2);

//Temperature:
//MUST USE 5V VOLTAGE REF
sensorInput = analogRead(TEMP_PIN);
voltageOut = sensorInput * (3.3 / 1023.0);
tempC = ((voltageOut - 0.48) * 100);

//Water Detection:
water1Val = analogRead(WATER1_PIN);
water2Val = analogRead(WATER2_PIN);
int flag = 0;
if (water1Val > 2){
  //There is water inside the compartment
  flag = 1;
  //return flag;
}
else if (water2Val > 2){
  flag = 2;
  //return flag;
}
```

```
  //No water inside
  else flag;

  //Force Sensor
  force1Input = analogRead(FORCE1_PIN);
  force1VoltageOut = force1Input * (3.3 / 1023.0);

  //encoder code
  if(millis() - lastReading >= 250){ //take a reading every QUARTER
SECOND
    lastReading = millis();
    //disable the interrupt and make a copy of the number of pulses
    detachInterrupt(2); //detach the interrupt
    double copyPulses = pulses;
    pulses = 0; //reset to zero for the next reading
    attachInterrupt(2, ISRpulses, RISING);
    //revolutionsPerQT = copyPulses / pulsesperturn;
    RPS = (copyPulses / pulsesperturn) * 4;
    double RPM = RPS * 60;
    Serial.print("  RPM:");
    Serial.print(RPM);
    Serial.print("  VBeforeMPPT:");
    Serial.print(VoltRead1, 4);
    Serial.print("  CBeforeMPPT");
    Serial.print(curr1, 4);
    Serial.print("  VBattCharge");
    Serial.print(VoltRead2, 4);
    Serial.print("  CBattCharge");
    Serial.print(curr2, 4);
    Serial.print("  TempinC:");
    Serial.print(tempC);
```

```
//    Serial.print("  Water?:");
//    if(flag == 1){
//      Serial.print("YES: Watertight Section");
//    }
//    else if (flag == 2){
//      Serial.print("YES: Electronics Module");
//    }
//    else
//    Serial.print("No water!");
//
    Serial.print("  ForceSensedV:");
    Serial.println(force1VoltageOut, 3);

   }
}

// This function is called by the interrupt for the encoder
void ISRpulses() {
  pulses++;
}
```